Buckling and Postbuckling response of laminated composite plates with interlaminar flaws

Nima Shabanijafroudi

A Thesis
In the Department
of
Mechanical, Aerospace and Industrial Engineering

Presented in Partial Fulfillment of the Requirements
For the Degree of
Doctor of Philosophy (Mechanical Engineering) at
Concordia University
Montreal, Quebec, Canada

January 2021

CONCORDIA UNIVERSITY
School of Graduate Studies

This is to certify that the thesis was prepared
By : Nima Shabanijafroudi

Entitled: Buckling and Postbuckling response of laminated composite plates with interlaminar flaws

and submitted in partial fulfilment of the requirements for the degree of
DOCTOR OF PHILOSOPHY (Mechanical Engineering)
complies with the regulations of the University and meets the accepted standards with respect to originality and quality.
Signed by the final examining committee:

Dr. Catherine Mulligan	Chair
Dr. Abdolhamid Akbarzadeh Shafaroudi	External Examiner
Dr. Khaled E. Galal	External to Program
Dr. Suong Van Hoa	Examiner
Dr. Mehdi Hojjati	Examiner
Dr. Rajamohan Ganesan	Supervisor
Dr. Anh Dung Ngô	Co-supervisor

,
Approved by

Dr. Ivan Contreras, Graduate Program Director

January15, 2021

Dr. Mourad Debbabi, Dean
Gina Cody School of Engineering & Computer Science

ABSTRACT

Buckling and Postbuckling response of laminated composite plates with interlaminar flaws

Nima Shabanijafroudi, Ph.D.
Concordia University, 2021.

High stiffness and strength, corrosion resistance, and ease of manufacturing have made laminated composites an excellent replacement for isotropic materials. The outstanding properties of composites especially appeal to industries such as the aerospace industry where lightweighting is of great importance. Despite the mentioned advantages, susceptibility to defects is a major drawback in using these materials. Being composed of several layers bonded together using an adhesive material, delamination or debonding of layers is one of the most common flaws in composite laminates. Delamination may drastically impact the mechanical behavior of laminates, especially in unstable conditions. Larger deflections and higher levels of stresses that a laminate experiences in the postbuckling state may, in turn, lead to the growth of a delamination. Given the complications that are caused by delamination, keeping delaminated plates in service requires an in-depth understanding of their postbuckling behavior including the possibility of the growth of the delamination. The objective of this thesis is to develop a comprehensive mathematical and mechanical methodology for accurately predicting the buckling and postbuckling behavior of delaminated composite plates including the fracture mechanical phenomena involved in the postbuckling state.

In all the formulations derived in the framework of the new methodology, the deformations of laminates are approximated using the first-order shear deformation theory and the equilibrium equations were derived using the principle of stationary total potential energy and the Ritz method. In both linear buckling and nonlinear postbuckling analyses, the effect of large rotations is incorporated by adopting Von Kármán's approximations of the Green strain tensor.

The present thesis work approaches the buckling and postbuckling behavior of delaminated plates through nonlinear analyses. However, conducting nonlinear analyses requires a preliminary knowledge of the potential buckling modes (local, mixed or global) and the loading level at which they may emerge. This preliminary information is used for determining the optimal configuration

of imperfections to be incorporated in the nonlinear analyses. In the present work, a novel eigenvalue buckling solution was developed for the required preliminary information. The developed formulation in order to account for the prebuckling stress field nonuniformity caused by in-plane constraints, bases the eigenvalue analysis on a calculated stress field obtained using a prebuckling stress analysis.

For interrogating the details of the postbuckling behavior of delaminated plates, a state of the art postbuckling solution is proposed. The proposed methodology uses a new partitioning scheme that splits the delaminated plate using the plane of the delamination. Outside the delaminated regions the bond between the sublaminates is modeled using a penalty function method. The penalty functions model the effect of an extremely thin layer of elastic adhesive gluing the sublaminates together. The use of the penalty function method offers the advantage of providing the distribution of interlaminar traction in the plane of the delamination. Given the availability of interlaminar tractions in the vicinity of the borders of the delaminated region, Irwin's crack closure integrals were integrated into the solution for calculating strain energy release rates corresponding to the three fracture modes separately.

Given the importance and the abundant industrial use of curved composite panels especially in the aerospace industries, in an attempt to extend the applicability of the developed methodology to delaminated curved panels, an eigenvalue buckling solution for curved plates subjected to rotational edge restraints is developed.

The validity of the deliverable results of each of the pieces of the developed methodology was verified by comparing the results with experimental data and numerical results obtained using finite element analyses.

Dedication

I dedicate this dissertation work to my spouse for
her patience, support, and encouragement

Acknowledgment

I would express my gratitude to my spouse and my son for without their support and understanding I couldn`t have succeeded in completing this thesis.

My gratitude also extends to my supervisor Dr. Rajamohan Ganesan whose supports and directions helped me strive and thrive.

Furthermore, I would like to thank Dr. Said Jazouli from whom I learned a lot.

I would like to acknowledge the financial supports provided by NSERC, CRIAQ, Bell Helicopter, L3 Technologies, Bombardier aerospace, and Concordia University.

Contents

List of tables

List of figures

Contribution of authors in co-authored journal articles

Title: "*Influence of in-plane constraints on the prebuckling and buckling responses of laminated composite plates*" Under review at European Journal of Mechanics - A/Solids
Nima Shabanijafroudi: Conceptualization, Methodology, Software, Validation, Formal analysis, Writing - Original Draft, Visualization
Rajamohan Ganesan: Supervision, Conceptualization, Funding acquisition, Methodology, Writing - Review & Editing.

Title: "*A penalty function based delamination model for postbuckling analysis of composite plates with delamination*" Composite Structures 2020 (Impact Factor 5.138)
Nima Shabanijafroudi: Conceptualization, Methodology, Software, Validation, Formal analysis, Writing - Original Draft, Visualization
Rajamohan Ganesan: Supervision, Conceptualization, Funding acquisition, Methodology, Writing - Review & Editing.

Title: "*A new methodology for buckling, postbuckling and delamination growth behavior of composite laminates with delamination*" Accepted for publication by Composite Structures (Impact Factor 5.138) with minor editorial revisions.
Nima Shabanijafroudi: Methodology, Software, Validation, Formal analysis, Writing - Original Draft, Visualization
Rajamohan Ganesan: Supervision, Conceptualization, Funding acquisition, Methodology, Writing - Review & Editing.

Title: *"Effect of rotational restraints on the stability of curved composite panels under shear loading*" Acta Mech. 231, 1805–1820 (2020).
Nima Shabanijafroudi: Methodology, Software, Validation, Formal analysis, Writing - Original Draft, Visualization
Said Jazouli: Supervision, Conceptualization, Methodology, Writing - Review & Editing.
Rajamohan Ganesan: Supervision, Conceptualization, Methodology, Funding acquisition, , Writing - Review & Editing.

Chapter 1: Introduction

1.1 Background and motivation

Thanks to their outstanding mechanical properties, corrosion resistance, lightweight, and ease of manufacturing, laminated composite materials have gained remarkable popularity, especially in the aerospace industry where these characteristics are highly preferred. However, given their nonhomogeneous structure, understanding and modeling their failure mechanisms have been challenging and the subject of numerous studies. Failure often occurs due to the growth and propagation of preexisting flaws and despite their excellent properties, composite laminates are susceptible to inherent flaws. Probably the most impactful of the flaws in composite laminates is delamination. Delamination is partial debonding of the plies that constitute a layered laminate and may exist as preexisting manufacturing defects or may appear later in service due to material degradation, fatigue, or low-speed impact. It is established that there is a connection between matrix cracking inside the layers and the appearance of delamination between the layers. The aforementioned matrix cracks are generally cause by shearing or bending deformations. Delamination generally appears between layers with different fiber orientation. When a growing crack fails to penetrate the adjacent layer with different fiber orientation propagates as a delamination[1]. Regardless of the reason for their presence, delamination may drastically impact the mechanical behavior and load-carrying capacity of laminates [2]. The impact of delamination on the stiffness and strength of a plate is more pronounced in unstable conditions where significantly larger deformations are expected. The large deformations experienced in the postbuckling state may trigger fracture mechanisms and lead to the growth of the delamination.

In thin-walled structures, static instability, or in other words buckling, happens due to a decrease in the bending stiffness of the structure caused by the reverse stress stiffening effect corresponding to in-plane compressive forces. In delaminated composite plates and shells, the manifestation of the instability phenomenon depends on the geometry, ply material properties, and the stacking sequence of the laminate as well as the size and the location of the delamination along the thickness of the laminate. A laminate with a near-surface delamination is expected to experience a local buckling followed by a mixed buckling mode, whereas, laminates with delaminations closer to their midplane generally experience either global or mixed buckling mode shapes (Figure 1.1).

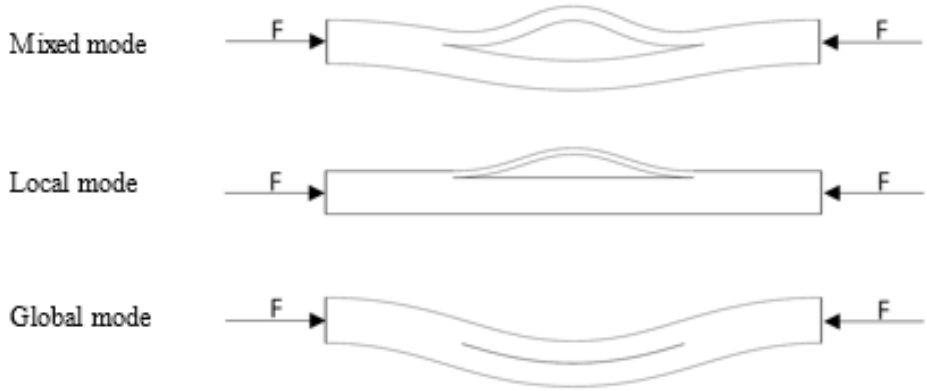

Figure 1.1 Schematic view of possible buckling mode shapes for a delaminated plate under compressive loading

The diminishment of the bending stiffness in a buckled plate may lead to radically large deflections and consequently induces higher levels of stresses. This is especially more pronounced and important in delaminated plates, where the boundaries of the delaminated region constitute the tips of internal cracks. Large buckling deflections may trigger either of the three fracture mechanisms (Figure 1.2) and lead to the propagation of the delamination. The growth of a delamination may eventually result in the complete failure of the composite laminate.

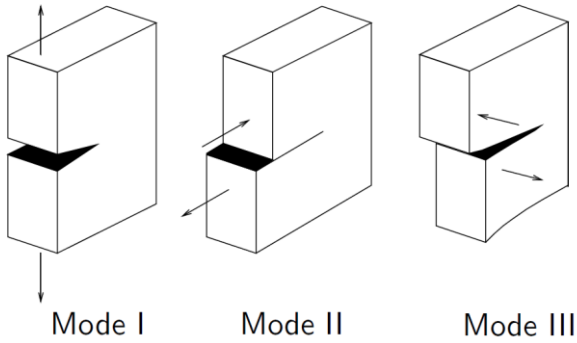

Figure 1.2 The three standard fracture modes (Mode I: opening, Mode II: shearing, Mode III: tearing)

Given the prevalence of delamination in composite laminates, the general practice doesn't involve discarding slightly defective laminates but rather keeping them in service while taking into account the ensuing consequences of the delamination. Given the complications that arise from the instability of delaminated plates, keeping such plates in service requires an in-depth understanding of their buckling and postbuckling behavior. Even though the aerospace industry relies vastly on testing, extrapolating the results of experiments necessitates an elaborate

methodology for predicting the buckling and postbuckling behavior of delaminated plates as well as the possibility of the propagation of a delamination.

To predict the behavior of delaminated plates under compressive loading either eigenvalue buckling analyses or nonlinear buckling and postbuckling analyses can be performed. The linear buckling solutions have the advantage of speed and conciseness of results, however, the information they provide is limited to the instability threshold and the buckling mode shape. In contrast, nonlinear postbuckling analyses can provide a wide range of information that can help designers have a clear picture of the behavior of structures beyond the instability threshold. Eventually, the information collected using these analyses can be used for determining the residual strength in delaminated plates and adjusting the design allowables.

1.2 Literature survey

In the literature, various parameters, and phenomena have been found influential, in the instability problem of delaminated plates and the effect of each parameter has been examined either qualitatively or quantitatively. Studies differ in the parameters accounted for, the techniques to incorporate them, and also in solution approaches. Here the literature has been viewed from the perspective of the present work and the phenomena accounted for are summarized along with the strategies used to incorporate them in the simulation. In the subsequent sections, different aspects of the implemented theories and techniques are briefly explained and the advantages and disadvantages of each of them are discussed.

1.2.1 Geometrical approach

Technically, delamination is a discontinuity in the thickness of a composite plate and hence delaminated plate needs to be treated differently than an intact piece of material. One of the earliest works on the buckling and postbuckling of delaminated plates was carried out by Chai et al [3]. They proposed a one-dimensional analytical scheme based on a beam-column model and proceeded with calculating the energy release rate. They regarded thin, near-the-surface delaminations as a film bonded to an infinite substrate and for arbitrarily positioned delaminations they proposed a partitioning scheme for accommodating the geometrical discontinuity across the delamination (Figure 1.3).

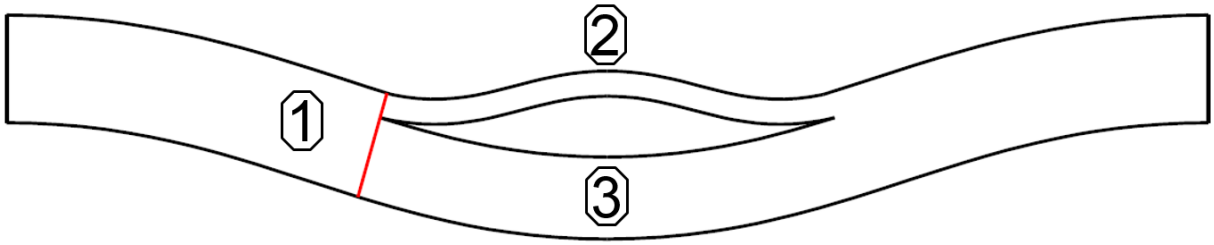

Figure 1.3 Schematic view of a multi-zone model [4]

The film modeling scheme as described was later used by many other researchers [2,5–8]. Larson [9] extended the applicability of the one-dimensional film model to multiple axisymmetric circular delaminations. The concept of modeling a thin debonded layer as an independent film was also extended to two-dimensional modeling and was used in several works for modeling the stability behavior of delaminated elliptical films [10–14]. The film model approach has been also used for buckling analysis of laminates with multiple delaminations[9]. In this approach delaminated layers are modeled as a separate films, however the contact between these films are taken into account. Despite the vast use of the film model for simulating near-surface delaminations, Nilsson et al [15] in a numerical work questioned the accuracy of this approach.

The partitioning scheme has also been widely used for the instability analysis of delaminated plates. The approach has been used for both one-dimensional [16–21] and two-dimensional [22–26] modeling of laminates with through-the-width delaminations. The same principle has been used to develop a multizone partitioning scheme for two-dimensional analysis of laminates with finite-width embedded delaminations [25,27–34]. In problems involving multiple delaminations, the application of the partitioning scheme leads to a more intricate combination of sublaminates separated by delamination planes [24,35–37].

Models based on layerwise theories treat the in-thickness discontinuity simply by modifying the assumed displacement field. Displacement discontinuity across the delamination is modeled by adding a jump function to the displacement field of the layerwise model [38–41]. The use of layerwise theories makes it possible to model a delaminated panel as a single plate without the need for partitioning. Ovesy et al [24] and Kharghani and Soares [42] however opted to use the partitioning scheme while modeling each segment using a layerwise theory.

1.2.2 Continuum modeling

A variety of theories have been used for modeling the mechanical behavior of composite laminates with delamination. The simplest approach has been using a one-dimensional beam-column model for simulating the different segments of a plate with through-the-width delaminations. In the majority of researches of this type the Euler-Bernoulli beam model has been used [3,7,8,16–18], however, to extend the applicability of the beam-column model to moderately thick laminates, some researchers have employed shear deformation theories [13,19]. In spite of the one-dimensional nature of these models, the essentially two-dimensional coupling effects have also been accounted for by modifying the bending stiffness of beams [5,21,43]. As was mentioned before the one-dimensional approach in conjunction with an axisymmetric formulation has been used for modeling axisymmetric geometries [9] as well.

One-dimensional models as described are incapable of simulating two-dimensional phenomena such as two-dimensional deformations and/or width-related phenomena in through-the-width and finite-width delaminations. To accommodate these essentially two-dimensional effects and conditions, plate and shell theories have been used. The Classical Laminated Plate Theory (CLPT) provides the simplest approximation of the behavior of laminates and has been widely used in the literature of delaminated composite plates [5,9,11,12,22,44]. The CLPT assumes a linear distribution of in-plane displacements in the out-of-plane direction and neglects out-of-plane shear deformations. The CLPT has been proved to fairly approximate the behavior of thin laminates, however, it is notorious for overestimating the bending stiffness of thick laminates. To avoid excessive stiffness, First-order Shear Deformation Theory (FSDT) [15,25,30–32,45–48] and Higher-Order Shear Deformation Theories (HSDTs) [27] have been used. Kharazi et al [23] studied the buckling behavior of laminates containing through-the-width delamination using CLPT, FSDT, and HSDT. They concluded that the HSDT had superior accuracy. However, they observed that the results obtained using FSDT match those of HSDT except for the cases with remarkably thick sublaminates. The FSDT despite taking into account shear deformations assumes a uniform distribution of transverse shear stresses in the thickness of a laminate and violates the traction free condition of the surfaces of a laminate and thus overestimates the bending stiffness. As a remedy to this problem, a shear correction factor is introduced to the shear stiffness of the laminate. Unlike isotropic materials, no single value can be prescribed as the shear correction factor of composite laminates. However, both the values prescribed for isotropic plates have been

used in the literature [49–52] both for pristine laminates and the sublaminates that constitute a delaminated plate and were proved to yield acceptable results. A more accurate approach for determining the shear correction factor of a laminate with a particular configuration is introduced by Whitney [53] and uses an energy equivalency method for estimating the shear stiffness of the laminate.

Thus far all the discussed theories consider a laminate as an Equivalent Single Layer (ESL). Layerwise theories [24,28,33] constitute a different class of approximation methods for modeling laminated plates. These theories by assuming only C^0 continuity of in-plane displacements in the out-of-plane direction of a laminate provide a more realistic picture of the behavior of a non-homogenous layered plate.

Besides the discussed plate and shell theories, solid models have been used in numerical studies as well. Both 2D [35,54–57] and 3D [38,58] Finite Elements (FEs) have been used in the literature to cover different aspects of the instability of delaminated composite plates. The major disadvantage of FE analysis is high computational costs. As a remedy to the high time and calculation costs associated with FE analyses, Whitcomb [59,60] employed a substructuring method to reduce the size of FE analyses.

1.2.3 Fundamental formulation

To derive and/or solve the buckling and postbuckling equations for composite laminates containing interlaminar flaws, a variety of formulations have been used.

In solutions developed based on the beam-column model [3,5,7,21], the general approach has been to assume that the buckling mode shape remains unchanged in the postbuckling state and the axial stress in the postbuckling state is equal to the buckling critical stress. In these solutions, the kinematic consistency equations are used for determining the amplitude of the buckled shape in terms of the applied end-shortening (the relative movement of the opposite edges of a plate). Apart from the discussed approach, the perturbation method [8,16–18] has also been used for obtaining buckling and postbuckling solutions of beam-column based models.

In the context of two-dimensional analysis of delaminated plates, fully analytical solutions are rare due to the complexity of the problem. The work of Xue et al [26] is one of the very few

analytical solutions introduced for two-dimensional buckling problems. These analytical approaches are majorly applicable in the absence of coupling effects.

Probably the most widely used method in delamination buckling and postbuckling studies is the Ritz method. The Ritz method is used for finding solutions to variationally expressed equations. In structural mechanics, the Ritz method is employed for finding an equilibrium state by minimizing the total potential energy functional. The Ritz method seeks the solution for the displacement field in the form of series of arbitrary approximate functions that satisfy the essential boundary conditions. The Ritz method can be used both for linear instability analyses [12,14,25,27,28,44] and for nonlinear buckling and postbuckling studies [22,28,44]. The major advantage of the Ritz method over other analytical and semi-analytical solutions is its flexibility with respect to geometry. Most of the discussed analytical and approximate solutions have been used to study through-the-width delaminations only, while, using the Ritz method embedded delaminations with more complicated shapes such as circular[25] and elliptical [12,14,44] shapes have been modeled as well. Using a piecewise integration scheme Ovesy et al[27] could expand the applicability of the Ritz method to modeling the buckling behavior of panels with arbitrarily shaped delaminations.

Besides the discussed analytical and semi-analytical methods, numerical methods and majorly the finite element method have been vastly used to investigate the buckling and postbuckling of plates containing one or multiple delaminations. The major advantage of the Finite Element Method (FEM) is its flexibility to accommodate any geometrical feature and continuum models (shell, layerwise, or solid). Besides FEM, other numerical approaches such as finite difference [43] and finite strip [38] solutions have also been used for delamination buckling studies.

1.2.4 Delamination growth

The ultimate goal in delamination buckling and postbuckling studies is determining the possibility of a buckling-driven delamination propagation. Technically the borders of a delaminated region are crack tips where damage may accumulate and lead to the propagation of the delamination. In the majority of the research works conducted on buckling-driven delamination growth, the possibility of the growth is determined by employing fracture or damage mechanics, and through the calculation of strain energy release rates.

On occasions when a closed-form expression for the strain energy of the structure is available, the Strain Energy Release Rate (SERR) can be calculated as the first derivative of the strain energy expression with respect to the length of the delaminated region[3]. In more general cases where a closed-form solution is not available, Crack Extension Techniques (CETs) have been employed for calculating SERR. The CETs work based on the assumption that a crack grows in a self-similar manner. The CETs determine the total strain energy release rate as the difference between the strain energy of the plate before and after an infinitesimal advancement of the crack front per unit surface area of the newly debonded region. The CET has been used in both one-dimensional [3,6,9] and two-dimensional [40,44,61] analyses. An exception to using a self-similar growth of a crack when using CET is the work of Wang et al [62]. They assumed that a circular delamination would grow into an elliptical shape and hence they accounted for the shape change that may occur in the process of the propagation of an existing delamination. There are two downsides associated with this method which are the self-similar delamination propagation assumption and its incapability of determining the contribution of each fracture mode in the delamination propagation.

Another approach that has been widely used for SERR calculation, is the path independent J-integral method [5,13,17,18]. In buckling-driven delamination analyses, the J-integral method has been only used in one-dimensional analyses and it is incapable of determining the contribution of different fracture modes.

In virtually all analytical and approximate solutions proposed for buckling and postbuckling problem in delaminated plates, the technique used for crack growth analysis is incapable of determining the contribution of the three fracture modes. An exception to this common shortcoming is the work of Chai [63] for thin debonded layers. Through combining thin plate solutions with crack tip elasticity results Chai developed a formulation capable of finding the distribution of SERR for the three fracture modes.

A more powerful technic for energy release rate calculation is the Virtual Crack Closure Technique (VCCT) which is almost exclusively used in conjunction with FEM [46,47,59,60]. The VCCT works on the basis of the assumption that the energy required to close a crack is equal to the energy required to make the crack grow. Using VCCT the contribution of each fracture mode in delamination growth is determinable.

Another family of techniques that have been exclusively used in conjunction with FEM [33,58,64] is the Cohesive Zone models (CZMs). CZM is a crack assessment approach based on

damage mechanics which works by assigning a decohesive constitutive equation to the plane of the propagation of the crack.

1.2.5 Contact

Depending on the buckling mode shape, the contact between delamination surfaces may be of great importance, and failing to incorporate it may lead to erroneous results [54]. Contact effects are mostly included in nonlinear FE buckling and postbuckling analyses [9,15,31,32,35,46–48,55,56,65] using algorithms such as Lagrange multiplier or penalty function methods. To avoid using complicated nonlinear contact algorithms, Sheinman et al [20] imposed controlled imperfections to their geometrical model and avoided unwanted self-penetrating mode shapes. Ning et al [45] used a creative approach and through a preliminary contact analysis could simulate the effect of contacting surfaces by fictitious springs and regarded the nonlinear problem as an eigenvalue problem. The effect of contacting surfaces has also been accounted for in some of the research works conducted using the Ritz method by assuming linear fictitious springs at the contacting regions [22,24,25,27]. Hosseini et al [33] used a modified CZM capable of accommodating contact effect in the delaminated zone to prevent the interpenetration of the touching surfaces of the delaminated sublayers.

1.2.6 Nonlinear solver

Nonlinear systems of algebraic equations are almost exclusively solved using iterative solutions. The most commonly used iterative methods are:

- Picard Iteration method (Direct iteration method),
- Newton-Raphson iteration method,
- Rik's and Modified Rik's methods

Amongst the mentioned methods Picard iteration method has the slowest convergence rate and is notorious for leading to diverged solutions. The most popular approach in solving nonlinear algebraic equations is adopting different variations of Newton's method [24,25,42,66]. However, the applicability of Newton's method is limited by the emergence of critical points close to which the tangent matrix becomes singular or ill-conditioned. Therefore in problems involving postbuckling phenomena such as snap-through or snap-back Newton's method is incapable of tracing the equilibrium path beyond the critical point. In order to trace the path of equilibrium past

the point of instability, a system of nonlinear equations can be solved using Rik's method also known as the Arc-length method. Rik's method by searching the solution at a definite distance from a previously determined equilibrium point can trace the entirety of the equilibrium path. Applying Rik's method requires changing the dimensions of matrices representing the nonlinear algebraic system of equations. To avoid complications arising from the alteration of matrices, modified Rik's method which base the iterative solution on the original matrices are more commonly used [67,68].

1.3 Objectives

The current thesis is inspired by the challenges that the aerospace industry faces in adjusting the design allowable of laminated composite plates having minor interlaminar defects. The High cost of preventing minor (micro) delamination makes designing based on damage tolerance an inevitable and integrated part of designing with composite materials[69]. Designing base on damage tolerance philosophy and keeping composite plates with potential delaminations in service requires an in-depth insight into their behavior especially under compressive loading where delaminations are prone to grow.

Such knowledge can be acquired using multipurpose FEM software packages. However, there are certain drawbacks to using these tools namely their significantly higher time computational costs compared to those of analytical and approximated solutions especially in problems concerning fracture mechanics where extra precautions in meshing are required. Furthermore using commercial software packages impose limitations with regard to implementing innovative and appropriate techniques for addressing the specific nature, mechanistic requirements and characteristics of the involved phenomena where an analytical solution can be tailor-made for the specific conditions of a problem.

Despite the vast number of research works dedicated to the buckling and postbuckling behavior of delaminated composite plates, neither of the previously developed analytical methodologies provide adequate information for determining the possibility of the growth of a delamination. The majority of the existing formulations are derived using a common partitioning scheme that regards the intact regions outside the borders of a delamination as an ESL and therefore, fail to detect the

highly localized effects in the vicinity of theses borderlines. Having missed these crucial pieces of information, these formulations remain incapable of incorporating fracture mechanics to provide a definitive assessment of the possibility of the growth of a delamination. Furthermore, the assumed displacement fields in these works suffer slight yet important inconsistencies that can lead to a lack of accuracy in the predicted deformations especially in the vicinity of the edges of a delaminated region.

The objective of this thesis is to develop a comprehensive mathematical and mechanical methodology for accurately predicting the buckling and postbuckling behavior of delaminated composite plates including the fracture mechanical phenomenon involved in the postbuckling state. Besides predicting the overall behavior of a plate under compressive loading the fulfillment of this main objective requires proposing models and formulations capable of capturing highly localized deformation gradients and interlaminar stresses near the edges of a delaminated region. Access to these highly localized deformations and stress distributions sets the ground for incorporating fracture mechanics into the methodology and addressing delamination growth.

The principal objective as explained can be broken down to sub-objectives summarized below:

- Determine buckling critical load and mode shapes of delaminated plates,
- Predict postbuckling behavior of delaminated plates including the deformations and load-deformation correlation,
- Determine interlaminar tractions in the plane of a delamination,
- Calculate Strain Energy Release Rates (SERRs) along the edges of delamination.

1.4 Organization of the manuscript based dissertation

This manuscript based dissertation has been prepared in compliance with the "Thesis Preparation and Thesis Examination Regulation" booklet of the School of Graduate Studies of Concordia University. This dissertation contains seven chapters, including an introduction, four chapters addressing the objective of the thesis, and a final chapter dedicated to the overall conclusions of the thesis and suggestions for future works. Chapter 1 provides an introduction to the problem being addressed and through an extensive literature survey explains the significance of the objective of the thesis work. Chapters 2-4 and 6 present the new developments done to fulfill the objective of the thesis in the form of 4 complete journal articles. Chapter 5 introduces a unified

methodology based on the developed linear and nonlinear buckling and postbuckling solutions. The developments presented in chapter 2 is a linear buckling solution that can be used for determining the buckling mode (local, mixed, global) of a delaminated plate. The buckling mode is used for determining the imperfections necessary in nonlinear postbuckling solutions presented in chapters 3 and 4. In chapter 3 a nonlinear solution is formulated for predicting the postbuckling behavior of delaminated plates. The developed formulation is capable of predicting the distribution of interlaminar tractions in the plane of an assumed delamination, however, it lacks the means for addressing the fracture mechanics aspect of the problem. To complement the findings of chapter 3, in chapter 4 a complete methodology based on similar principles is developed which has the advantage of addressing the fracture mechanics involved in the postbuckling state and can yield the SERRs along the crack tips. Chapter 5 describes the interconnection between the linear solution of chapter 2 and the postbuckling solutions presented in the two following chapters. The linear buckling solution presented in chapter 6 is the first step in developing a buckling and postbuckling methodology for curved laminated plates. The developments of the other pieces of the curved shell methodology are recommended as a topic for potential future research works. The linear buckling solution presented in chapter 6 serves the same purpose in the context of the stability of curved laminates as the solution presented in chapter 2 in the context of stability of flat plates.

And finally, chapter 6 summarizes the conclusions of the entire research and offers suggestions for future works that may be undertaken to complement the achievements of the current research. The articles constituting chapters 2-4 and 6 that are extracted through different stages of the research are either published or submitted to peer-reviewed journals. The contents of these articles are briefly summarized below:

Chapter 2: Nima Shabnijafroudi, Rajamohan Ganesan, “Influence of in-plane constraints on the prebuckling and buckling responses of laminated composite plates” under review in Acta Mechanica

This article presents an eigenvalue buckling solution based on a calculated prebuckling stress field. Generally, the presence of in-plane constraints renders the prebuckling stress field nonuniform and biaxial. This nonuniformity that was majorly overlooked in earlier researches can have a drastic effect on both the instability threshold and buckling mode shape of a plate. In this

article, by proposing a two-step solution these effects are accounted for and a realistic picture of the instability phenomenon of laminated composite plates is provided. The presented technique is applicable for investigating the behavior of individual plates as well as debonded films. In the context of the instability of delaminated composite plates, the linear buckling analysis serves the purpose of determining the buckling mode shape of plates (local, mixed, global). Based on the determined mode shape the shape of the initial imperfection to be considered in postbuckling analyses can be determined.

Chapter 3: Nima Shabaniafroudi, Rajamohan Ganesan "A penalty function based delamination model for postbuckling analysis of composite plates with delamination" Composite Structures 2020.

In this article, a novel methodology for determining the buckling and postbuckling behavior of composite plates containing a delaminated region is presented. The new model is developed based on a nonlinear formulation capable of capturing high rotations involved in a postbuckling state. The major contribution of this article is proposing a model for remedying inherent inconsistencies of earlier works as well as offering insight into the interlaminar tractions in the plane of the delamination. The model uses a penalty function method for modeling delamination and through that provides access to the said interlaminar tractions. Furthermore, to address the local deformations that can be expected in problems involving delaminations a modification to the original Ritz method is proposed.

Chapter 4: Nima Shabanijafroudi, Rajamohan Ganesan "A new methodology for buckling, postbuckling and delamination growth behavior of composite laminates with delamination" Accepted for publication by Composite Structures with minor editorial revisions.

This article by employing fracture mechanics complements the development of chapter 3 and addresses the ultimate objective of the dissertation which is proposing a formulation capable of assessing the state of the crack tip. The model uses a new partitioning scheme in conjunction with a penalty function method for modeling a plate with a delamination. The new model sets the ground for calculating the strain energy release rate through Irwin's crack closure integrals. The developed formulation for postbuckling analysis was verified through the comparison of its results with experimental data taken from the literature. The applicability and precision of the SERR calculation approach were examined by comparing the results with FEM results obtained using VCCT.

Chapter 6: Nima Shabaniafroudi, Said Jazouli, Rajamohan Ganesan "Effect of rotational restraints on the stability of curved composite panels under shear loading" Acta Mechanica. 231, 1805–1820 (2020).

In this article, as a first step in extending the applicability of the developed methodology to curved delaminated panels, a formulation for predicting the instability characteristics of thin composite laminates with rotationally restrained edges is presented. The presented methodology offers insight into the buckling behavior of composite laminates through an eigenvalue buckling analysis. The developed formulation can be used for determining the instability threshold and buckling mode shapes of individual composite plates as well as delaminated films. This information can then be used for determining the buckling mode (local, mixed, or global) of a delaminated curved panel.

The figures in each of the articles introduced above have similar formatting, however as these articles are either published or in publication, to remain loyal to the original published articles, no uniform formatting is imposed on the figures of different chapters.

Chapter 2: Influence of in-plane constraints on the prebuckling and buckling responses of laminated composite plates

2.1 Introduction

The proven advantages of laminated composite plates have led to their ever-increasing industrial use. Due to complications that may arise after instability, often composite structures are designed to work in fully stable conditions. Therefore, one of the major criteria in designing composite structures is their buckling strength. Given the importance of determining the stability characteristics of composite plates, tremendous attention has been paid to the study of the buckling problem of these plates.

Essentially, buckling is a large deformation (nonlinear) phenomenon that is often approached through a linear eigenvalue problem. Based on the assumption that the membrane stress-resultant field remains unchanged at the instance of instability, the eigenvalue buckling analysis utilizes a previously known prebuckling membrane force field to generate a linearized formulation. This necessitates an accurate assessment of the prebuckling state. Considering the complexity of calculating the prebuckling stress resultants, in the majority of the published articles, it has been conveniently assumed that the distribution of stress resultants is uniform [52,70–74]. The assumption of uniform stress-resultant field implicitly indicates that no in-plane restraining boundary conditions are considered. For the cases of thermal buckling [75], the uniformity of stress resultants would also imply that the temperature field, as well as the thermal expansion coefficient, is assumed to be uniform. There have been works in which non-uniform distributions for the prebuckling membrane forces have been considered, however, the non-uniformity has been due to phenomena other than in-plane constraints. Examples of these basically variable stress resultant distributions are cases with non-uniform application of boundary tractions [51,76], arbitrarily assumed stress distributions [77], or material property heterogeneity [78,79]. The common aspect of all these works is a priori known or obtainable stress resultant field.

Most of the attempts made to incorporate the real in-plane stress field instability analyses involve non-uniformities caused by tow angle variations. Gurdal et al [79] used the Ritz method to investigate the effect of stiffness variation on the buckling response of variable tow laminates. They based their buckling analysis on a stress resultant field that was obtained by solving the governing partial differential equation of the in-plane elastic case using a general-purpose software package. Raju et al [80] studied the buckling of variable angle tow plates based on a calculated prebuckling stress field. They used a stress function formulation to derive the governing prebuckling equations and solved them numerically using the differential quadrature method. Wu

et al [81] also tackled the buckling problem of variable angle tow plates. They used the Ritz method for determining the prebuckling stress state. They used the Ritz method to minimize the complementary total energy expression of a plate derived in terms of a stress function. Broderick et al [82] applied the stress function based Ritz method to the buckling analysis of stiffened panels. The formulations developed in terms of stress functions use the total complementary energy as the governing functional. Thus, the essential boundary conditions to be satisfied through the selection of proper approximate functions are the stress boundary conditions. Most of the analyses carried out using stress functions involve solely balanced laminates with no shear-stretching coupling. Furthermore, these solutions are only applied to a specific category of problems involving shear free-boundary conditions.

Apart from the assumed prebuckling state, the existing buckling methodologies differ in the treatment of laminates, boundary conditions, and solution methods. In the study of thin to moderately thick laminates, the most common approach is regarding laminates as an equivalent single layer (ESL). The simplest and most easily applied ESL is the classical laminated plate theory (CLPT) [73,74,78,79]. The CPLT is notorious for overestimating the critical buckling load for relatively thick laminates. As a remedy to this problem, first-order [52,83–85] and higher-order [86–88] Shear deformation theories have been used. Apart from the well-known shear deformation theories, more sophisticated distribution functions [89,90] have also been used to improve the accuracy of buckling analyses.

The solution methods may be classified in the three major categories of analytical [70,91], approximate [51,73,74,77,92,93] and numerical [68,75,89,94–97] solutions. The Ritz method, which belongs to the category of approximate solutions, is probably the most widely used approach in the context of the instability of composite plates.

In spite of the vast studies carried out on the buckling of composite plates, little attention has been paid to the effect of in-plane constraints. The present work aims to incorporate the effect of these constraints by addressing the prebuckling elasticity problem and bases the eigenvalue buckling analysis on a calculated in-plane stress field. In the entirety of this work, the FSDT is used for modeling laminates and both elasticity and stability equations are obtained using the Ritz method. In employing the Ritz method approximate functions corresponding to a specific set of boundary conditions were used, however, in deriving the formulation no restrictive assumptions have been made and the formulation is applicable to any arbitrary boundary conditions.

2.2 Theoretical formulation

In the current work, a two-step solution is used for studying the buckling behavior of laminated composite plates subjected to in-plane constraints. The first step constitutes solving the in-plane elasticity problem in order to find the distribution of the stress resultants and in the second step, the findings of the first steps are used for obtaining the linear stability equations. In both steps, the laminate is modeled using the FSDT and the solution is obtained using the Ritz method.

In the subsequent sections, first, the kinematics and the constitutive equations are presented and next, the details of each of the aforementioned two steps are explained.

2.2.1 Kinematics

In the FSDT, the in-plane displacements are assumed to vary linearly in the thickness of a laminate, and the out-of-plane displacement is assumed to be a function of the in-plane coordinates only. The distribution field is mathematically expressed as:

$$u = u_0(x, y) + z\varphi_x \tag{2.1}$$
$$v = v_0(x, y) + z\varphi_y \tag{2.2}$$
$$w = w_0(x, y) \tag{2.3}$$

where x and y are coordinates in a Cartesian coordinate system parallel to the plate edges, u and v are the in-plane displacements in x and y respectively, w is the out-of-plane displacement, and ϕ_x and ϕ_y are the rotations of the cross-section about y and x-axes respectively. The variables denoted by $_0$ are the displacements associated with the mid-plane of the laminate.

Given the aforementioned displacement distribution, the infinitesimal mid-plane strains and curvatures of a laminate are expressed in terms of the displacements as:

$$\{\epsilon\} = \begin{Bmatrix} \varepsilon_x^0 \\ \varepsilon_y^0 \\ \gamma_{xy}^0 \\ k_x \\ k_y \\ k_{xy} \end{Bmatrix} = \begin{Bmatrix} \dfrac{\partial u_0}{\partial x} \\ \dfrac{\partial v_0}{\partial y} \\ \dfrac{\partial u_0}{\partial y} + \dfrac{\partial v_0}{\partial x} \\ \dfrac{\partial \varphi_x}{\partial x} \\ \dfrac{\partial \varphi_y}{\partial y} \\ \dfrac{\partial \varphi_y}{\partial x} + \dfrac{\partial \varphi_x}{\partial y} \end{Bmatrix} \tag{2.4}$$

The transverse shear strains to be incorporated in the shear deformation theory are defined as:

$$\{\Gamma\} = \begin{Bmatrix} \gamma_{yz} \\ \gamma_{xz} \end{Bmatrix} = \begin{Bmatrix} \dfrac{\partial v}{\partial z} + \dfrac{\partial w}{\partial y} \\ \dfrac{\partial u}{\partial z} + \dfrac{\partial w}{\partial x} \end{Bmatrix} \tag{2.5}$$

Taking the assumptions of Eq. (2.3) into consideration, Eq. (2.5) can be rewritten in the form:

$$\{\Gamma\} = \begin{Bmatrix} \gamma_{yz} \\ \gamma_{xz} \end{Bmatrix} = \begin{Bmatrix} \varphi_y + \dfrac{\partial w_0}{\partial y} \\ \varphi_x + \dfrac{\partial w_0}{\partial x} \end{Bmatrix} \tag{2.6}$$

Given the large-rotation nature of the buckling phenomenon, a nonlinear definition of strains that is capable of accommodating large rotation effects is required. Here Von Karman's approximations are used as complementary nonlinear terms for obtaining the mid-plane strains due to the out-of-plane deflection. The additional nonlinear terms introduced by these approximations are:

$$\{\epsilon'\} = \begin{Bmatrix} \varepsilon_x' \\ \varepsilon_y' \\ \gamma_{xy}' \end{Bmatrix} = \begin{Bmatrix} \dfrac{1}{2}\left(\dfrac{\partial w_0}{\partial x}\right)^2 \\ \dfrac{1}{2}\left(\dfrac{\partial w_0}{\partial y}\right)^2 \\ \dfrac{\partial w_0}{\partial x}\dfrac{\partial w_0}{\partial y} \end{Bmatrix} \tag{2.7}$$

2.2.2 Constitutive equations

In an FSDT, the relationship between the generalized strain vector (vector of strains and curvatures) and stress and moment resultants is given as:

$$\begin{Bmatrix} N \\ \mathrm{M} \end{Bmatrix} = \begin{bmatrix} [A] & [B] \\ [B] & [D] \end{bmatrix} \{\epsilon\} \tag{2.8}$$

where N and M are the vectors of stress and moment resultants respectively and are expressed as:

$$\begin{Bmatrix} N_x \\ N_y \\ N_{xy} \\ M_x \\ M_y \\ M_{xy} \end{Bmatrix} = \int_{-h/2}^{h/2} \begin{Bmatrix} \sigma_x \\ \sigma_y \\ \tau_{xy} \\ z\sigma_x \\ z\sigma_y \\ z\tau_{xy} \end{Bmatrix} dz \tag{2.9}$$

The elements of the stiffness or the so-called ABD matrix are:

$$\left(\mathrm{A_{ij}}, \mathrm{B_{ij}}, \mathrm{D_{ij}}\right) = \int_{-h/2}^{h/2} \overline{Q}_{i,j}(1, z, z^2) dz \tag{2.10}$$

where $\bar{Q}_{ij}$ are the elements of the transformed plane stress stiffness matrix of each ply in a reference coordinate system.

The constitutive equation which describes the relationship between the out-of-plane shear stress resultants and shear strains reads as:

$$\begin{Bmatrix} Q_x \\ Q_y \end{Bmatrix} = [H]\{\Gamma\} \tag{2.11}$$

where Q_x and Q_y are the shear resultants on xz and yz planes respectively and H is the shear stiffness matrix. The shear stress resultants are expressed as:

$$\begin{Bmatrix} Q_{xz} \\ Q_{yz} \end{Bmatrix} = \int_{-h/2}^{h/2} \begin{Bmatrix} \tau_{xz} \\ z\tau_{yz} \end{Bmatrix} dz \tag{2.12}$$

The elements of the shear stiffness matrix are obtained using the corresponding elements of the full anisotropic stiffness matrix as follows:

$$H_{\mathrm{ij}} = k_{ij} \int_{-\frac{h}{2}}^{\frac{h}{2}} \overline{C}_{i,j}\, dz \quad for \quad i = 4{,}5 \tag{2.13}$$

where $\mathrm{k_{ij}}$ are shear correction factors and $\mathrm{C_{ij}}$ are the elements of the complete anisotropic stiffness matrix of the ply material.

The FSDT assumptions lead to a constant shear stress distribution in the thickness of a laminate which violates the condition of traction-free top and bottom surfaces. This inconsistency generates excessive stiffness, especially for relatively thick laminates. To alleviate this problem, the shear correction factors are introduced to the shear stiffness matrix. Unlike isotropic materials, no single optimum value can be prescribed for layered composite materials and the correction factors need to be calculated for each laminate separately. However, to avoid the complexity of obtaining a customized shear correction factor, in most of the published works in the field of the instability of composite plates, the values prescribed for isotropic materials are used[51,52,87,98,99]. In this work a correction factor of 2/3 was used and later through the validation process, it is shown that the generated results with this correction factor are satisfactory.

2.2.3 Prebuckling analysis

In order to calculate the prebuckling distribution of membrane forces, the in-plane elasticity problem needs to be addressed in the first step. Here the solution to the elasticity problem is obtained using the Ritz method which is a variational method based on the stationary total potential energy principle. The general expression of the total potential energy for a plate subjected to external forces reads as:

$$\Pi = U + W \tag{2.14}$$

where U is the strain energy stored in the plate and W is the potential energy of the applied forces.

The strain energy of a plate is given by:

$$U = \frac{1}{2}\left\{\iint \{\epsilon\}^T \begin{bmatrix}[A] & [B]\\ [B] & [D]\end{bmatrix}\{\epsilon\}dA + \iint \{\Gamma\}^T[H]\{\Gamma\}dA\right\} \tag{2.15}$$

For symmetrically stacked laminates subjected to in-plane forces only, no out-of-plane deflections are expected. Thus the strain energies corresponding to bending and out-of-plane shearing vanish and the expression for strain energy can be reduced to:

$$U = \frac{1}{2}\left\{\iint \begin{Bmatrix}\varepsilon_x^0\\ \varepsilon_y^0\\ \gamma_{xy}^0\end{Bmatrix}^T [A] \begin{Bmatrix}\varepsilon_x^0\\ \varepsilon_y^0\\ \gamma_{xy}^0\end{Bmatrix} dA\right\} \tag{2.16}$$

where $[A]$ is the in-plane stiffness matrix.

The general form of the potential energy of boundary forces is:

$$W = -\oint \vec{N} \cdot \vec{u}\, ds \tag{2.17}$$

where $\vec{N}$ the traction vector on the boundary and $\vec{u}$ is the displacement vector.

For the special case of a rectangular plate of dimensions *a* and *b* under biaxial distributed loading Eq. (6.15) transforms to:

$$W = -\int_0^b (N_x^* u)_{x=0,a}\, dy - \int_0^a (N_y^* v)_{y=0,b}\, dx \tag{2.18}$$

where N_x^* and N_y^* are distributed loads applied on the edges of the plate

The Ritz method approximates the displacements in the form of a series of separable functions as follows.

$$\begin{aligned} w_0 &= \sum_{m=1}^{I}\sum_{n=1}^{J} W_{mn} W_m^x W_n^y \\ u_0 &= \sum_{m=1}^{I}\sum_{n=1}^{J} U_{mn} U_m^x U_n^y \\ v_0 &= \sum_{m=1}^{I}\sum_{n=1}^{J} V_{mn} V_m^x V_n^y \\ \varphi_x &= \sum_{m=1}^{I}\sum_{n=1}^{J} \Phi_{mn} \Phi_m^x \Phi_n^y \\ \varphi_y &= \sum_{m=1}^{I}\sum_{n=1}^{J} \Psi_{mn} \Psi_m^x \Psi_n^y \end{aligned} \tag{2.19}$$

where $W_m^x, W_n^y, U_m^x, U_n^y, V_m^x, V_n^y, \Phi_m^x, \Phi_n^y, \Psi_m^x,$ and Ψ_n^y are arbitrary functions that satisfy the essential boundary conditions of a specific problem and W_{mn}, U_{mn}, V_{mn}, Φ_{mn}, and Ψ_{mn} are the unknown coefficients to be determined. The Ritz approximate functions are required to be complete and capable of accommodating any possible deflected shape of the plate and must be linearly independent and have derivatives up to half the order of the corresponding partial differential equation [100].

Substituting Eq. (2.19) in Eqs. (2.18) and 2.16) and subsequently, in Eq. (2.14), the expression of total potential energy in terms of the approximate functions is obtained. The variables in the latter equation would be the coefficients W_{mn}, U_{mn}, V_{mn}, Φ_{mn}, Ψ_{mn}. Having obtained the expression of total potential energy in terms of these coefficients, the principle of stationary potential energy

will be applied by minimizing this expression with respect to these variables. The minimization leads to a system of linear equations as follows:

$$\frac{\partial \Pi}{\partial W_{mn}} = 0,\ \frac{\partial \Pi}{\partial U_{mn}} = 0,\ \frac{\partial \Pi}{\partial V_{mn}} = 0,\ \frac{\partial \Pi}{\partial \Phi_{mn}} = 0,\ \frac{\partial \Pi}{\partial \Psi_{mn}} = 0 \tag{2.20}$$

The coefficients W_{mn}, U_{mn}, V_{mn}, Φ_{mn}, and Ψ_{mn} for the linear prebuckling state are determined by solving the system of equations. Substituting the calculated coefficients in Eq.(2.19), the displacements of the plate under the applied in-plane loading are calculated. Substituting the obtained displacement functions in Eq.(2.4) and subsequently in Eq.2.8), the expressions for the prebuckling stress resultants are obtained:

$$\begin{aligned}
N_x^0 = \sum_{m=1}^{I}\sum_{n=1}^{J}\Big[&A_{11}U_{mn}^0 U_{x,x}^m U_y^m + A_{12}V_{mn}^0 V_x^m V_{y,y}^n \\
&+ A_{16}\left(U_{mn}^0 U_x^m U_{y,y}^n + V_{mn}^0 V_{x,x}^m V_y^n\right) + B_{11}\Phi_{mn}^0 \Phi_{x,x}^m \Phi_y^n \\
&+ B_{12}\Psi_{mn}^0 \Psi_x^m \Psi_{y,y}^m + B_{16}\left(\Phi_{mn}^0 \Phi_x^m \Phi_{y,y}^n + \Psi_{mn}^0 \Psi_{x,x}^m \Psi_y^n\right)\Big] \\
N_y^0 = \sum_{m=1}^{I}\sum_{n=1}^{J}\Big[&A_{12}U_{mn}^0 U_{x,x}^m U_y^m + A_{22}V_{mn}^0 V_x^m V_{y,y}^n \\
&+ A_{26}\left(U_{mn}^0 U_x^m U_{y,y}^n + V_{mn}^0 V_{x,x}^m V_y^n\right) + B_{12}\Phi_{mn}^0 \Phi_{x,x}^m \Phi_y^n \\
&+ B_{22}\Psi_{mn}^0 \Psi_x^m \Psi_{y,y}^m + B_{26}\left(\Phi_{mn}^0 \Phi_x^m \Phi_{y,y}^n + \Psi_{mn}^0 \Psi_{x,x}^m \Psi_y^n\right)\Big] \\
N_{xy}^0 = \sum_{m=1}^{I}\sum_{n=1}^{J}\Big[&A_{16}U_{mn}^0 U_{x,x}^m U_y^m + A_{26}V_{mn}^0 V_x^m V_{y,y}^n \\
&+ A_{66}\left(U_{mn}^0 U_x^m U_{y,y}^n + V_{mn}^0 V_{x,x}^m V_y^n\right) + B_{16}\Phi_{mn}^0 \Phi_{x,x}^m \Phi_y^n \\
&+ B_{26}\Psi_{mn}^0 \Psi_x^m \Psi_{y,y}^m + B_{66}\left(\Phi_{mn}^0 \Phi_x^m \Phi_{y,y}^n + \Psi_{mn}^0 \Psi_{x,x}^m \Psi_y^n\right)\Big]
\end{aligned} \tag{2.21}$$

where coefficients denoted by the superscript ^{0} are the values obtained through the prebuckling analysis. For the sake of brevity, differentiation with respect to *x* and *y* is denoted by the subscripts $_{,x}$ and $_{,y}$ respectively. Evidently, for symmetrically stacked laminates, the terms containing elements of the B matrix vanish.

2.2.4 Linear buckling analysis

Buckling by definition is a point of instability where a second path of equilibrium becomes possible. When approaching the plate buckling problem through energy methods, a level of in-plane compressive load is sought under which even in the absence of any transversal loading an out-of-plane deflection becomes possible. The degradation of the transversal stiffness that leads to the possibility of an out-of-plane deflection occurs due to an adverse stress stiffening phenomenon. Thus in a buckling problem, the energy corresponding to stress stiffening is incorporated in the total potential energy and it is expressed as:

$$\Pi = U + V \tag{2.22}$$

where V is the stress stiffening energy and reads as:

$$V = \iint \{N^0\}^T \{\epsilon'\} dA \tag{2.23}$$

where $\{N^0\}$ is the vector of prebuckling in-plane stress resultants. The main distinction between the present work and the existing works lies in the use of a calculated stress resultant field to constitute the expression of the potential energy related to stress softening. Through the calculated stress resultant field, the effect of in-plane constraints is incorporated in the stability analysis. The components of this spatially varying stress resultant vector are determined in the prebuckling analysis through Eq. (2.19). Given the spatial nonuniformity of $\{N^0\}$, it cannot be taken out of the integral and the integration needs to be carried out on the entirety of the integrand product.

For symmetrically laminated composites, the in-plane and out-of-plane displacements are decoupled, hence the strain energy corresponding to in-plane displacements would have no effect on the eigenvalue buckling analysis. In this regard Eq.(2.13) can be rewritten in the form:

$$U = \frac{1}{2}\left\{ \int_0^a \int_0^b \begin{Bmatrix} k_x \\ k_y \\ k_{xy} \end{Bmatrix}^T [D] \begin{Bmatrix} k_x \\ k_y \\ k_{xy} \end{Bmatrix} dxdy + \int_0^a \int_0^b \{\Gamma\}^T [H] \{\Gamma\} dxdy \right\} \tag{2.24}$$

Essentially linear buckling analysis is based on the assumption that the distribution of in-plane stresses in the instance of buckling, remains similar to that of the unbuckled structure on the verge of instability. Basically, before instability, the structure is believed to experience no out-of-plane deformation. A cursory look at the nonlinear strains defined in Eq. 2.8) reveals that in the absence of out-of-plane displacements a linear behavior of the structure can be expected. Hence up to the point of instability, the stress stiffening energy is assumed to be linearly proportional to the applied forces. Therefore the total potential energy for the buckling problem can be rewritten in the form:

$$\Pi = U + \lambda V^0 \tag{2.25}$$

where V^0 is the stress stiffening energy calculated for an arbitrary level of external load and λ is a scalar to be determined? Thus minimization of the total potential energy yields:

$$\begin{aligned}
\frac{\partial U}{\partial W_{mn}} + \lambda \frac{\partial V^0}{\partial W_{mn}} = 0 \\
\frac{\partial U}{\partial U_{mn}} + \lambda \frac{\partial V^0}{\partial U_{mn}} = 0 \\
\frac{\partial U}{\partial V_{mn}} + \lambda \frac{\partial V^0}{\partial V_{mn}} = 0 \\
\frac{\partial U}{\partial \Phi_{mn}} + \lambda \frac{\partial V^0}{\partial \Phi_{mn}} = 0 \\
\frac{\partial U}{\partial \Psi_{mn}} + \lambda \frac{\partial V^0}{\partial \Psi_{mn}} = 0
\end{aligned} \tag{2.26}$$

Rearranging these equations in the matrix form we will have

$$[K + \lambda K_s] \begin{Bmatrix} \{W_{mn}\} \\ \{U_{mn}\} \\ \{V_{mn}\} \\ \{\Phi_{mn}\} \\ \{\Psi_{mn}\} \end{Bmatrix} = \{0\}_{5IJ} \tag{2.27}$$

where $[K]$ is the matrix composed of the first terms in Eqs. (3.26) and $\lambda[Ks]$ is the matrix composed of the second terms of the same system of equations.

In the absence of the potential energy of transversely applied forces, this system of equations has a trivial solution. By multiplying Eq. (2.27)by K^{-1} and dividing it by λ, we will have:

$$\left[K^{-1}K_s + \frac{1}{\lambda} I\right] \begin{Bmatrix} \{W_{mn}\} \\ \{U_{mn}\} \\ \{V_{mn}\} \\ \{\Phi_{mn}\} \\ \{\Psi_{mn}\} \end{Bmatrix} = \{0\}_{5IJ} \tag{2.28}$$

Eq. (2.28) is a classical eigenvalue problem and the largest eigenvalue of the matrix $K^{-1}K_s$ will give the smallest λ that makes the structure unstable and is known as the buckling coefficient. This coefficient multiplied by the applied forces N_x^* and N_y^* gives the buckling strength of the plate. The corresponding eigenvector gives the buckled shape of the plate.

2.3 Validation

In order to validate the new development, for a variety of cases the calculated results were compared with the results obtained using finite element analysis (FEA). The FEA was carried out using ANSYS commercial software and the results were used for validating both in-plane elasticity and eigenvalue buckling solutions. Both the FE and the Ritz analyses were performed using the boundary conditions depicted in Figure 2.1. The approximate Ritz functions used to satisfy the prescribed boundary conditions are presented in appendix A. The ply material properties used for all the numerical examples are E_I= 26.25 Mpsi, E_{II}=1.49 Mpsi, G_{12}=1.04 Mpsi, ν_{12}=0.28, and the ply thickness is 0.008 in

In the FEA, the 8-node, six-degree of freedom SHELL281 element with a quadratic shape function was used. The element uses a first-order shear deformation theory and is suitable for modeling moderately thick shells. In all of the analyses, mesh quality was gradually improved until mesh independence was achieved.

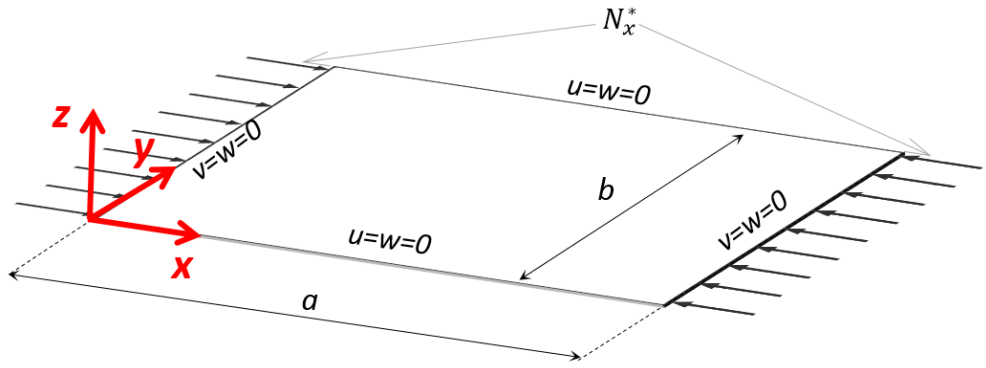

Figure 2.1 Schematic view of a rectangular plate under distributed uniaxial loading

Through comparison of the results with FEA for a variety of cases with different layup configurations and aspect ratios, it was established that an acceptable agreement in the calculated stress resultant distribution is achievable. The comparison is illustrated in Figure 2.2**Error! Reference source not found.** is obtained using a 15×150 term solution and shows an impeccable similarity in the distribution of the stress resultants for an arbitrarily selected case.

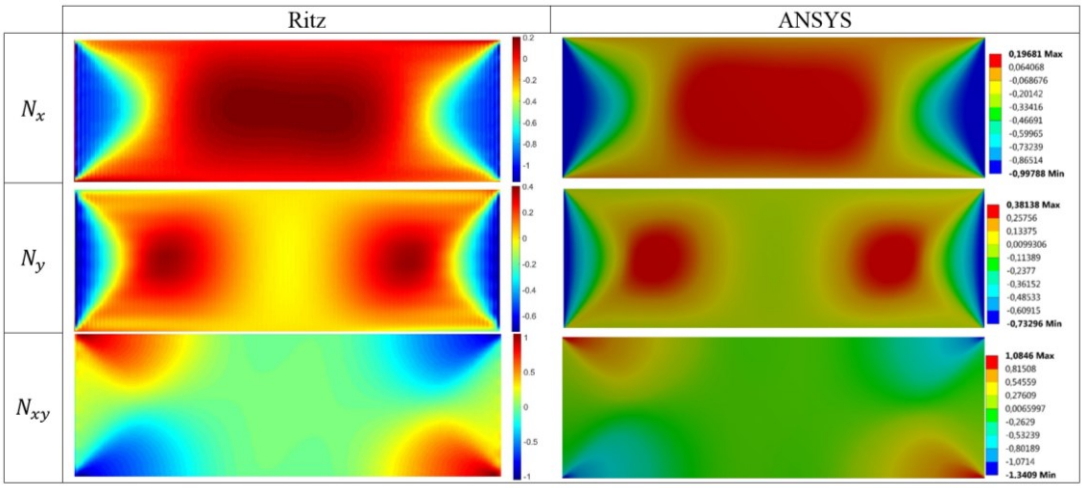

Figure 2.2 Comparison of stress resultant with ANSYS results (right column: Ritz, left column ANSYS) for a $[(\pm 45)_2/(45)]_s$ laminate with an aspect ratio of 3 under uniaxial loading in the x-direction

Table 2.1 lists critical buckling loads calculated using the developed method and FEA for a variety of stacking sequences and geometrical arrangements. The comparisons show a good agreement for the majority of cases, however, it can be observed that for larger aspect ratios the results deviate further from FEA.

Table 2.1 Comparison of critical buckling loads Ritz vs ANSYS

$[(0/90)_2/(0)]_s$ ply thickness 0.008”				
a (in)	b (in)	FEM (lb/in)	Ritz (lb/in)	Difference %
3	10	839.5	843.4	-0.5
5	10	331.8	331.0	0.3
10	10	149.7	148.6	0.7
20	10	167.4	166.1	0.8
30	10	193.9	191.4	1.3
$[(\pm 30)_2/(30)]_s$ ply thickness 0.008”				
a (in)	b (in)	FEM (lb/in)	Ritz (lb/in)	Difference %
3	10	824.2	822.4	0.2
5	10	349.7	345.5	1.2
10	10	175.7	172.5	1.8

20	10	372.3	360.1	3.4
30	10	339.8	324.7	4.6
$[(\pm 45)_2/(45)]_s$ ply thickness 0.008”				
a (in)	b (in)	FEM (lb/in)	Ritz (lb/in)	Difference %
3	10	485.3	476.0	1.9
5	10	231.7	225.8	2.6
10	10	359.4	346.0	3.9
20	10	392.1	371.5	5.6
30	10	383.2	358.3	6.9
$[(\pm 70)_2/(70)]_s$ ply thickness 0.008”				
a (in)	b (in)	FEM (lb/in)	Ritz (lb/in)	Difference %
3	10	168.8	166.2	1.6
5	10	169.7	165.6	2.5
10	10	254.8	247.1	3.1
20	10	259.1	244.5	6.0
30	10	268.0	244.5	9.6

2.4 Results and discussion

In this section, the results for both prebuckling and buckling problems are presented and discussed. In generating numerical results the same boundary conditions and ply properties as those presented in the validation section were used.

Regarding the in-plane elasticity results, the first observation was that in spite of the capability of the approximate solution to accurately estimate the deflections of a plate using a few terms, with the same number of terms, the obtained stress resultants exhibit oscillations and lack accuracy (see Figure 2.2 left). It was observed that the amplitude of the oscillations majorly depends on the aspect ratio of the panel, while the direction of the ripples depends on the direction of the application of the external forces. Figure 2.3 shows that for a uniaxial loading applied in the *x*-direction, these ripples are normal to the loading axis and the number of ripples is roughly half the number of the utilized terms. These oscillations or ripples were previously addressed by other

researchers [101,102] and some remedies were proposed for smoothening the computed stress resultants.

In the present work, instead of the proposed techniques in references [101,102], a smoother solution was achieved by increasing the number of terms in the approximate functions. When using simple polynomial functions, the number of terms is limited by the emergence of ill-conditioned matrices. The employed trigonometric functions (see appendix A) have the advantage of orthogonality which guaranties well-conditioned matrices regardless of the number of terms used. In order to control the computation size of the analyses, the number of terms to be used in each direction were selected separately based on the direction of the application of external forces and the aspect ratio. Figure 2.3 shows that for a uniaxial loading in *x*-direction to get a smooth distribution of stress resultants it is enough to increase the number of terms in *x* solely.

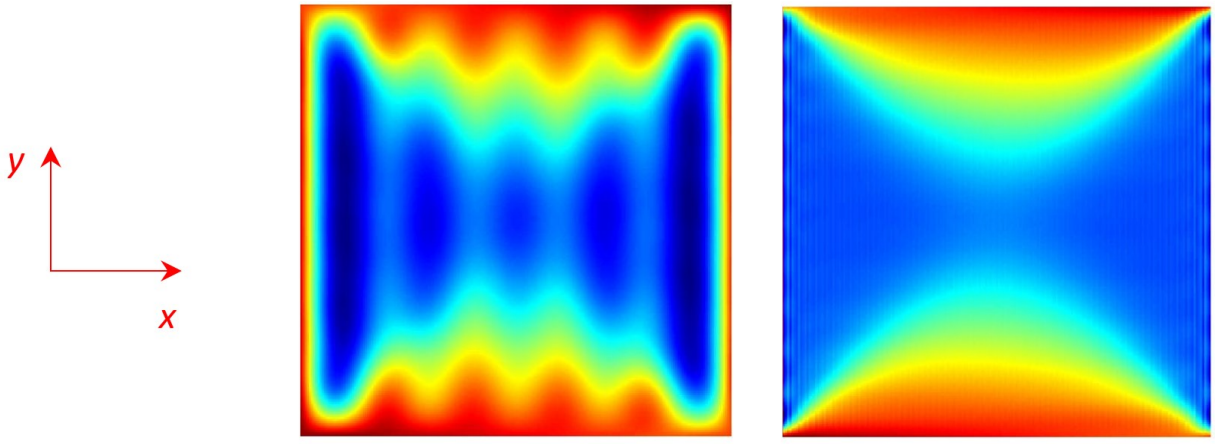

Figure 2.3 Calculated N_x for a $[(\pm 45)_2/(45)]_s$ plate under uniform loading of unity in the x-direction. Left: 10×10 terms and Right: 150×15 terms.

A closer look into the results reveals that as pointed out by other researchers [102], the obtained solutions slightly violate the expected natural boundary conditions, however, it was observed that the extent of this violation diminishes when a higher number of terms is used.

Another important observation is the biaxiality of the stress resultant field due to the existence of in-plane constraints. The biaxial stress resultant due to a uniaxial loading is reflected in Figure 2.2. It can be noticed that N_y and N_{xy} are of comparable magnitudes as N_x and may affect the buckling solution significantly.

Based on the calculated resultants, eigenvalue buckling analyses were undertaken. It was observed that the number of terms used in the in-plane elasticity analysis may significantly impact

the accuracy of the calculated critical buckling loads. Figure 2.4 shows the trend of the convergence of the calculated critical buckling load with the number of terms used in the prebuckling analysis. As it was mentioned before, for a plate under uniaxial loading, in order to eliminate the stress resultant oscillations, it is enough to increase the number of terms corresponding to the direction of the application of the external force. Therefore, the number of terms in the y-direction was kept constant at 15 and the number of terms in the x-direction (the direction of the application of the external force) was varied. These curves were produced using a symmetrical 15 terms solution for the eigenvalue buckling analysis. These convergence curves reveal that for higher aspect ratios convergence rate is remarkably slower.

The eigenvalue buckling analysis was found relatively insensitive to the number of terms of approximate functions. Figure 2.5 shows the trend of convergence of the buckling solution with the number of terms used in the eigenvalue buckling (second step) analysis. These results were obtained using a 15×50 term prebuckling solution. It can be observed that by increasing the number of terms from 5 to 22 no more than 0.5% enhancement can be achieved.

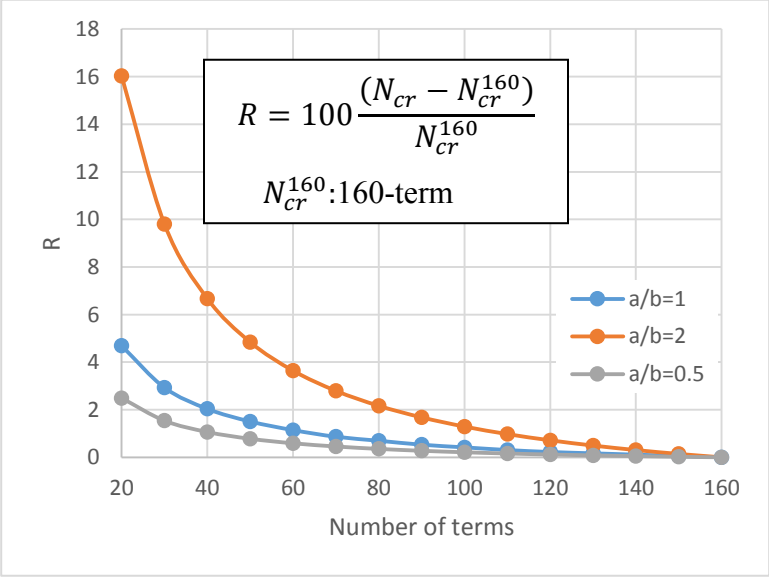

Figure 2.4 The trend of convergence with the number of terms corresponding to the prebuckling analysis (10"×10" $[(\pm 45)_2/(45)]_s$)

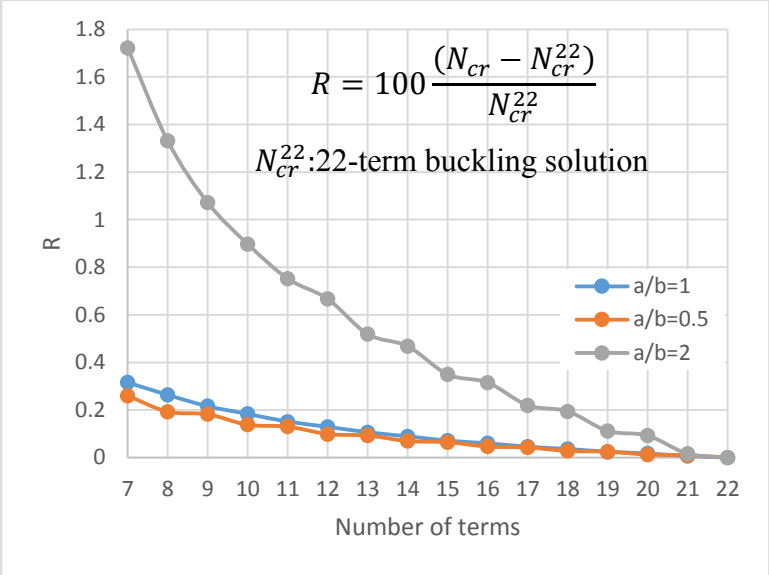

Figure 2.5 The trend of convergence with the number of terms corresponding to the eigenvalue analysis (10"×10" $[(\pm 45)_2/(45)]_s$

Figure 2.6 shows the trend of variation of buckling critical loads with aspect ratio for a variety of symmetrically laminated plates under uniaxial compressive loading. In order to present numerical results in a more insightful manner, the results are presented in terms of non-dimensional parameters. The non-dimensional parameters used to characterize the buckling behavior of laminates are defined as follows:

$$\alpha = \frac{a}{b}\left(\frac{D_{22}}{D_{11}}\right)^{1/4} \tag{2.29}$$

$$\bar{N}_x = \frac{N_x^0 b^2}{\pi^2 (D_{11} D_{22})^{1/2}} \tag{2.30}$$

where α is the nondimensional aspect ratio and $\bar{N}_x$ is the shear coefficient.

Figure 2.7 presents the same results as those in Figure 2.6 obtained by neglecting the in-plane constraints (based on a uniform stress distribution). A comparison of the buckling curves in Figure 2.6 and Figure 2.7 reveals that in general, incorporating the in-plane constraints as prescribed leads to higher buckling strengths, especially for plates with higher aspect ratios. This can be explained by taking into account the distribution of the prebuckling stress resultants. Figure 2.8 depicts a transition in the distribution of the stress resultants with the variation of aspect ratio. It can be noticed that under uniaxial loading, in plates with higher aspect ratios, a central zone with positive (tensile) stress resultants in both x and y directions develops. The stress

stiffening effect associated with these positive stress resultants increases the buckling critical load and makes the buckling mode shape relatively local. Whereas, neglecting these constraints leads to a uniform, uniaxial compressive stress resultant field.

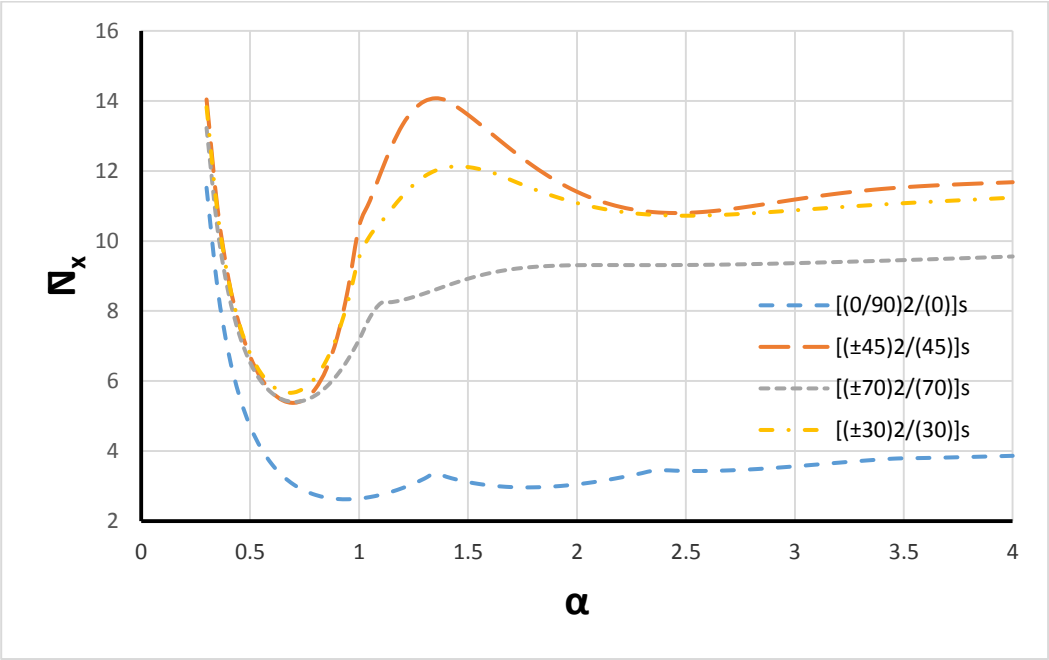

Figure 2.6 variation of non-dimensional buckling load with non-dimensional aspect ratio.

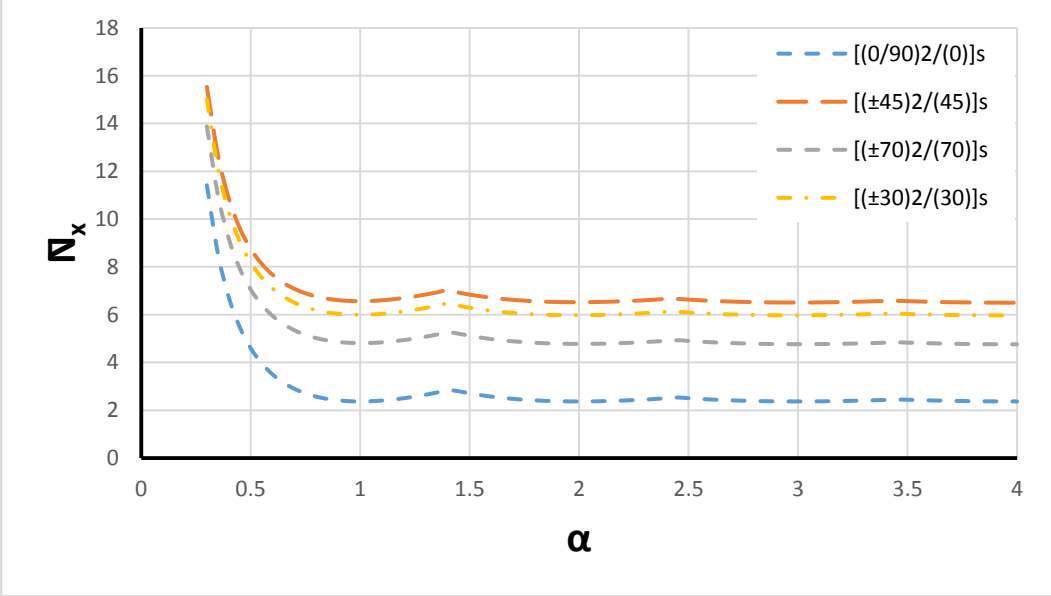

Figure 2.7 variation of non-dimensional buckling load with non-dimensional aspect ratio without consideration of in-plane constraint.

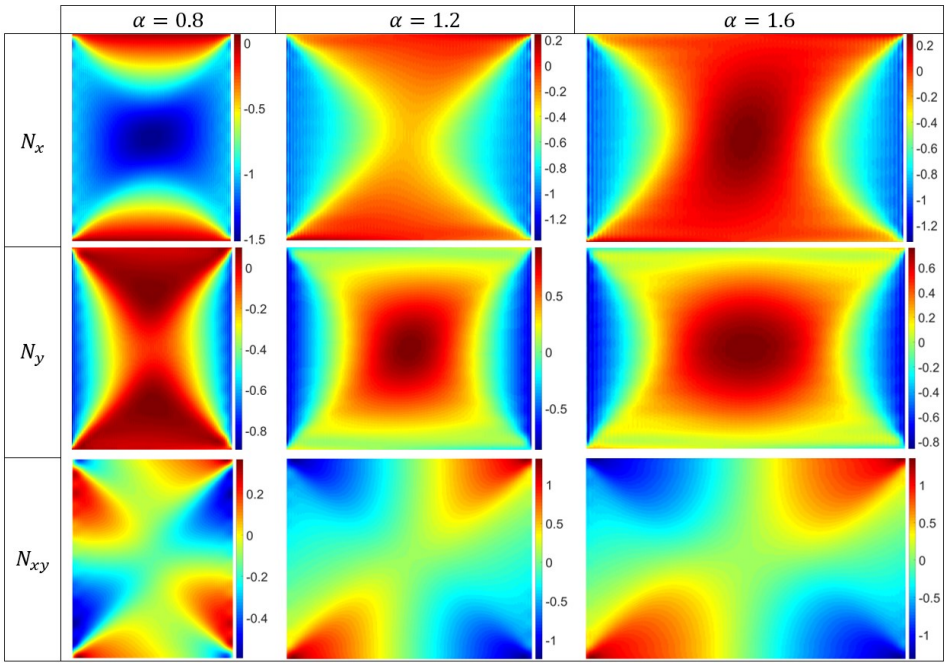

Figure 2.8 Variation of stress resultant distribution with non-dimensional aspect ratio α under uniaxial loading in the x-direction

The kink points on the curves in Figure 2.6 are the aspect ratios at which a shift in the buckling mode shape occurs. Figure 2.9 depicts the transition of buckling mode shapes for the $[(\pm 45)_2/(45)]_s$ laminate. The mode shape transition for the other $[(\pm\theta)_2/(\theta)]_s$ laminates happens in a similar manner except for the α values at which the transition takes place. The $[(0/90)_2/(0)]_s$ laminate, however, exhibits different buckling mode shape transition pattern (Figure 2.10).

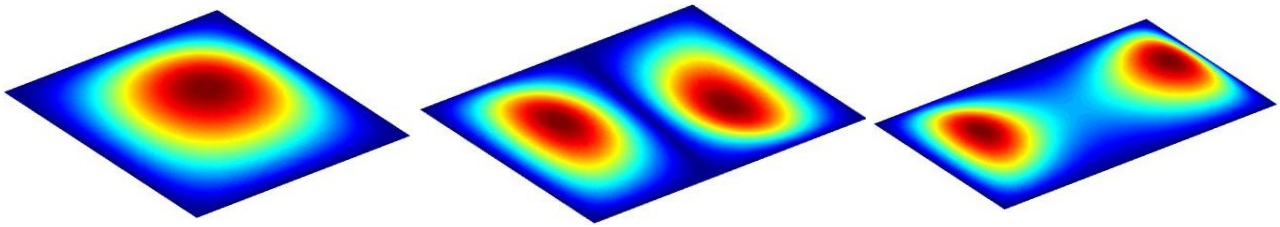

α=0.8 α=1.2 α=1.6

Figure 2.9 buckling mode shape transition with aspect ratio variations for a $[(\pm 45)2/(45)]_s$ laminate

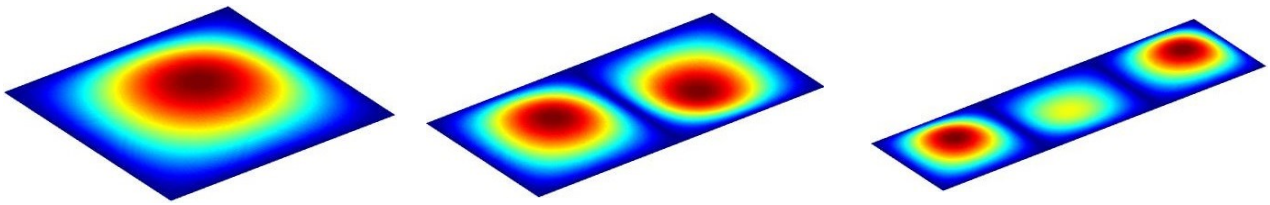

α=0.9 α=1.7 α=3

Figure 2.10 Buckling mode shape transition with aspect ratio variations a $[(0/90)2/(0)]_s$ laminate

2.5 Conclusion

The effect of introducing in-plane constraints on the buckling behavior of composite panels was investigated. In order to account for these constraints, a linear static analysis was carried out and the calculated stress resultant distribution was incorporated in the eigenvalue buckling analysis. Using the developed formulation a variety of laminates and geometric configurations were studied and the characteristic graphs were generated. Through the undertaken studies the following conclusions were drawn.

- The formulation was proved capable of generating reliable results that reflect the effect of in-plane constraints.
- The in-plane constraints severely impact the critical buckling behavior of composite plates including critical forces and mode shapes.
- Laminates with shearing-stretching coupling, seem to be more sensitive to the application of in-plane constraints.
- The stress resultants obtained in the prebuckling analysis exhibit oscillations which are normal to the direction of the external of loading and their amplitude mainly depends on the aspect ratio of the plate.
- By increasing the number of terms used in the Ritz method the inaccuracy caused by the oscillations can be controlled. Under uniaxial loading to achieve smooth distributions of stress resultants, it is sufficient to increase the number of terms in the direction of the application of the external force.
- Compared to the in-plane elasticity problem the buckling analysis is much less sensitive to the number of terms used in the Ritz method.

2.6 Appendices

2.6.1 Appendix A: Approximate functions

Trigonometric approximate functions corresponding to the boundary conditions described in Figure 2.1

$$W_x = \sin\frac{m\pi x}{a} \qquad W_y = \sin\frac{n\pi y}{b}$$

$$U_x = \cos\frac{m\pi x}{a} \qquad U_y = \sin\frac{n\pi y}{b}$$

$$V_x = \sin\frac{m\pi x}{a} \qquad V_y = \cos\frac{n\pi y}{b}$$

$$\Phi_x = \cos\frac{m\pi x}{a} \qquad \Phi_y = \sin\frac{n\pi y}{b}$$

$$\Psi_x = \sin\frac{m\pi x}{a} \qquad \Psi_y = \cos\frac{n\pi y}{b}$$

2.6.2 Appendix B: Supplementary Results with clamped boundary conditions:

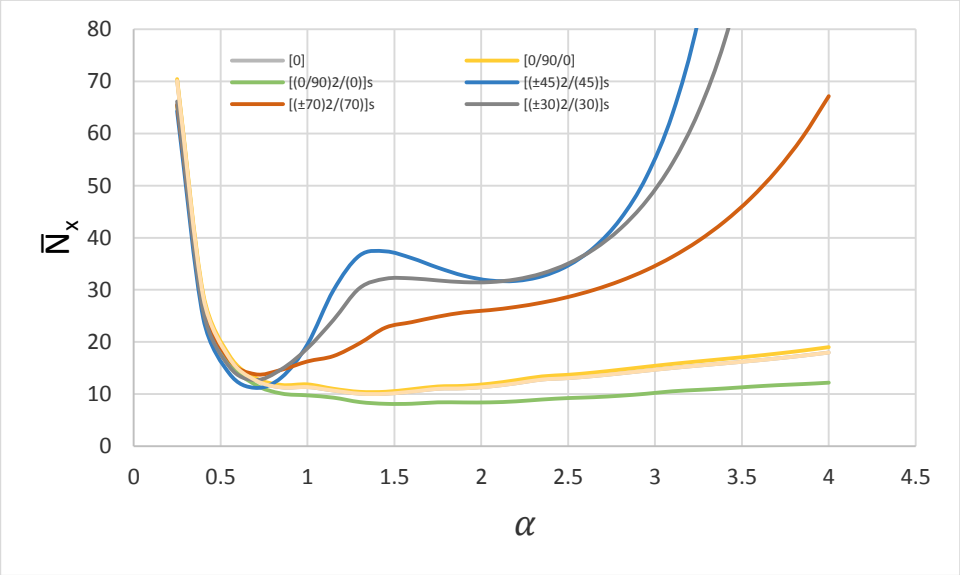

Figure 2.11 variation of non-dimensional buckling load with non-dimensional aspect ratio for a plate with clamped boundary conditions .

Chapter 3: A penalty function based delamination model for postbuckling analysis of composite plates with delamination

Nomenclature

a, b	*Dimensions of the rectangular plate*
d_x, d_y	*Dimensions of the rectangular delamination*
u, v	*In-plane displacement in x and y-direction*
u_0, v_0, w_0	*Midplane displacements*
ϕ_x	*Clockwise rotation of cross-section normal to x-axis about the y-axis*
ϕ_y	*Clockwise rotation of cross-section normal to y-axis about the x-axis*
δ	*End-shortening*
$\varepsilon_x^0,\ \varepsilon_y^0,\ \gamma_{xy}^0$	*Midplane strains*
k_x, k_y, k_{xy}	*Midplane curvatures*
N_x, N_y, N_{xy}	*Stress resultants*
M_x, M_y, M_{xy}	*Moment resultants*
U	*Strain energy*
W	*Potential energy of external forces*
U_P	*Penalty term corresponding to interlaminar adhesion*
Π	*Total Potential energy functional*
u^1, v^1, w^1	*Displacements of the interface of the bottom sublaminate*
u^2, v^2, w^2	*Displacements of the interface of the top sublaminate*

3.1 Introduction

Thanks to their outstanding mechanical and corrosion properties and lightweight, laminated composite materials have gained remarkable popularity, especially in the aerospace industry. However, despite their advantages, they are susceptible to various types of flaws among which delamination is probably the most impactful. Delaminations are partial debondings of the plies that constitute a laminate and may exist as manufacturing defects or may appear later in service due to material degradation, fatigue, or impact. Regardless of the reason for their existence, delaminations may drastically reduce the load-carrying capacity of laminates, especially under compressive loading. Delaminations pose an imbalance to symmetrically stacked laminates and promote instability. In the postbuckling regime, the distribution of strains changes, and the laminate undergoes remarkably higher levels of stresses. The elevated level of stresses in turn often leads to the growth of delaminations and the failure of structures. The critical effect of delaminations on the performance of composite structures necessitates a meticulous determination of the residual strength of delaminated composites. In the aerospace industry, the performance of laminates containing flaws is evaluated by measuring the deflections and the surface stains under compressive loading. In the present work this approach used by the industry is kept in focus and the prediction of the same measured parameters is targeted.

Given the importance of determining the residual strength of delaminated plates, their compressive response has been the subject of many studies. One of the earliest works on the buckling and postbuckling of delaminated plates was carried out by Chai et al [3]. They developed a one-dimensional analysis scheme based on a beam-column model and proceeded with calculating the energy release rate. They regarded thin, near-the-surface delaminations as a film bonded to an infinite substrate and for arbitrarily positioned (in thickness) delaminations they proposed a partitioning scheme for accommodating the geometrical discontinuity across the debonded region. Chai[63] later proposed a three-dimensional solution for investigating the state of a crack and the possibility of the propagation of the delamination. The thin-film model which was borrowed from the work of Kachanov [103] was later widely used in both one-dimensional [2,5–8] and two-dimensional [11–14,44,104,105] studies. The same scheme in conjunction with an axisymmetric formulation was used to predict the postbuckling behavior of circular delaminations [106,107]. The partitioning approach has been more vastly used in the literature of delaminated composite plates [16–21] and its modified two-dimensional variations are being used

to date [25,27–34,108]. Partitioning despite its practicality and ease of application, suffers from a slight inconsistency in the displacement field and provides no information on the interlaminar tractions. Moreover, it increases the size of the analysis and consequently adds to its computational cost. By adopting a different approach for addressing the discontinuity across the delamination, Zhang et al [109] used a layerwise theory with a non-continuous displacement field in the delaminated region. A similar technique was also used by Marjanovic et al [39] in conjunction with a different solution method. Numerical solutions offer high versatility with respect to the geometric shape of structures and can easily accommodate the delamination discontinuity without any need for partitioning techniques, however, this facility comes at the expense of much higher computational and modeling costs.

To model the mechanical behavior of anisotropic laminates a variety of theories have been used. The most common theories used in the context of instability analysis of laminated plates are Equivalent Single Layer (ESL) theories. The simplest ESL theory is the Classical Laminated Plate Theory (CLPT) which is notorious for overestimating the bending stiffness, especially for thicker plates. First-Order Theory (FSDT) and Higher-Order Shear Deformation Theory (HSDT) have been proven to more accurately represent the mechanical behavior of composite laminates without significantly overestimating their flexural stiffness. Kharazi et al [23] compared the accuracy of these theories in predicting the stability behavior of plates containing through-the-width delaminations and concluded that the efficiency of HSDT was superior. However, they observed that the results obtained using FSDT match those of HSDT except for the cases with remarkably thick sublaminates.

In the present work, a novel technique for modeling delamination is proposed. The delamination is simulated by splitting the laminate into two sublaminates at the plane of the delamination. The bonding of sublaminates formed on the two sides of the delamination plane is modeled using a penalty function in the intact (nondelaminated) regions. Each of the sublaminates is separately modeled using the first-order shear deformation theory. The equilibrium equations are obtained using a modified Ritz method capable of capturing local deflections as well as global deformations. The penalty method offers access to the interlaminar tractions corresponding to the three fracture mode shapes. The availability of these tractions sets a foundation for assessing the possible growth of a delamination.

Using the developed formulation a MATLAB® program was developed and validated through the comparison of results with three-dimensional finite element analyses carried out using the multipurpose commercial software ANSYS®.

3.2 Problem definition

The present work focuses on the compressive response of rectangular laminated composite plates with arbitrary stacking sequences containing a finite-width rectangular delamination. Figure 3.1 illustrates the geometry of such a delaminated plate including the symbols that are used to designate the dimensions of the plate and the delamination. To trace the equilibrium path beyond the instability threshold, throughout this work the stability analyses are carried out under a displacement-controlled loading system.

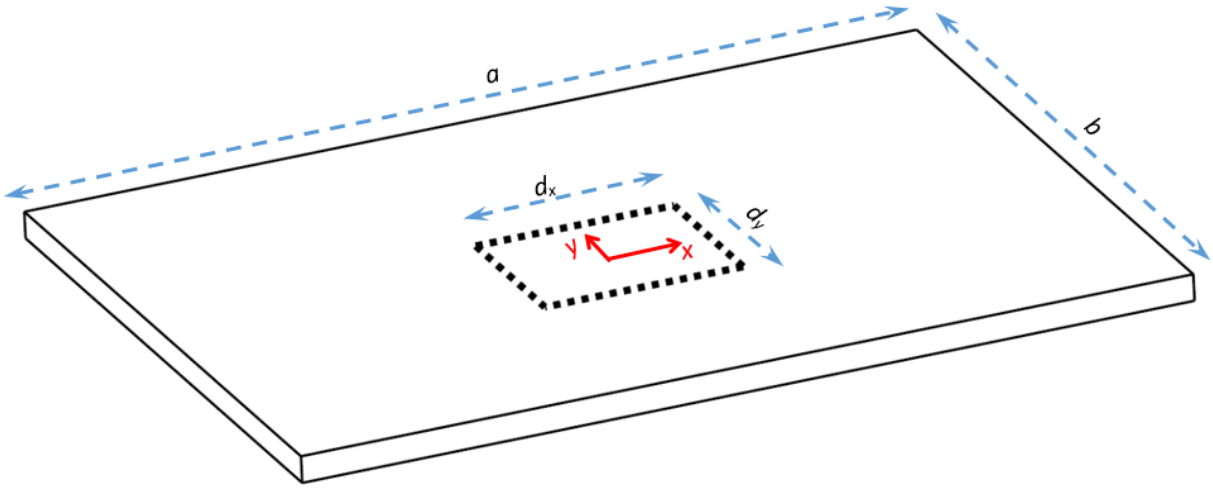

Figure 3.1 Schematic view of a plate containing an embedded delamination

3.3 Theory and formulation

3.3.1 Kinematics

In the proposed method, the delaminated plate is assumed to be composed of two sublaminates on the two sides of the plane of the delamination. The displacement fields in both of these sublaminates are approximated by the FSDT. Despite the common aspect of adopting a linear displacement field, unlike CLPT, FSDT does account for the out-of-plane shear deformations and

by doing so avoids overestimating the stiffness of moderately thick laminates. The FSDT assumes a linear distribution of in-plane displacements in the thickness direction of the laminate while assuming that the out-of-plane displacement is a function of the in-plane coordinates only. The explained displacement field can be mathematically expressed in the form:

$$u\,(x,y,z) = u_0(x,y) + z\phi_x(x,y) \tag{3.1}$$
$$v\,(x,y,z) = v_0(x,y) + z\phi_y(x,y) \tag{3.2}$$
$$w(x,y,z) = w_0(x,y) \tag{3.3}$$

The instability and post-instability behaviors of anisotropic laminates generally involve small strains and moderately large rotations. Therefore, in order to model the behavior of a composite plate in these conditions, a strain definition capable of accommodating large rotations is required. For planar structures, large rotations are conventionally accounted for by using Von Kármán's approximations of the Green strain tensor.

Given the FSDT displacement field as described in Eqs.(4.1-4.3), Von Kármán's in-plane strains can be expressed as:

$$\begin{Bmatrix} \varepsilon_x \\ \varepsilon_y \\ \gamma_{xy} \end{Bmatrix} = \begin{Bmatrix} \varepsilon_x^0 \\ \varepsilon_y^0 \\ \gamma_{xy}^0 \end{Bmatrix} + z\begin{Bmatrix} k_x \\ k_y \\ k_{xy} \end{Bmatrix} = \begin{Bmatrix} \dfrac{\partial u_0}{\partial x} + \dfrac{1}{2}\left(\dfrac{\partial w_0}{\partial x}\right)^2 \\ \dfrac{\partial v_0}{\partial y} + \dfrac{1}{2}\left(\dfrac{\partial w_0}{\partial y}\right)^2 \\ \dfrac{\partial u_0}{\partial y} + \dfrac{\partial v_0}{\partial x} + \dfrac{\partial w_0}{\partial x}\dfrac{\partial w_0}{\partial y} \end{Bmatrix} + z\begin{Bmatrix} \dfrac{\partial \varphi_x}{\partial x} \\ \dfrac{\partial \varphi_y}{\partial y} \\ \dfrac{\partial \varphi_y}{\partial x} + \dfrac{\partial \varphi_x}{\partial y} \end{Bmatrix} \tag{3.4}$$

Based on the same displacement field the out-of-plane shear strains read as:

$$\begin{Bmatrix} \gamma_{yz} \\ \gamma_{xz} \end{Bmatrix} = \begin{Bmatrix} \varphi_y + \dfrac{\partial w_0}{\partial y} \\ \varphi_x + \dfrac{\partial w_0}{\partial x} \end{Bmatrix} \tag{3.5}$$

3.3.2 Constitutive equations

Assuming a plane-stress condition the constitutive equation at an arbitrary point in the laminate is expressed as:

$$\begin{Bmatrix} \sigma_x \\ \sigma_y \\ \tau_{xy} \\ \tau_{yz} \\ \tau_{xz} \end{Bmatrix} = \begin{bmatrix} Q_{11} & Q_{12} & Q_{16} & 0 & 0 \\ Q_{12} & Q_{22} & Q_{26} & 0 & 0 \\ Q_{16} & Q_{26} & Q_{66} & 0 & 0 \\ 0 & 0 & 0 & Q_{44} & Q_{45} \\ 0 & 0 & 0 & Q_{45} & Q_{55} \end{bmatrix} \begin{Bmatrix} \varepsilon_x \\ \varepsilon_y \\ \gamma_{xy} \\ \gamma_{yz} \\ \gamma_{xz} \end{Bmatrix} \tag{3.6}$$

where Q_{ij}s are the elements of the reduced plane-stress stiffness matrix of the corresponding ply.

As the FSDT treats the laminate as an ESL the constitutive equation is stated in the form of an equation that defines the relationship between the stress and moment resultants and the so-called laminate strain vector as:

$$\begin{Bmatrix} N_x \\ N_y \\ N_{xy} \\ M_x \\ M_y \\ M_{xy} \\ Q_x \\ Q_y \end{Bmatrix} = \int_{-h/2}^{h/2} \begin{Bmatrix} \sigma_x \\ \sigma_y \\ \tau_{xy} \\ z\sigma_x \\ z\sigma_y \\ z\tau_{xy} \\ \tau_{yz} \\ \tau_{xz} \end{Bmatrix} dz = \begin{bmatrix} [A] & [B] & 0 \\ [B] & [D] & 0 \\ 0 & 0 & [H] \end{bmatrix} \begin{Bmatrix} \varepsilon_x^0 \\ \varepsilon_y^0 \\ \gamma_{xy}^0 \\ k_x \\ k_y \\ k_{xy} \\ \gamma_{yz} \\ \gamma_{xz} \end{Bmatrix} \tag{3.7}$$

where the elements the stiffness matrices are obtained using the following equations:

$$\left(\mathrm{A_{ij}}, \mathrm{B_{ij}}, \mathrm{D_{ij}}\right) = \int_{-h/2}^{h/2} Q_{ij}(1, z, z^2) dz \quad for \quad i,j = 1,2,6 \tag{3.8}$$

And

$$H_{\mathrm{ij}} = k \int_{-h/2}^{h/2} C_{ij}\, dz \quad for \quad i,j = 4,5 \tag{3.9}$$

where k is the shear correction factor.

The assumptions of FSDT dictate a uniform shear stress distribution in the thickness of a laminate and thus violate the condition of traction-free upper and lower surfaces. This results in an overestimation of the shear stiffness. To alleviate this excessive stiffness, the correction factor k is introduced to the shear stiffness matrix. Unlike for isotropic materials, no unique value can be advocated for composite laminates. However, the same values used for isotropic plates have been used in a multitude of research works and satisfactory accuracy has been achieved. In the present work, a k value of 5/6 is used.

When considering the laminate as two sublaminates bonded to each other, each sublaminate is considered as a separate ESL. Therefore, in order to model the mechanical behavior of the

delaminated plate, the stiffness matrices of each sublaminate need to be determined based on the stacking sequence of that particular sublaminate. Given the bonding between the sublaminates, unlike the top and bottom surfaces of the laminate, the traction-free assumption does not hold for the interface. However, the excessive stiffness imposed by the assumption of a linear displacement field still needs to be remedied using a correction factor.

3.3.3 A modified Ritz method

The equilibrium equations for the quasi-static nonlinear problem are found using the principle of minimum total potential energy applied through the Ritz method.

According to the stationary total potential energy principle, equilibrium corresponds to a condition in which the total potential energy functional is stationary and minimum for a stable configuration. The total potential energy of a structural system consists of the strain energy stored in the structure and the potential energy of external forces:

$$\Pi = U + W \tag{3.10}$$

For a laminate assumed to be composed of two sublaminates, the strain energy is the sum of the strain energies of the two sublaminates. The bonding between the two sublaminates is enforced using a penalty function that ensures the continuity of the displacement field across the interface. The total potential energy of the assembled sublaminates that form a whole laminate is expressed as:

$$\Pi = U_1 + U_2 + U_P + U_c + W \tag{3.11}$$

where U_1 and U_2 are the strain energy terms corresponding to the bottom and top sublaminates respectively, U_p is the penalty term corresponding to the energy stored in an elastic bonding, and U_c is the energy corresponding to contacting surfaces.

For an anisotropic plate the deflection of which is represented by the FSDT, the strain energy is expressed as:

$$U = \frac{1}{2}\left\{\iint \{\epsilon\}^T \begin{bmatrix} [A] & [B] & 0 \\ [B] & [D] & 0 \\ 0 & 0 & [H] \end{bmatrix} \{\epsilon\}\, dA\right\} \tag{3.12}$$

where $\{\epsilon\} = \begin{bmatrix} \varepsilon_x^0 & \varepsilon_y^0 & \gamma_{xy}^0 & k_x & k_y & k_{xy} & \gamma_{yz} & \gamma_{xz} \end{bmatrix}^T$

In assessing the compressive response of plates, solution nonlinearities generally lead to extremum points beyond which the slope of the force-displacement curve becomes negative, that is, further deflection can take place without any increase in the magnitude of external forces.

Hence, in a force-controlled analysis, it is impossible to capture the equilibrium path past such extremum points. In order to trace the complete equilibrium path, post-instability analyses are often conducted under a displacement-controlled loading. Therefore, in the present work, the external forces are absent and the external loading is considered in the form of an incremental displacement imposed on the edges of the plate.

Once the expression of the total potential energy of the assembly is derived, the minimization of the functional is done through the application of the Ritz method. The Ritz method approximates the displacements corresponding to an equilibrium state in the form of finite series of linearly independent functions with unknown coefficients. These functions need to satisfy the essential boundary conditions of the problem and have non-zero derivatives to the highest degree of the derivatives that appear in the total potential energy expression. For the two-dimensional problem of a plate, the common approach is to seek the solution in the form of series with separable continuous functions. The general form of such approximate functions reads as:

$$\psi = \sum_{m=1}^{M} \sum_{n=1}^{N} \Psi_{mn} X_m Y_n \tag{3.13}$$

where X_m and Y_n are definite functions of x and y respectively.

In the aforementioned 2D plate problem, ψ represents the displacements $u, v,$ and w or the rotations φ_x and φ_y while Ψ_{mn} represents the corresponding coefficients U_{mn}, V_{mn}, W_{mn}, $\Phi_{x_{mn}}$, and $\Phi_{y_{mn}}$. For Each of the displacement fields $u, v, w, \varphi_x,$ and φ_y, X_ms and Y_ns need to be defined consistent with the corresponding boundary conditions.

The adopted series is supposed to be capable of generating every possible deformed shape of the physical domain while respecting the essential boundary conditions.

By substituting the approximate functions into Eq. (3.4) and subsequently into Eqs. (3.11) and (3.12), The expression of the strain energy in terms of the unknown coefficients Ψ_{mn} is obtained. The minimization of the total potential energy is then done with respect to the unknown coefficients and it leads to a system of nonlinear equations as follows:

$$\frac{\partial \Pi}{\partial U_{mn}} = 0, \frac{\partial \Pi}{\partial V_{mn}} = 0, \qquad \frac{\partial \Pi}{\partial W_{mn}} = 0, \qquad \frac{\partial \Pi}{\partial \Phi_{x_{mn}}} = 0, \qquad \frac{\partial \Pi}{\partial \Phi_{y_{mn}}} = 0 \tag{3.14}$$

where U_{mn}, V_{mn}, W_{mn}, $\Phi_{x_{mn}}$, and $\Phi_{y_{mn}}$ are the coefficients of the approximate functions for *u, v, w* , φ_x, and φ_y respectively.

Conventionally, the Ritz approximate functions are continuous over the mathematical domain which is equivalent to the physical span of the plate. Being of a continuous nature, these functions can very hardly accommodate high gradient local deformations that are expected in a delaminated region. As a remedy for this problem, the superimposition of a set of supplementary non-continuous functions on the conventional continuous approximate functions is proposed in the present work. The supplementary functions which serve as a local refinement, are complete functions with a value of zero outside the delaminated region. To maintain displacement continuity across the plate, these functions are designed in a way that they satisfy the condition of C1 continuity at the borders of the delaminated region. That is, their values, as well as their first derivatives, vanish at the edges of the delamination. The requirements of C1 continuity as described are built in the approximate functions while their zero value outside the delaminated region is secured by multiplying the series by a step function. With this adjustment, the Ritz approximate functions take the form:

$$\psi = \sum_{m=1}^{M}\sum_{n=1}^{N}\left[\Psi_{mn}X_mY_n + R_d\Psi_{mn}\acute{\Psi}_{mn}\acute{X}_m\acute{Y}_n\right] \tag{3.15}$$

where R_d is a step function with a value of unity inside the delaminated region and a value of zero outside the delaminated zone and can be defined using the Heaviside step function. For the particular geometric configuration depicted in Figure 3.1 Schematic view of a plate containing an embedded delamination**Error! Reference source not found.**, R_d can be expressed in the form:

$$R_d = \left[H\left(y+\frac{dy}{2}\right) - H\left(x-\frac{dy}{2}\right)\right]\left[H\left(x+\frac{dx}{2}\right) - H\left(x-\frac{dx}{2}\right)\right] \tag{3.16}$$

When using such a combination of functions, the continuous functions are responsible for capturing the global deformations while the local deformations are captured by the noncontinuous functions.

Even though the choice of the Ritz approximate functions is arbitrary, it is well established that using higher-order simple polynomials can lead to the emergence of ill-conditioned matrices and subsequently to an inaccurate numerical solution[100,110]. In the present work, acceptable approximate functions compatible with the boundary conditions of a problem are constructed based on simple polynomial functions. To avoid numerical complications as explained, the Gram-Schmidt orthonormoalization procedure is used to convert the simple polynomial functions into sets of orthogonal functions. The general form of simple polynomial functions to satisfy the essential boundary conditions of an arbitrary problem may be expressed as:

$$X_m = R_x x^m \quad m = 0,1,2..M \tag{3.17}$$
$$Y_m = R_y y^n \quad n = 0,1,2..N \tag{3.18}$$

where R_x and R_y are the functions that enforce the essential boundary conditions for a particular physical degree of freedom of a problem and they are dubbed Boundary Condition Coefficient Functions (BCCF).

Similarly, the local noncontinuous polynomial functions used for a rectangular delaminated region are constructed as:

$$\acute{X}_m = \acute{R}_x x^m \quad m = 0,1,2..M \tag{3.19}$$
$$\acute{Y}_n = \acute{R}_y y^n \quad n = 0,1,2..N \tag{3.20}$$

where $\acute{R}_x$ and $\acute{R}_y$ are the BCCFs that provide the C1 continuity across the edges of the delamination. That is, both the BCCFs and their first derivatives are supposed to vanish at the edges of the delamination. For a delamination the center of which coincides with the center of the plate, these BBCFs are defined as:

$$\acute{R}_x = (x^2 - \frac{{d_x}^2}{4})^2 \tag{3.21}$$
$$\acute{R}_y = (y^2 - \frac{{d_y}^2}{4})^2 \tag{3.22}$$

Once the original polynomial functions are constructed, the corresponding orthonormal functions are obtained through the application of the Gram-Schmidt procedure. For the global functions, the orthonormalization is carried out over the intervals *[-a/2 a/2]* and *[-b/2 b/2]* whilst for the local functions, the intervals *[-dx/2 dx/2]* and *[-dy/2 dy/2] are used*. Figure 3.2 illustrates the first five terms of global and local orthonormalized approximate functions that are compatible with clamped boundary conditions (CCCC).

To set up a displacement-controlled analysis an additional definite linear term is added to the approximate function corresponding to the in-plane displacements. For a uniaxial compressive loading in the x-direction, the approximate function for *u* is modified as:

$$u = x\frac{\delta}{a} + \sum_{m=1}^{M}\sum_{n=1}^{N}\left[U_{mn}X_mY_n + R_d\acute{U}_{mn}\acute{X}_m\acute{Y}_n\right] \tag{3.23}$$

where δ is the relative edge displacement.

If the BCCFs in the series are defined in a way that they do not allow any in-plane movement of the edge, then the movement of the edge is dictated by the value selected for δ. This relative displacement of the opposite edges is often referred to as end-shortening.

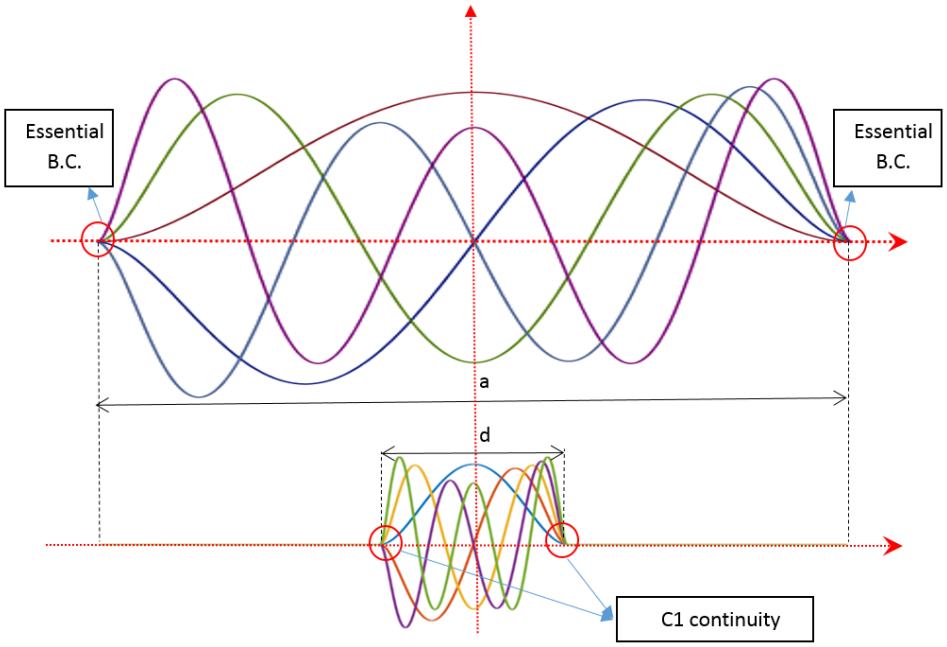

Figure 3.2 Continuous global functions (top) versus noncontinuous local functions (bottom)

3.3.4 Delamination modeling

The new delamination modeling scheme considers the laminate containing a delamination as two sublaminates on the two sides of the plane of the delamination. As for the real-life case where the plies are bonded to each other using an adhesive, in the new model the sublaminates are bonded together using penalty functions. The penalty functions are essentially equivalent to the potential energy corresponding to distributed elastic bonds which restrain the relative movements of the touching surfaces (interface) of the sublaminates in the intact regions. By selecting infinitely high stiffness values for these distributed elastic springs a zero relative displacement can be achieved. Figure 3.3 shows the arrangement of the sublaminates. As it is depicted in the figure the interface of the two sublaminates is located on the upper surface of the lower sublaminate as well as the lower surface of the upper sublaminate.

For the three physical degrees of freedom of any point on the interface, three separate penalty functions are to be defined to prevent all possible relative movements of the interface. As the out-of-plane displacement w is assumed not to vary with the location in the thickness, the relative out-of-plane movement of the sublaminates at the interface is equal to the difference between the out-of-plane displacements of the midplanes of the two sublaminates. Hence the penalty term corresponding to the out-of-plane displacement reads as:

$$U_N = \frac{1}{2} K_w \iint_I (w^1 - w^2)^2 dA = \frac{1}{2} K_w \iint_I (w_0^1 - w_0^2)^2 dA \tag{3.24}$$

Similarly, the penalty term corresponding to in-plane relative displacements are:

$$U_S = \frac{1}{2} \iint_I [K_u (u^1 - u^2)^2 + K_v (v^1 - v^2)^2] dA \tag{3.25}$$ (1)

where I designates the intact region and K_u, K_v, and K_w are the penalty stiffnesses in x, y, and z-directions respectively.

In order to account for the debonding in the delaminated region, the integration in Eqs.(3.24) and (3.25) are carried out over the intact region and the debonded region is excluded.

Taking into account the displacement fields of Eqs. (3.1) and (3.2) the displacements of the upper surface of the bottom sublaminate can be presented in terms of its midplane parameters as:

$$u^1 = u_{01} + \varphi_{x1} \frac{h_1}{2} \tag{3.26}$$

$$v^1 = v_{01} + \varphi_{y1} \frac{h_1}{2} \tag{3.27}$$

Similarly, the displacements of the bottom surface of the top sublaminate can be expressed in terms of its midplane parameters as:

$$u^2 = u_{02} - \varphi_{x2} \frac{h_2}{2} \tag{3.28}$$

$$v^2 = v_{02} - \varphi_{y2} \frac{h_2}{2} \tag{3.29}$$

The overall penalty term U_p to be considered in Eq.(3.10) is the sum of penalty functions:

$$U_P = U_N + U_S \tag{3.30}$$

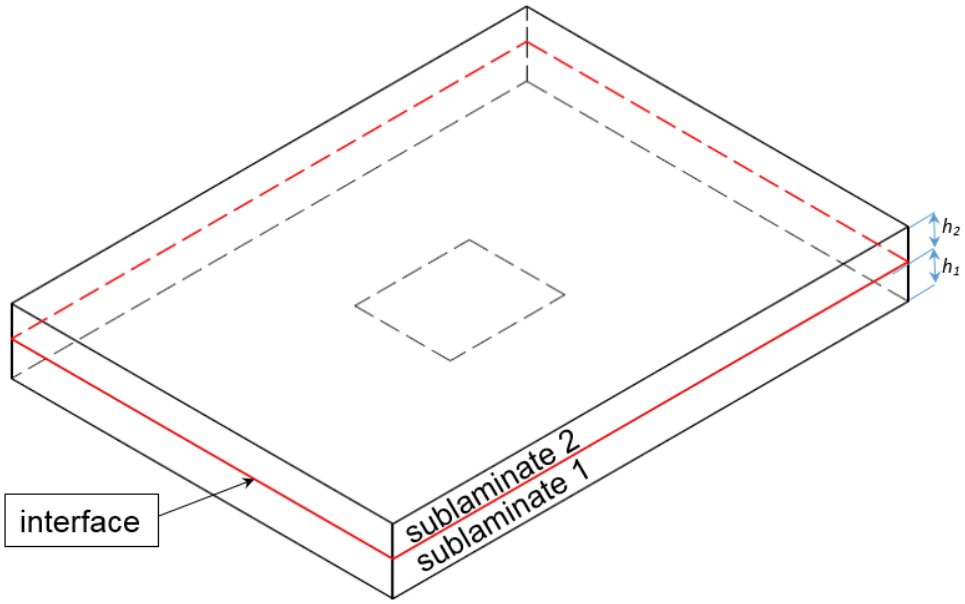

Figure 3.3 Schematic view of sublaminates and their interface

3.3.5 Aspects of contact

The defection of the delaminated region may involve the touching (contact) of the delamination surfaces. In order to account for this phenomenon and to prevent the interpenetration of delamination surfaces. This contact is modeled using a scattered distribution of fictitious compression-only springs. To ensure the compression-only behavior, in an iterative procedure their status is checked and the springs under tension are eliminated. The energy stored in a $K \times L$ rectangular array of springs is expressed as:

$$U_c = \frac{1}{2} K_c \sum_{k=1}^{K} \sum_{l=1}^{L} C_s (w^1(x_k, y_l) - w^2(x_k, y_l))^2 \tag{3.31}$$

where (x_k, y_l) is the location of an individual spring of the array in the delaminated region and C_s is a binary parameter defining the status of a spring.

3.4 Customized Arc-length method

In solving nonlinear equations, the most popular approach is adopting different variations of Newton's method. However, the applicability of Newton's method is limited by the emergence of critical points close to which the tangent matrix becomes singular or ill-conditioned. In order to trace the path of equilibrium past the point of instability, in the present work, the system of nonlinear equations obtained through the application of the Ritz method was solved using an Arc-

length method. The Arc-length method by controlling the size of steps taken in an iterative solution traces almost the entirety of an equilibrium path. In the present work, Crisfield's [67] version of the Arc-length method is modified to meet the special requirements of the system of nonlinear equations in hand. In Crisfield's method, it is assumed that the terms in the system of nonlinear equations are separable into functions of external loading magnitude and functions of the solution vector $\{U\}$ (internal forces) and therefore, the nonlinear system of equations can be expressed in the form:

$$f(\{U\}) + \lambda\{\bar{\mathrm{F}}\} = 0 \tag{3.32}$$

where λ is a scalar defining the magnitude of the external loading and $\{\bar{\mathrm{F}}\}$ is the loading vector corresponding to an arbitrary loading level.

However, as in the present work a forced edge displacement is imposed through the addition of a specific linear function to the displacement approximate function, such a distinction between the terms does not exist and the internal forces depend on the level of the applied end-shortening as well. Therefore, the equation should be expressed in the form:

$$\left\{\frac{\partial \Pi}{\partial \Psi_{mn}}\right\}_{\psi=u,v,w,\varphi_x,\varphi_y} = f(\{U\},\lambda) + \lambda\{\bar{\mathrm{F}}\} = 0 \tag{3.33}$$

R_n^r the residual vector in rth iteration of the nth load step is defined as:

$$\{R\}_n^r = f(\{U\}_n^r, \lambda_n^r) + \lambda_n^r\{\bar{\mathrm{F}}\} \tag{3.34}$$

Assuming that the solution for the $(r-1)^{th}$ iteration of the nth load step is $\{U\}_n^{r-1}$ and the corresponding load parameter is λ_n^{r-1}, to find a solution that renders the residual zero in the rth iteration, R is expanded using the first-order terms of Taylor's series as follows:

$$\{R\}_n^r = \{R(\{U\}_n^{r-1}, \lambda_n^{r-1})\} + \left(\frac{\partial\{R\}}{\partial\lambda}\right)^{r-1} \delta\lambda^r + \left(\frac{\partial\{R\}}{\partial\{U\}}\right)^{r-1} \delta\{\mathrm{U}\}^r \tag{3.35}$$

Where $\delta\lambda^r$ and $\delta\{\mathrm{U}\}^r$ are the corrections to the $(r-1)^{th}$ iteration solution.

Substituting Eq.(3.34) into Eq.(3.35) one has:

$$\{R\}_n^r = \{R(\{U\}^{r-1}, \lambda^{r-1})\} + \left(\frac{\partial f}{\partial\lambda} + \{\bar{\mathrm{F}}\}\right) \delta\lambda_n^r + \frac{\partial f}{\partial\{U\}} \{\delta\mathrm{U}\}_n^r \tag{3.36}$$

where $\frac{\partial f}{\partial\{U\}}$ is by definition the tangent stiffness matrix K_T.

Setting the residual to 0 and solving for $\{\delta\mathrm{U}\}^r$ one has:

$$\{\delta\mathrm{U}\}_n^r = -[K_T]^{-1}\{R\}_n^{r-1} + \delta\lambda^r[K_T]^{-1}\left(\frac{\partial f}{\partial\lambda} + \{\bar{\mathrm{F}}\}\right) \equiv \{\overline{\delta U}\}_n^r + \delta\lambda_n^r\{\widehat{\delta U}\} \tag{3.37}$$

The solution of the r[th] iteration is therefore given as:

$$\{U\}_n^r = \{U\}_n + \{\Delta U\}_n^r \tag{3.38}$$

$$\{\Delta U\}_n^r = \{\Delta U\}_n^{r-1} + \{\delta U\}_n^r \tag{3.39}$$

The length of the load-step progress vector $\{\Delta U\}_n^r$ is expressed as:

$$\Delta S = \sqrt{\{\Delta U\}_n^r . \{\Delta U\}_n^r} \tag{3.40}$$

The value of the scalar $\delta\lambda_n^r$ is determined by selecting an appropriate value for ΔS and substituting Eqs.(3.37)-(3.39) into Eq.(3.40) and solving for $\delta\lambda_n^r$.

Further details on the procedure of finding the equilibrium path can be found in Ref.[67].

3.5 Numerical examples

The formulation explained in the previous sections was derived for general boundary conditions. Numerical results are obtained and presented for an arbitrarily selected combination of boundary conditions with two opposite clamped edges and two free edges. All the five physical degrees of freedom the plates are fully constrained along the clamped edges. Displacement–controlled loading was applied uniformly on the two opposite clamped edges simultaneously. **Error! Reference source not found.** depicts the described boundary conditions. The selected boundary conditions require similar approximate functions for all the 5 physical degrees of freedom of the problem (*u, v, w, φ_x and φ_y*) which are enforced by adopting the following BCCFs:

$$R_x = (x^2 - \frac{a^2}{4}) \tag{3.41}$$

$$R_y = 1 \tag{3.42}$$

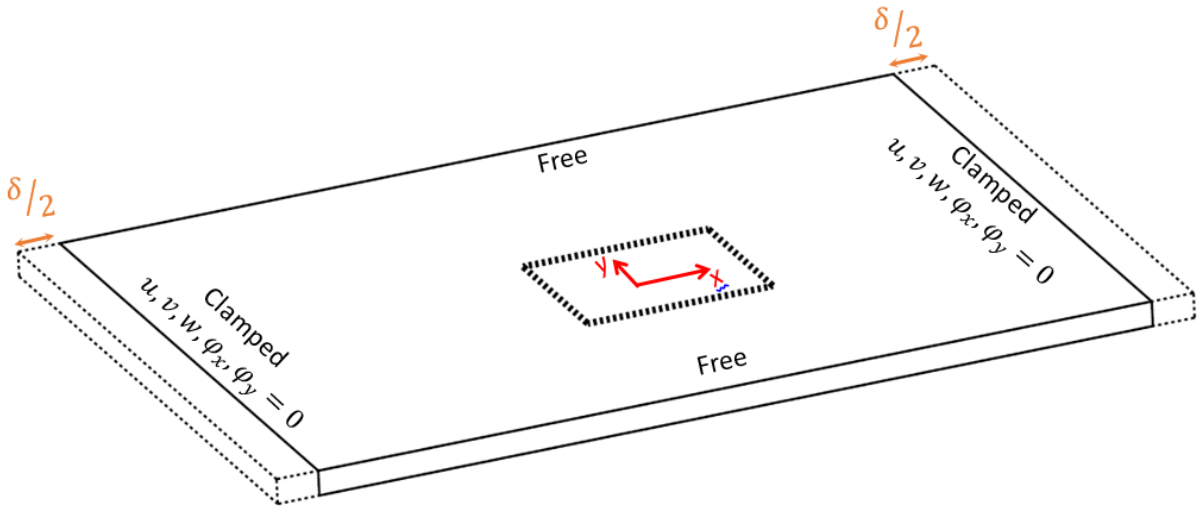

Figure 3.4 Loading and boundary conditions used for numerical examples

Analyses were undertaken on a laminate with a stacking sequence of $(0/90/90/0)_3$ with a ply thickness of 0.2 mm. Additionally, a laminate with a stacking sequence of $(0/90)_6$ was analyzed to demonstrate the capability of the developed formulation to handle asymmetrically stacked laminates. The overall size of the specimen in all analyses was kept constant at 150 mm×100 mm and the dimensions and the location of the delamination in the thickness-direction were varied. The material properties used are listed in Table 3.1.

Table 3.1 Orthotropic material properties

E_{11}(GPa)	E_{22}(GPa)	G_{12}(GPa)	ν_{12}
181	10.3	7.17	0.28

The selected combination of boundary conditions, material properties and laminate lay-up would lead to symmetric deformed shapes that could be simulated using a quarter model, however, as the methodology was meant to be applicable for any arbitrary laminate and boundary conditions, it was developed based on a full modeling scheme.

As a benchmark, every analyzed case was compared with the results obtained through Finite Element Method (FEM). The FEM simulations were conducted using ANSYS® multipurpose commercial software. The modeling was done using the 3-dimensional SOLID185 element which is a linear element capable of accommodating stress stiffening and large deflection effects. The element is constructed with 8 nodes each of which has 3 translational degrees of freedom. Each ply of the laminate was modeled using two layers of hexahedral elements.

Given the fact that symmetrically stacked laminates do not generally become unstable under pure compressive in-plane loading, similar shape and amount of imperfection were considered in both analyses (FEM and present). The imperfections were generated by applying a very small equal and opposite distributed pair forces on the touching surfaces of the sublaminates in the delaminated region. As the sum of the forces applied on the plate is zero no global imperfection is caused.

In the first series of analyses, the delamination was placed between the second and third plies from the top of the laminate. The analyses show that in this arrangement with a gradual increase in the end-shortening, instability first occurs in the thinner sublaminate in the form of a dome. With a further increase in the applied end-shortening, a mixed-mode buckling takes place after which the whole laminate including the thinner sublaminate moves in the opposite direction.

Figure 3.5 depicts both local and mixed buckled shapes for a plate with a square shaped delamination of 30 mm×30 mm.

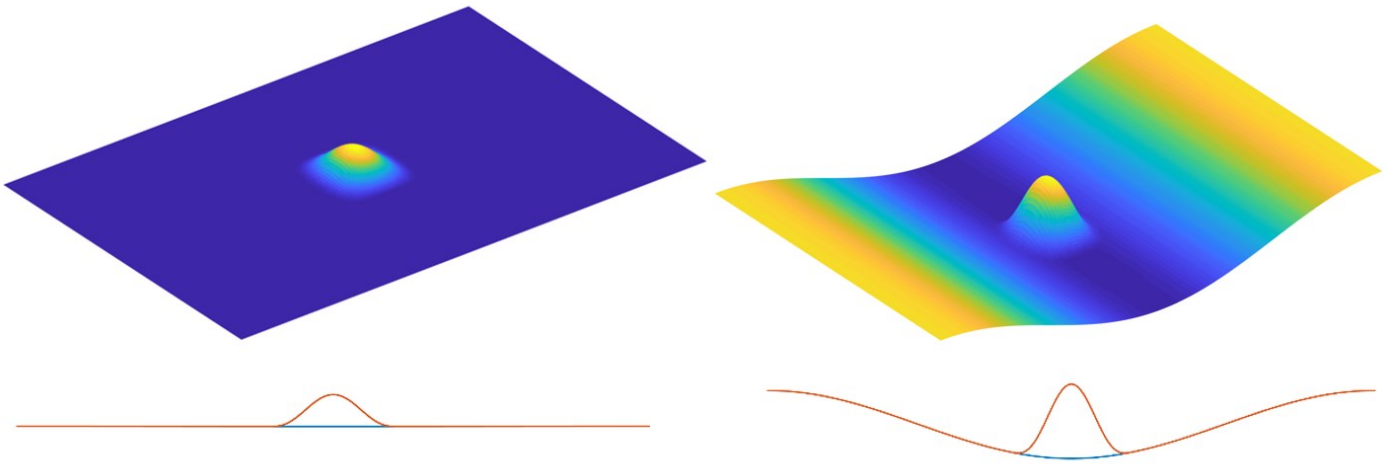

Figure 3.5 Local (left) and mixed-mode (right) shapes for a delamination between 2nd and 3rd plies of the $(0/90/90/0)_3$ laminate

Analyses involving other delamination sizes exhibit similar instability phenomena, however, the loading level at which these instabilities occur vary.

Figure 3.6-3.8 demonstrate the variation of the out-of-plane displacement and the normal strain in the longitudinal direction (ε_x) at the center of the sublaminates versus the applied end-shortening. These figures correspond to delaminations of sizes 30 mm×30 mm, 40 mm×40 mm, and 50 mm×50 mm respectively. To visualize the impact of the delamination on the compressive response, the load vs out-of-plane displacement curve is presented for an intact plate (without delamination) as well. Given the fact that in these analyses the bottom sublaminate is of a thickness close to the thickness of the intact laminate, it mostly follows the global deflection of the whole plate. Therefore, a radical change in the slope of the out-of-plane displacement of the center point of the bottom sublaminate can be regarded as the onset of the mixed instability. A drastic change in the out-of-plane displacement of the center point of the upper laminate happens without any noticeable change in the behavior of the whole plate and it can be interpreted as the onset of the local buckling. It was noticed the emergence of the global deflection led to the closure of the delamination at its longitudinal extremities (transversal edges) and the material surfaces on the two sides of the delamination plane came in partial contact.

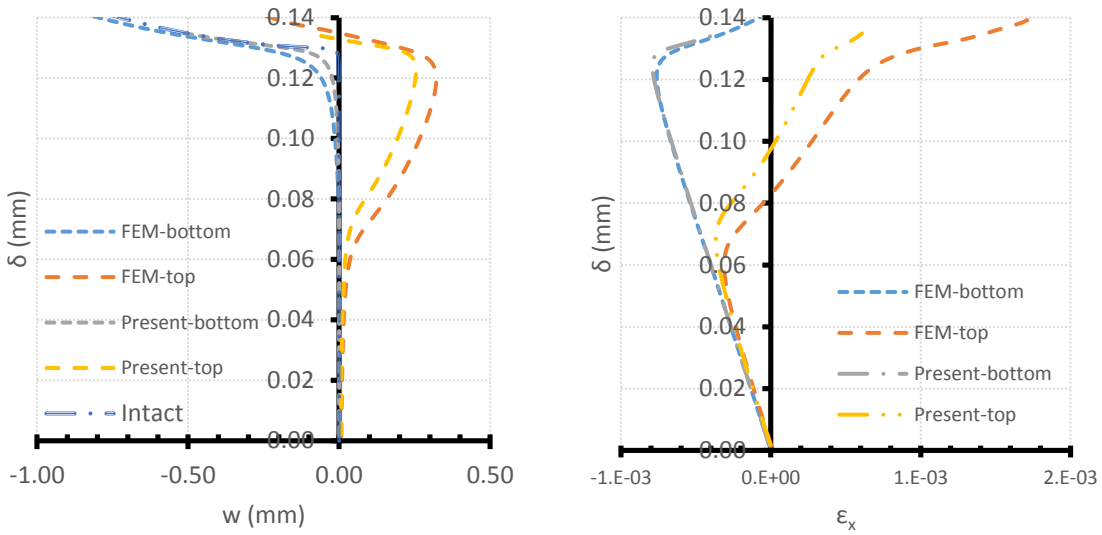

Figure 3.6 Center point out-of-plane displacement (left) and x-direction strain (right) vs end-shortening for a 30mm×30mm delamination

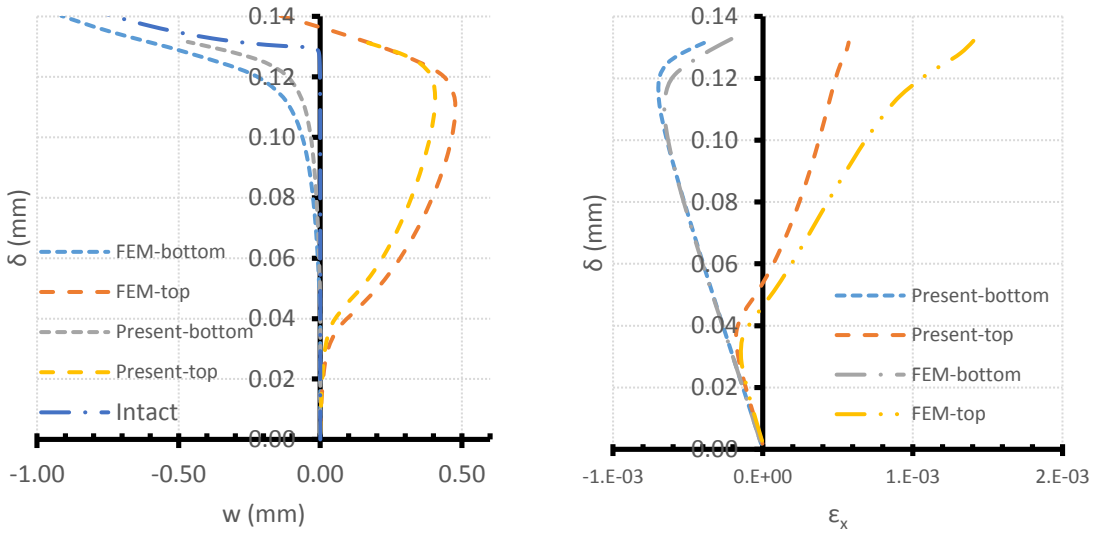

Figure 3.7 Center point out-of-plane displacement (left) and x-direction strain (right) vs end-shortening for a 40 mm×40 mm delamination

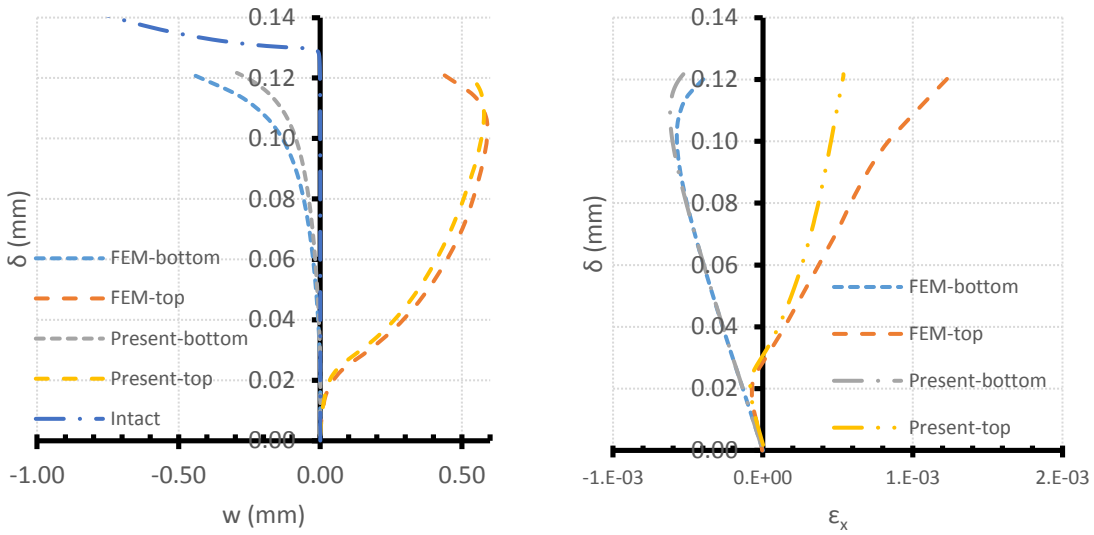

Figure 3.8 Center point out-of-plane displacement (left) and x-direction strain (right) vs end-shortening for a 50 mm×50 mm delamination

A cursory look at the results presented in Figure 3.6-3.8 reveals that larger delaminations tend to buckle under lower levels of loading. It can be observed that for smaller delaminations (30 mm×30 mm, 40 mm×40 mm), the delamination mostly causes a shift forward of the instability onset rather than changing the ultimate behavior of the whole plate in the postbuckling regime. The largest delamination, however, changed the correlation between the end-shortening and out-of-plane displacement in the postbuckling regime as well. It should be taken into account that the smooth transition into the postbuckling regime is partly due to the preexisting imperfection. The results obtained using the present method perfectly agree with the FEM results in predicting the deformed shapes and the emerging phenomena as well as in the load level at which the local instability takes place. In predicting the second (mixed mode) buckling, however, the difference in the calculated onset of instability is more pronounced. The results obtained for strains show a rise proportional to externally applied end-shortening up to the onset of instability. Beyond the instability point, the bending strains come into the picture so as to change the trend of variation of the center point strain. The predicted strains for the thicker sublaminate very closely match the FEM results while the calculated strain on the thinner sublaminate deviates more significantly from FEM result.

To explore the effect of the aspect ratio of the delaminated region, a variety of rectangular delaminations were analyzed. The rectangular delaminations were made by changing the width of the 30mm×30mm delamination the results for which were presented in Figure 3.6. Therefore,

plates containing rectangular delamination of the dimensions 30mm×15mm, 30mm×20mm, and 30mm×45mm were considered. It was observed that for the plate with the 30mm×45mm delamination, similar to the previous cases, the instability involved a local buckling followed by a mixed-mode shape. The out-of-plane displacement and x-direction strains of the center point of the two sublaminates are depicted in Figure 3.9. The analyses of the plates with 30mm×15mm and 30mm×20mm delaminations, showed that the global buckling preceded a potential local instability. Therefore, unlike the previous cases, the buckled shape involved the deflection of the whole plate towards the direction of the thinner sublaminate. The onset of this deflection was followed by the touching (contact) of the delamination surfaces. Given the identical nature of the results obtained for the two delamination dimensions, only the results for the plate with 30mm×20mm delamination are presented in Figure 3.10. The obtained results for the deformed shape and the strains exhibit impeccable agreement with FEM results.

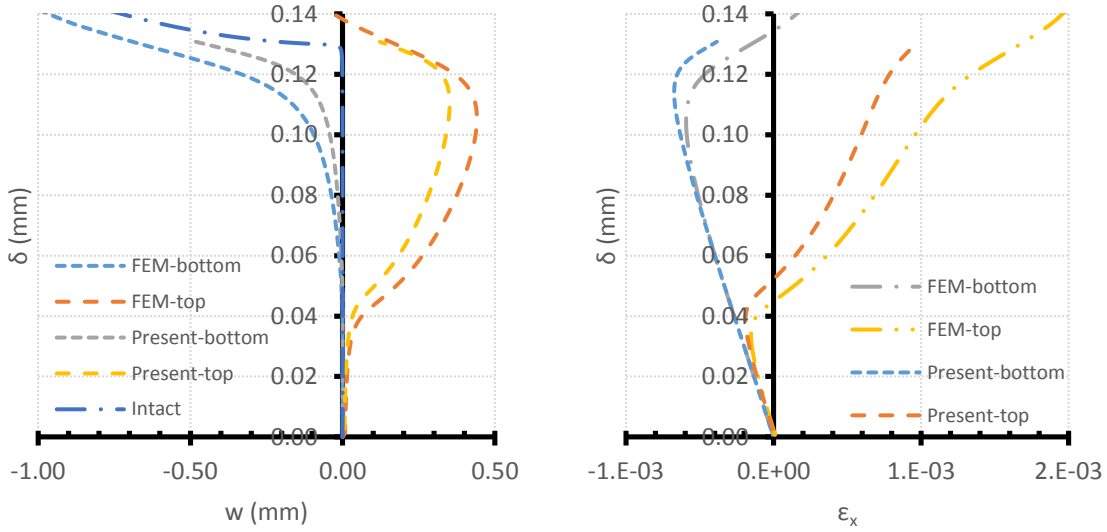

Figure 3.9 Center point out-of-plane displacement (left) and x-direction strain (right) vs end-shortening for a 30 mm×45 mm delamination

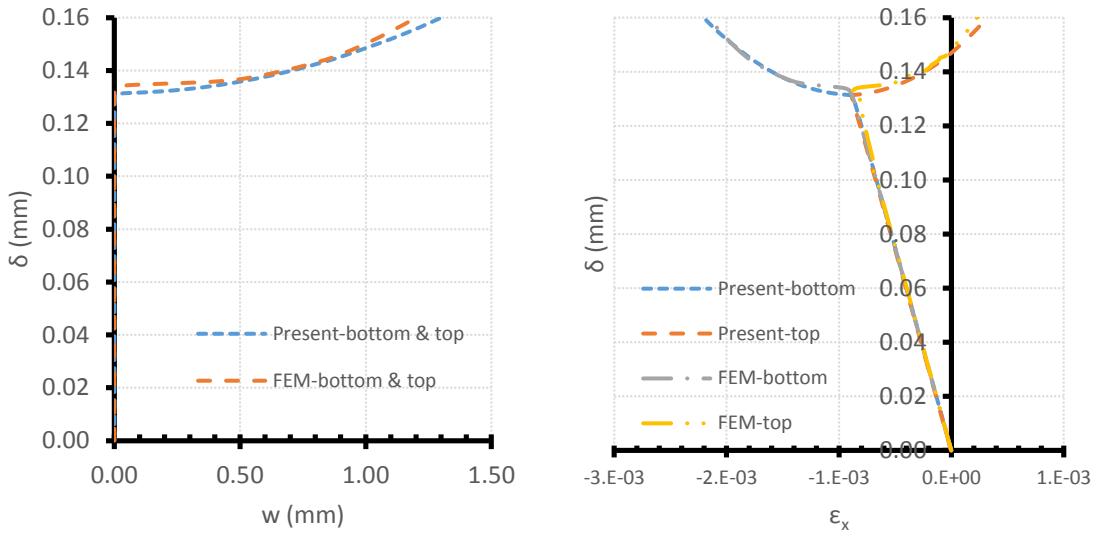

Figure 3.10 Center point out-of-plane displacement (left) and x-direction strain (right) vs end-shortening for a 30 mm×20 mm delamination

In the next step, the delamination was placed between the 4th and the 5th plies of the laminate from the top. In this arrangement, no local buckling was observed and the first buckling mode shape involved a global deformation. Considering the similarity of the results obtained for different sizes of the delamination, for the sake of brevity, the results for a plate with a 30 mm×30 mm delamination are presented solely Figure 3.11 shows the variation of the out-of-plane displacement the x-direction strain at the center of the plate versus the applied end-shortening. Of course, as the buckling does not involve any local deformations, the displacements of the center point of both sublaminates have similar values. The results obtained for all different sizes of delaminations show a very good agreement with the results obtained using FEM. A comparison of the critical buckling load obtained for such delaminated plates with an intact plate reveals that these delaminations barely change the load-carrying capacity of the plate.

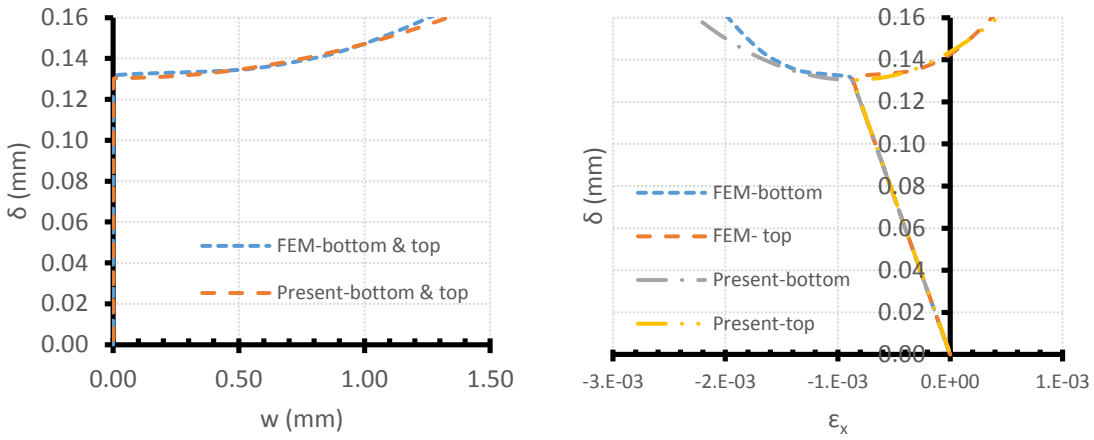

Figure 3.11 Center point out-of-plane displacement (left) and x-direction strain (right) vs end-shortening for a 30mm×30mm delamination

As an example of an asymmetrically stacked laminate, a plate with a lay-up of $(0/90)_6$ containing a 30mm×30mm delamination between the 2nd and the 3rd plies was analyzed. Despite the coupling effects associated with asymmetrical laminates, as the rotations of end edges were constrained an immediate out-of-plane displacement due to in-plane loading did not take place. Similar to symmetrically stacked laminates, the buckling mode shape was a local deformation followed by a mixed-mode buckled shape. The out-of-plane displacement and the x-direction strain at the center point of the top and the bottom surfaces of the plate are presented in Figure 3.12

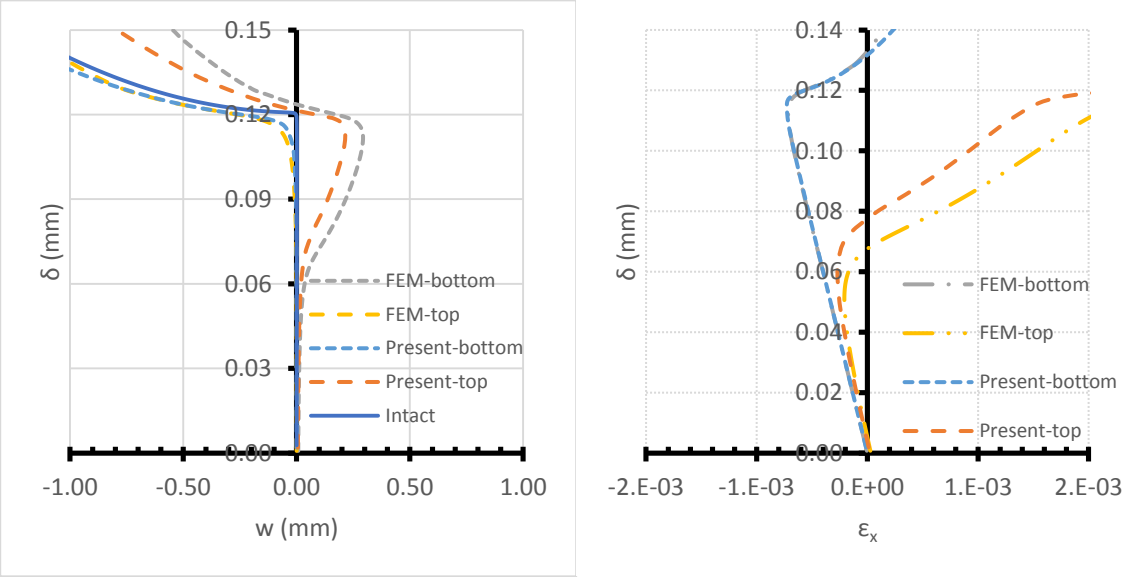

Figure 3.12 Center point out-of-plane displacement (left) and x-direction strain (right) vs end-shortening for a 30 mm×30 mm delamination with a stacking sequence of $(0/90)_6$

The major advantage of the present methodology lies in its capability of estimating interlaminar tractions. By post-processing the relative displacement of the sublaminates, the distribution of

bonding tractions between sublaminates is obtainable. This facility provides the possibility of assessing interlaminar bonds under loading. The calculated interlaminar tractions do not provide the means for determining the possibility of the growth of the delamination, however, they do provide an insight into the location where crack growth may initiate. Furthermore, having access to these tractions along with an accurate estimation of the displacements at the vicinity of the edges of the delamination sets a foundation for calculating the strain energy release rate distribution along the edges of the delamination. Having used isolated penalty functions for each of the three degrees of freedom of a physical point on the interface, the tractions corresponding to each fracture mode (opening, shearing, and tearing) can be determined separately. It is worthy of attention that theoretically, the stress field at the tip of a crack is singular. However, using finite penalty stiffness values, finite values for interlaminar tractions are obtained. Therefore, the magnitudes of the calculated tractions greatly depend on the applied penalty stiffness.

In the following, the interlaminar tractions are plotted along the edges of the delamination introduced in Figure 3.5 (30mm×30mm delamination between the 2nd and 3rd plies) at an end-shortening level of 0.06mm which is above the local buckling threshold and below the global instability limit, for, it was observed that opening tractions are more pronounced in this range. It is worth mentioning that once the delaminated plate reaches the global instability the delamination starts to close up and as the closing initiates from the vicinity of the edges of the delamination, the edges experience no opening traction. Given the dependency of the calculated stress levels on the adopted penalty stiffness, normalized traction values are plotted to demonstrate the distribution of the traction along the delamination edge. The normalization was carried out by scaling the tractions to have a value between -1 and 1. The scaling was done by dividing the tractions by the highest absolute value of tractions experienced along a given edge. Figure 3.13-3.15 show the normalized tractions corresponding to the three principal fracture modes along the axial (parallel to the x-axis) and transversal (parallel to the y-axis) edges of the 30 mm×30 mm delamination. The obtained distributions are in good agreement with the distribution obtained using FEM. The presented curves show a better agreement for the tractions along the axial edge. Obtaining a smooth distribution of interlaminar traction along the edges using FEM requires an extremely fine mesh.Figure 3.15 shows that despite using a fine mesh (an element size of 1 mm), the calculated tractions suffer some significant oscillations while the present method using no more than 10 terms

generates comparable smooth results. The oscillations in FEM results are particularly more pronounced in tearing mode tractions along all of the edges.

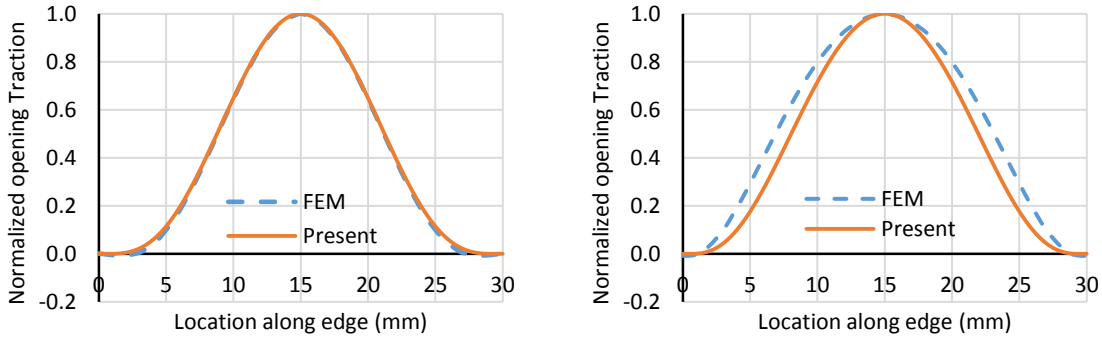

Figure 3.13 Opening traction along the axial (left) and transversal (right) edges of the delamination

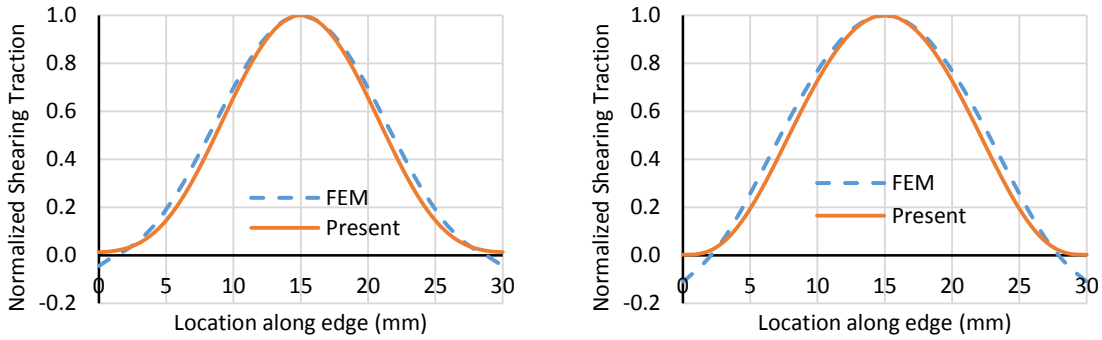

Figure 3.14 Shearing traction along the axial (left) and transversal (right) edges of the delamination

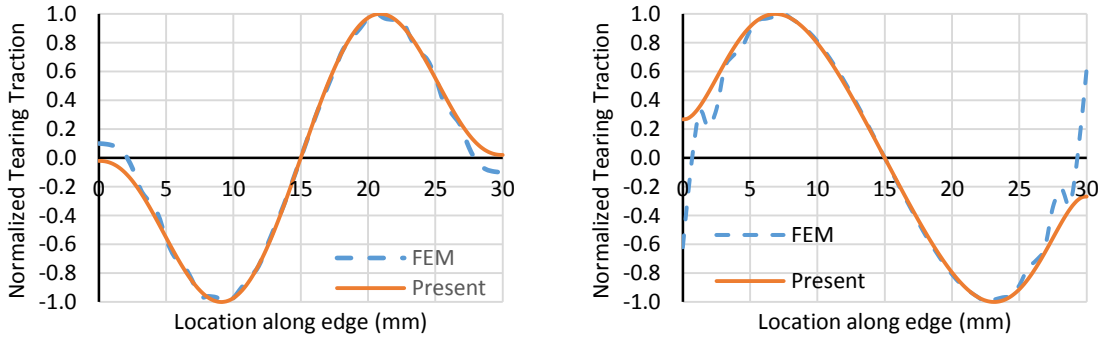

Figure 3.15 Tearing traction along the axial (left) and transversal (right) edges of the delamination

3.6 Conclusions

A new technique for mathematically modeling delaminated composite plates based on a penalty function method is proposed. The laminate and the sublaminates it is composed of are modeled

using the FSDT. The equilibrium states were determined using a modified Ritz method specially designed for problems involving highly localized deformations and high deformation gradients.

Based on the developed formulation a Matlab code was created and the generated results were compared with those obtained using FEM. Comparisons revealed a good agreement in the buckled shapes and in predicting the stability threshold and postbuckling deformations.

The newly implemented technique has the advantage of generating interlaminar traction data which can, in turn, be used for determining the distribution of strain energy release rate in future works. The new method proved to be capable of outperforming FEM in generating smooth interlaminar tractions while reducing the computation cost of the solution.

Chapter 4: A new methodology for buckling, postbuckling, and delamination growth behavior of composite laminates with delamination

Nomenclature

l_x, l_y	*Dimensions of rectangular plate*
h_1, h_2, h	*Thickness of bottom, top, and whole sublaminate*
d	*Dimensions of the rectangular delamination*
u, v	*In-plane displacement in x and y-direction*
u_0, v_0, w_0	*Midplane displacements*
ϕ_x	*Clockwise rotation of cross-section normal to x-axis about the y-axis*
ϕ_y	*Clockwise rotation of cross-section normal to y-axis about the x-axis*
δ	*End-shortening*
δ_t	*Center point out-of-plane deflection*
$\varepsilon_x^0,\ \varepsilon_y^0,\ \gamma_{xy}^0$	*Midplane strains*
k_x, k_y, k_{xy}	*Midplane curvatures*
N_x, N_y, N_{xy}	*Stress resultants*
M_x, M_y, M_{xy}	*Moment resultants*
U	*Strain energy*
W	*Potential energy of applied forces*
U_P	*Penalty term corresponding to elastic adhesions*
U_C	*Penalty term corresponding to contact*
Π	*Total Potential energy functional*
G_I	*Opening mode strain energy release rate*
G_{II}	*Shearing mode strain energy release rate*
G_{III}	*Tearing mode strain energy release rate*
K_u, K_v, K_w	*Penalty stiffness in x, y, and z axes*
$K_{\varphi_x},\ K_{\varphi_y}$	*Rotational penalty stiffness about y and x axes*
K_c	*Stiffness of fictitious contact springs*
L_i	*Lagrange polynomial of i^{th} degree*
$\delta u,\ \delta v,\ \delta w$	*Relative movements of the open surfaces of a crack*

4.1 Introduction

High strength and low density have made laminated composites great candidates for replacing conventional isotropic materials. The advantages of composites especially appeal to industries such as the aerospace industry where lightweight is essential. Despite their outstanding mechanical properties, laminated structures are prone to interlaminar flaws or in other words delaminations. This type of flaw can impact the mechanical behavior and load-carrying capacity of such structures in various ways. In interrogating the behavior of partially delaminated composite plates, probably the most important problem to be addressed is the possibility and the extent of the growth of an existing delamination. This is especially of significance in unstable conditions such as the postbuckling state where the spread of an interlaminar flaw is most expected.

Composite laminates similar to other thin-walled structures when subjected to in-plane compressive loading lose their bending stiffness and start to deflect laterally at their critical buckling loads. Beyond this level of loading, the behavior of the structure changes drastically, and the plate undergoes relatively larger deformations. In laminates containing delaminations, the manifestation of the instability phenomenon depends on the geometry, ply material properties, and the stacking sequence of the laminate as well as the size and the location of the delamination through the thickness of the laminate. A laminate with a near-surface delamination is expected to experience a local buckling followed by a mixed buckling mode. While laminates with delaminations closer to their midplane generally experience either global or mixed buckling mode shapes.

The larger deflections in the postbuckling regime increase the strain energy available for the propagation of the delamination. A global buckling leads to a rise in Strain Energy Release Rate (SERR) corresponding to the fracture Mode *II* (shearing) while in local or mixed buckling mode shapes, a rise in both Mode *I* (opening) and Mode *II* SERRs is expected. Under uniaxial compressive loading, laminates with through-the-with delaminations generally experience negligible values of Mode *III* (tearing) SERR. Once enough energy for the propagation of the delamination is available, it starts growing and the change in its shape and size, in turn, contributes to a further stiffness loss in the plate, and consequently larger deflections. The loading level under which an uncontrolled growth of delamination occurs may be regarded as the ultimate load-carrying capacity of a plate with delamination.

Given the inevitable existence of interlaminar flaws and the possibility of their growth under unstable conditions, the postbuckling behavior of partially delaminated composite plates has been the subject of concern to a large number of researchers. To the knowledge of the authors, the earliest work on predicting the buckling behavior of delaminated composite plates was done by Chai et al [4]. Using an analytical one-dimensional model, they calculated the Strain Energy Release Rate (SERR) as the first variation of the total strain energy of a structure with respect to the length of the delaminated region. A similar technique was later used along with a different asymptotic solution[111]. The application of the aforementioned approach requires the availability of a closed-form expression for the strain energy of the plate. In more general cases where a closed-form expression is not at hand, Crack Extension Techniques (CET) have been employed for calculating SERR. The CET work based on the assumption that a crack grows in a self-similar manner. The CET determines the total strain energy release rate as the difference between the strain energies of the plate before and after an infinitesimal advancement of the crack front per unit surface area of the newly cracked region. The CET has been used in both one-dimensional [6,9] and two-dimensional [40,44,61] analyses. An exception to using CET based on the self-similar growth of a crack is the work of Wang et al [62]. They assumed that a circular delamination would grow into an elliptical shape and hence they accounted for the shape change that may occur in the process of the propagation of an existing delamination. In a different and unique approach, Chai [63] used a combination of thin-plate nonlinear solution and crack tip elasticity solution for calculating the SERRs corresponding to the three fracture modes individually.

Another widely implemented method for delamination growth assessment in approximate solutions is the J-integral method [5,13,17,18]. The calculation of SERR using the path independent J-integral method involves selecting a path along which the integrand is easily obtainable and carrying out the integration along that path. In buckling driven delamination analyses the J-integral method has been used for one-dimensional cracks only.

Finite Element Method (FEM) brings about the liberty of using more complicated techniques that are capable of providing a more detailed picture of the state of a crack. In a vast number of studies on buckling induced delamination growth, the Virtual Crack Growth Technique (VCCT) is used [46,47,59,60,112]. VCCT is developed based on the assumption that the energy released during the growth of a crack is equal to the energy required for closing it. Using VCCT in

conjunction with FEM, the energy release rates corresponding to the three fracture modes can be determined individually.

Besides the techniques that stem from fracture mechanics, Cohesive Zone Models (CZMs) have also been used with FEM for modeling the progressive growth of delaminations [33,58,64]. Given the apriori known plane for the growth of an existing delamination. CZMs work by assigning a decohesive constitutive law to an imaginary interface located in the plane of a delamination. By gradually degrading the stiffness and based on the maximum tolerable traction in the cohesive zone, CZMs predict both the possibility and the extent of the growth of a delamination.

In virtually all the published research works dedicated to the analytical or semianalytical study of the buckling and postbuckling problems of delaminated composite plates, the employed techniques are incapable of distinguishing the contributions of the three fracture modes individually. An exception to this rule is the method proposed by Chai [63] which is applicable to thin-film debonds only. The VCCT and the CZM despite being powerful means for studying the potential growth of delaminations have never been adapted to be used in conjunction with analytical or approximate solutions.

In the current work, with the goal of using Irwin's crack closure integrals for SERR calculation, a new formulation for modeling the buckling and postbuckling behavior of delaminated composite plates is proposed. The proposed approach is capable of predicting the distribution of interlaminar tractions in the plane of an existing delamination. The availability of these tractions makes it possible to calculate the distribution of the SERRs corresponding to each fracture mode individually. The proposed formulation is developed based on the First-Order Shear Deformation Theory (FSDT) and Von Kármán's nonlinear strains and the equilibrium equations are obtained using the Ritz method. The mechanical behavior and the effect of delamination are accounted for by a laminate partitioning scheme in conjunction with a penalty function method that is used for bonding the partitioned sublaminates of the delaminated plate.

4.2 Problem statement

The problem being addressed is the buckling and postbuckling behavior of rectangular composite plates with through-the-width delaminations. For the sake of comparability of the results with experimental data available in the literature [113], the loading and boundary conditions are selected similar to those of the previously conducted experiments. The adopted boundary

conditions and loading are illustrated in Figure 4.1. The compressive load is applied in the form of a uniform forced displacement of the transversal (parallel with y-axis) edges while their rotations and transversal displacement are constrained. The other two edges (parallel with x-axis) are considered free.

considering the symmetry of the rectangular plate and the absence of in-plane coupling effects due to the cross-ply stacking sequence used for experiments, the simulation is performed using a half model in conjunction with symmetry boundary conditions.

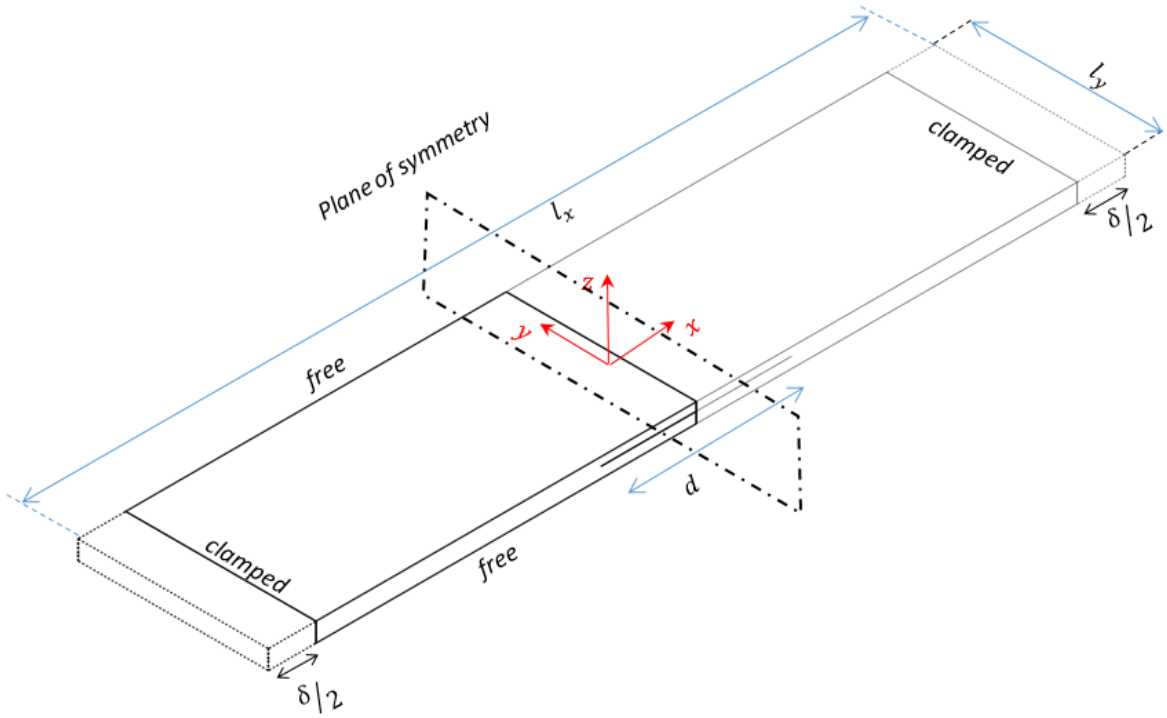

Figure 4.1 Schematic view of the plate and the boundary conditions

The developed formulations are meant to determine the critical buckling load of the delaminated plate as well as its postbuckling behavior including the correlation between the applied end-shortening and the out-of-plane displacements. Furthermore, it is desired to assess the possibility of the propagation of the delamination in the plate through determining the SERRs corresponding to the three fracture modes.

4.3 Theory and formulation

4.3.1 Kinematics and constitutive equations

Throughout the present work, the laminate is modeled as Equivalent Single Layer (ESL) the deformation of which is approximated using the FSDT. The FSDT assumes a linear variation of the in-plane displacements in the out-of-plane direction while assuming that the out-of-plane displacement is a function of in-plane coordinates only. The explained displacement field can be mathematically expressed as follows:

$$u = u_0(x,y) + z\phi_x \tag{4.1}$$

$$v = v_0(x,y) + z\phi_y \tag{4.2}$$

$$w = w_0(x,y) \tag{4.3}$$

where u and v are the in-plane displacements in x and y directions respectively and w is the out-of plane dispalcemnt. The subscript $_0$ denotes the displacements of the midplane of the laminate.

Aiming to address the buckling and postbuckling problems of delaminated plates, a strain definition capable of accommodating the moderately large rotations involved in these problems is required. In buckling and postbuckling problems of composite laminates where large in-plane strains are not involved, Von Kármán's approximations of the Green strain tensor are used. Based on the assumed displacement field described in Eqs. (5.1-5.3), the Von Kármán strains are expressed as:

$$\begin{Bmatrix} \varepsilon_x \\ \varepsilon_y \\ \gamma_{xy} \end{Bmatrix} = \begin{Bmatrix} \varepsilon_x^0 \\ \varepsilon_y^0 \\ \gamma_{xy}^0 \end{Bmatrix} + z\begin{Bmatrix} k_x \\ k_y \\ k_{xy} \end{Bmatrix} = \begin{Bmatrix} \dfrac{\partial u_0}{\partial x} + \dfrac{1}{2}\left(\dfrac{\partial w_0}{\partial x}\right)^2 \\ \dfrac{\partial v_0}{\partial y} + \dfrac{1}{2}\left(\dfrac{\partial w_0}{\partial y}\right)^2 \\ \dfrac{\partial u_0}{\partial y} + \dfrac{\partial v_0}{\partial x} + \dfrac{\partial w_0}{\partial x}\dfrac{\partial w_0}{\partial y} \end{Bmatrix} + z\begin{Bmatrix} \dfrac{\partial \varphi_x}{\partial x} \\ \dfrac{\partial \varphi_y}{\partial y} \\ \dfrac{\partial \varphi_y}{\partial x} + \dfrac{\partial \varphi_x}{\partial y} \end{Bmatrix} \tag{4.4}$$

where ε_x^0, ε_y^0, γ_{xy}^0 are the mdplane strains and k_x, k_y, $k_{xy}$are the midplane curvatures

By neglecting the quadratic terms, the out-of-plane shear strains for the FSDT read as:

$$\begin{Bmatrix} \gamma_{yz} \\ \gamma_{xz} \end{Bmatrix} = \begin{Bmatrix} \varphi_y + \dfrac{\partial w_0}{\partial y} \\ \varphi_x + \dfrac{\partial w_0}{\partial x} \end{Bmatrix} \tag{4.5}$$

Assuming that all the sublaminates are in a plane stress condition, the constitutive equations describing the relations between the stresses and strains at any arbitrary material point are expressed as:

$$\begin{Bmatrix} \sigma_x \\ \sigma_y \\ \tau_{xy} \\ \tau_{yz} \\ \tau_{xz} \end{Bmatrix} = \begin{bmatrix} Q_{11} & Q_{12} & Q_{16} & 0 & 0 \\ Q_{12} & Q_{22} & Q_{26} & 0 & 0 \\ Q_{16} & Q_{26} & Q_{66} & 0 & 0 \\ 0 & 0 & 0 & Q_{44} & Q_{45} \\ 0 & 0 & 0 & Q_{45} & Q_{55} \end{bmatrix} \begin{Bmatrix} \varepsilon_x \\ \varepsilon_y \\ \gamma_{xy} \\ \gamma_{yz} \\ \gamma_{xz} \end{Bmatrix} \tag{4.6}$$

where Q_{ij}s are the elements of the reduced plane stress stiffness matrix of the ply in which the point is located.

The constitutive equation relating the force and moment resultants of a laminate modeled as an ESL to the corresponding midplane strains and curvatures reads as:

$$\begin{Bmatrix} N_x \\ N_y \\ N_{xy} \\ M_x \\ M_y \\ M_{xy} \\ Q_x \\ Q_y \end{Bmatrix} = \int_{-h/2}^{h/2} \begin{Bmatrix} \sigma_x \\ \sigma_y \\ \tau_{xy} \\ z\sigma_x \\ z\sigma_y \\ z\tau_{xy} \\ \tau_{yz} \\ \tau_{xz} \end{Bmatrix} dz = \begin{bmatrix} [A] & [B] & 0 \\ [B] & [D] & 0 \\ 0 & 0 & [H] \end{bmatrix} \begin{Bmatrix} \varepsilon_x^0 \\ \varepsilon_y^0 \\ \gamma_{xy}^0 \\ k_x \\ k_y \\ k_{xy} \\ \gamma_{yz} \\ \gamma_{xz} \end{Bmatrix} \tag{4.7}$$

where the elements of the 3×3 A, B and D matrices are given as:

$$\left(\mathrm{A_{ij}}, \mathrm{B_{ij}}, \mathrm{D_{ij}}\right) = \int_{-h/2}^{h/2} Q_{ij}(1, z, z^2) dz \quad for \quad i,j = 1,2,6 \tag{4.8}$$

The elements of the 2x2 out-of-plane shear stiffness matrix H can be obtained as:

$$H_{\mathrm{ij}} = k \int_{-h/2}^{h/2} C_{ij}\, dz \quad for \quad i,j = 4,5 \tag{4.9}$$

where C_{ij}s are the elements of the complete three-dimensional stiffness matrix at any material point and k is the so-called shear correction factor.

The assumptions of the FSDT by violating the stress-free plate surfaces lead to an overestimation of the shear stiffness of plates. To alleviate this excessive stiffness, the shear correction factor is introduced to the out-of-plane shear stiffness matrix. Even though unlike plates made of isotropic materials, no single value can be prescribed for laminated composites, the findings of earlier publications [51,52,87,98,99] have proven that using the same values used for

isotropic plates, acceptable accuracy can be obtained. In this work, a shear correction factor of 2/3 is used.

4.3.2 Delamination model

In modeling the buckling and postbuckling response of partially delaminated plates, the conventional approach has been to divide the debonded region into two sublaminates on the two sides of the plane of the delamination while regarding the intact regions as an Equivalent Single Layer (ESL). However, the local deformations ahead of the crack tip (edge of the delamination) in the intact region are too complex to be represented using an ESL. Figure 4.2 illustrates the near crack deformation field in a Double Cantilever Beam (DCB) test simulation obtained using Finite Element (FE) analysis. It can be noticed that the portions above and below the delamination plane experience different magnitudes of rotation. When modeling the intact region as an ESL this discontinuity in the rotation field is overlooked and its corresponding effects are lost. This discrepancy in the deformation field not only may affect the predicted behavior of the plate but also hinders access to interlaminar data that can be used for delamination propagation assessment.

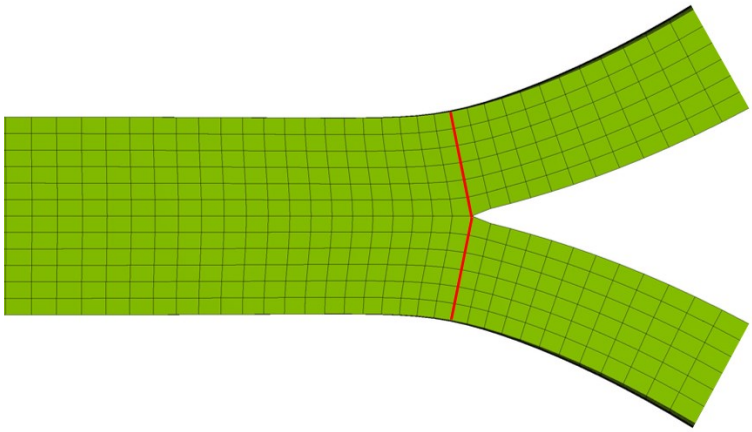

Figure 4.2 Near crack displacement field in DCB test simulation

As a remedy to the mentioned inconsistency, in the present new model, three distinct regions are recognized: the delaminated region, a small intermediate region located in the laminate immediately ahead of the edge of the delamination where very high gradients of displacements and interlaminar stresses are expected, and finally the intact region at a distance from the delaminated region. Experience with approximate solutions has shown that a single set of continuous approximate functions is incapable of capturing the mechanistic aspects of all the three

regions. Therefore, in this work, the laminate is partitioned into five zones as shown in Figure 4.3 in a fashion that each of these regions is modeled separately. Zone 1 represents the intact region where no high gradients of deformations or interlaminar stresses are expected, zones 2 and 3 represent the region immediately ahead of the tip of the crack, and zones 4 and 5 are representative of the debonded region. Zones 2 and 3 despite being modeled separately are assumed to be perfectly bonded at their touching interfaces. Through the simulation of this bond, the interlaminar tractions to be used for the crack growth assessment can be determined (unlike in zone 1 where the ESL does not provide reliable and accurate interlaminar data).

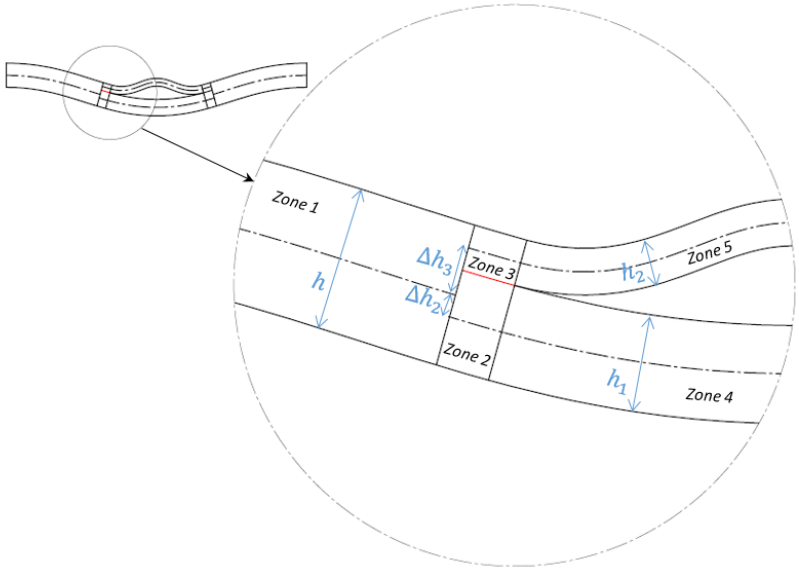

Figure 4.3 The new partitioning scheme to accommodate the effect of delamination

Modeling the sublaminates that correspond to the above mentioned regions individually necessitates additional constraint equations to properly "re-attach" these sublaminates to one another and to maintain the continuity in the structure. As all the sublaminates are modeled using the FSDT, the constraint equations need to be expressed in terms of the midplane displacements and rotations of the connected sublaminates. Figure 4.4 shows the notations used for addressing the Degrees Of Freedom (DOF) of the interfaces between the sublaminates. The subscripts denote the zones and the superscripts - and + denote left and right transversal edges respectively. In the following, the constraint equations describing the continuity condition are presented.

As all the sublaminates are modeled as ESLs, the boundaries of each sublaminate is represented by a line (as opposed to a 3D solid model in which the boundaries constitute flat planes). Therefore, in order to connect zones 1 and 2, the midplane displacements and rotations of zone 2 are set equal

to those of zone 1 along an imaginary line coinciding with the edge of the midplane of zone 2. The displacements of the mentioned imaginary line are expressed in terms of the midplane displacements and rotations of zone 1 using the displacement fields presented in Eqs. (1-3). Hence, the constraint equations read as:

$$\begin{aligned} u_{0_2}^{-} &= u_{0_1}^{+} - \Delta h_2 \varphi_{x_1}^{+} \\ v_{0_2}^{-} &= v_{0_1}^{+} - \Delta h_2 \varphi_{y_1}^{+} \\ w_{0_2}^{-} &= w_{0_1}^{+} \\ \varphi_{x_2}^{-} &= \varphi_{x_1}^{+} \\ \varphi_{y_2}^{-} &= \varphi_{y_1}^{+} \end{aligned} \tag{4.10}$$

where $\Delta h_2$is the distance between the midplane of the whole laminate and the midplane of sublaminate 2.

Similarly, the constraint equations connecting sublaminates 1 and 3 read as:

$$\begin{aligned} u_{0_3}^{-} &= u_{0_1}^{+} + \Delta h_3 \varphi_{x_1}^{+} \\ v_{0_3}^{-} &= v_{0_1}^{+} + \Delta h_3 \varphi_{y_1}^{+} \\ w_{0_3}^{-} &= w_{0_1}^{+} \\ \varphi_{x_3}^{-} &= \varphi_{x_1}^{+} \\ \varphi_{y_3}^{-} &= \varphi_{y_1}^{+} \end{aligned} \tag{4.11}$$

where Δh_3 is the distance between the midplane of the whole laminate and the midplane of the sublaminate 3.

Given the coplanarity of the sublaminates 2 and 4 it is simply enough to equate the displacements and the rotations of the two zones along their meeting edges.

$$\begin{aligned} u_{0_4}^{-} &= u_{0_2}^{+} \\ v_{0_4}^{-} &= v_{0_2}^{+} \\ w_{0_4}^{-} &= w_{0_2}^{+} \\ \varphi_{x_4}^{-} &= \varphi_{x_2}^{+} \\ \varphi_{y_4}^{-} &= \varphi_{y_2}^{+} \end{aligned} \tag{4.12}$$

In a similar way the constraint equations for zones 3 and 5 are:

$$\begin{aligned} u_{0_5}^{-} &= u_{0_3}^{+} \\ v_{0_5}^{-} &= v_{0_3}^{+} \\ w_{0_5}^{-} &= w_{0_3}^{+} \\ \varphi_{x_5}^{-} &= \varphi_{x_3}^{+} \\ \varphi_{y_5}^{-} &= \varphi_{y_3}^{+} \end{aligned} \tag{4.13}$$

As explained before the touching surfaces of the sublaminates 2 and 3 are bonded in a fashion that a through-thickness continuity is attained across the touching surfaces. To maintain the

through-thickness continuity the displacements of the touching surfaces of these two sublaminates need to be equal:

$$u_{0_2} + \varphi_{x_2}\frac{h_1}{2} = u_{0_3} - \varphi_{x_3}\frac{h_2}{2}$$

$$v_{0_2} + \varphi_{y_2}\frac{h_1}{2} = v_{0_3} - \varphi_{y_3}\frac{h_2}{2} \tag{4.14}$$

$$w_{0_2} = w_{0_3}$$

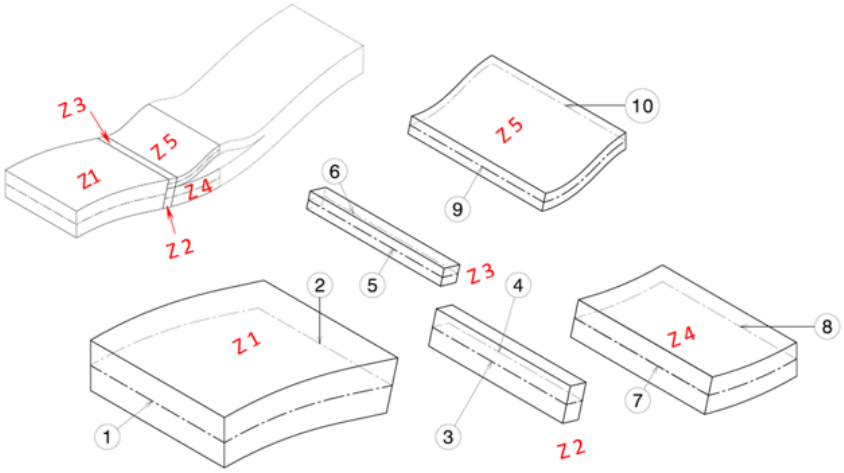

Interface	DOF
1	$u_{0_1}^-, v_{0_1}^-, w_{0_1}^-, \varphi_{x_1}^-, \varphi_{y_1}^-$
2	$u_{0_1}^+, v_{0_1}^+, w_{0_1}^+, \varphi_{x_1}^+, \varphi_{y_1}^+$
3	$u_{0_2}^-, v_{0_2}^-, w_{0_2}^-, \varphi_{x_2}^-, \varphi_{y_2}^-$
4	$u_{0_2}^+, v_{0_2}^+, w_{0_2}^+, \varphi_{x_2}^+, \varphi_{y_2}^+$
5	$u_{0_3}^-, v_{0_3}^-, w_{0_3}^-, \varphi_{x_3}^-, \varphi_{y_3}^-$
6	$u_{0_3}^+, v_{0_3}^+, w_{0_3}^+, \varphi_{x_3}^+, \varphi_{y_3}^+$
7	$u_{0_4}^-, v_{0_4}^-, w_{0_4}^-, \varphi_{x_4}^-, \varphi_{y_4}^-$
8	$u_{0_4}^+, v_{0_4}^+, w_{0_4}^+, \varphi_{x_4}^+, \varphi_{y_4}^+$
9	$u_{0_5}^-, v_{0_5}^-, w_{0_5}^-, \varphi_{x_5}^-, \varphi_{y_5}^-$
10	$u_{0_5}^+, v_{0_5}^+, w_{0_5}^+, \varphi_{x_5}^+, \varphi_{y_5}^+$

Figure 4.4 Interfaces of the laminate sublaminates

The constraint Eqs. (10-14) are enforced using a penalty function method which can be interpreted as considering an elastic adhesive with extremely high stiffness to hold the sublaminates together. The details of the penalty function method are discussed in a following section.

4.3.3 Equilibrium equations

The equilibrium equations are established using the stationary total potential energy principle. The total potential energy is expressed as:

$$\Pi = U + W \tag{4.15}$$

where U is the strain energy stored in the structure and W is the potential energy corresponding to external forces.

In the absence of body forces the potential energy of the applied forces reads as:

$$W = -\iint_S \vec{T} \cdot \vec{u}\, ds \tag{4.16}$$

where S is the boundary surface, $\vec{T}$ is the surface traction vector over the boundary and $\vec{u}$ is the displacement vector.

The equilibrium states are found as states in which the first variation of the total potential energy functional vanishes. The described condition is mathematically stated as:

$$\delta\Pi = 0 \tag{4.17}$$

In a displacement controlled postbuckling analysis, the external loading is applied in the form of an imposed movement of the edge of the plate. This edge displacement appears in the expression of strain energy, and therefore the potential energy of external forces is absent.

In the present work, the bond between different sublaminates is modeled using penalty functions which are analogous to assuming elastic adhesives holding the sublaminates in one piece. Given the elastic nature of these bonds, they too store energy once the plate is subjected to loading. Hence, in the particular structure under consideration, the energy is stored as the strain energy of sublaminates as well as in the elastic adhesive bonds:

$$U = \sum_{i=1}^{5} U_i + U_p \tag{4.18}$$

where U_i is the strain energy of zone i and U_p is the energy term corresponding to penalty functions collectively.

For a plate, the constitutive equation of which is presented in Eq.(4.7) the strain energy is expressed as:

$$U = \frac{1}{2}\left\{\iint \{\epsilon\}^T \begin{bmatrix} [A] & [B] & 0 \\ [B] & [D] & 0 \\ 0 & 0 & [H] \end{bmatrix} \{\epsilon\}\, dA\right\} \tag{4.19}$$

where $\{\epsilon\} = \begin{bmatrix} \varepsilon_x^0 & \varepsilon_y^0 & \gamma_{xy}^0 & k_x & k_y & k_{xy} & \gamma_{yz} & \gamma_{xz} \end{bmatrix}^T$

The penalty functions can be classified into three categories: The functions providing span wise continuity of displacement field, the functions providing interlaminar bonds in the plane of the delamination, and finally, the functions used for imposing the desired boundary conditions and loading.

The penalty function used to bond the edges of the sublaminates *1 and 2 reads as:*

$$U_p^{(1,2)} = \frac{1}{2}\int_{-\frac{l_y}{2}}^{\frac{l_y}{2}} \Big\{K_u(u_{0_1}^{+} - \Delta h_2 \varphi_{x_1}^{+} - u_{0_2}^{-})^2 + K_v(v_{0_{i1}}^{+} - \Delta h_2 \varphi_{y_1}^{+} - v_{0_2}^{-})^2 + K_w(w_{0_1}^{+} - w_{0_2}^{-})^2 + K_{\varphi_x}(\varphi_{x_1}^{+} - \varphi_{x_2}^{-})^2 + K_{\varphi_y}(\varphi_{y_1}^{+} - \varphi_{y_2}^{-})^2\Big\} dy \tag{4.20}$$

Similarly the penalty function used for connecting zones 1 and 3 is:

$$U_p^{(1,3)} = \frac{1}{2}\int_{-\frac{l_y}{2}}^{\frac{l_y}{2}} \Big\{K_u(u_{0_1}^{+} + \Delta h_3 \varphi_{x_1}^{+} - u_{0_2}^{-})^2 + K_v(v_{0_{i1}}^{+} + \Delta h_3 \varphi_{y_1}^{+} - v_{0_2}^{-})^2 + K_w(w_{0_1}^{+} - w_{0_2}^{-})^2 + K_{\varphi_x}(\varphi_{x_1}^{+} - \varphi_{x_2}^{-})^2 + K_{\varphi_y}(\varphi_{y_1}^{+} - \varphi_{y_2}^{-})^2\Big\} dy \tag{4.21}$$

In an abridged form the penalty functions bonding zone 2 to zone 4 and zone 3 to zone 5 are expressed as:

$$U_p^{(i,j)} = \frac{1}{2}\int_{-\frac{l_y}{2}}^{\frac{l_y}{2}} \Big\{K_u(u_{0_i}^{+} - u_{0_j}^{-})^2 + K_v(v_{0_i}^{+} - v_{0_j}^{-})^2 + K_w(w_{0_i}^{+} - w_{0_j}^{-})^2 + K_{\varphi_x}(\varphi_{x_i}^{+} - \varphi_{x_j}^{-})^2 + K_{\varphi_y}(\varphi_{y_i}^{+} - \varphi_{y_j}^{-})^2\Big\} dy \quad (i,j) = (2,4),(3,5) \tag{4.22}$$

The functions used to model the interlaminar adhesion between sublaminates 2 and 3 are the mathematical equivalent of a distributed elastic stiffness acting upon the differential movement of the touching surfaces of the two sublaminates and read as:

$$U_p^{(2,3)} = \frac{1}{2}\iint \Big\{K_u\Big[\Big(u_{0_2} + \varphi_{x_2}\frac{h_1}{2}\Big) - \Big(u_{0_3} - \varphi_{x_3}\frac{h_2}{2}\Big)\Big]^2 + K_v\Big[\Big(v_{0_2} + \varphi_{y_2}\frac{h_1}{2}\Big) - \Big(v_{0_3} - \varphi_{y_3}\frac{h_2}{2}\Big)\Big]^2 + K_w(w_{0_2} - w_{0_3})^2\Big\} dA \tag{4.23}$$

Theoretically, penalty stiffness values are supposed to be infinitely high to provide perfectly rigid bonds between the sublaminates, however, practically, choosing excessively high stiffness values would lead to numerical complications and oscillatory results. Attention must be paid to the fact that Eqs. (4.20)-(4.22) represent the bonds that act along a straight edge and provide span wise continuity while Eq.(4.23) introduces interlaminar bonds that provide in-thickness continuity. Given the different nature of these functionals, the proper values for the stiffnesses that appear in these equations are not generally similar.

Besides the bonds between the sublaminates, the boundary conditions are also applied using penalty functions and their corresponding penalty terms need to be included in the total potential energy functional. Throughout this work, the longitudinal (parallel to the x-axis) edges are assumed to be free to move in any direction and thus would require no additional constraint

equations. The boundary conditions considered along the transversal edge of the plate (as depicted in Figure 4.1) can be expressed as:

$$\begin{aligned} u_{0_1}^{-} &= \delta/2 \\ v_{0_1}^{-}, w_{0_1}^{-}, \varphi_{x_1}^{-}, \varphi_{y_1}^{-} &= 0 \end{aligned} \tag{4.24}$$

The symmetry boundary conditions along the transversal edges of zones 4 and 5 are applied by constraining the rotation about the y-axis and the longitudinal (x-direction) component of the displacements:

$$u_4^{+}, \varphi_{x_4}^{+}, u_5^{+}, \varphi_{x_5}^{+} = 0 \tag{4.25}$$

The penalty term corresponding to the boundary conditions described in Eqs. (21) and (22) reads as:

$$\begin{aligned} U_p^b = \frac{1}{2}\int_{-\frac{l_y}{2}}^{\frac{l_y}{2}} \Big\{ & K_u\left(u_{0_1}^{-} - \delta\right)^2 + K_v\left(v_{0_1}^{-}\right)^2 + K_w\left(w_{0_1}^{-}\right)^2 + K_{\varphi_x}(\varphi_{x_1}^{-})^2 + K_{\varphi_y}(\varphi_{y_1}^{-})^2 \Big\} dy \\ & + \frac{1}{2}\int_{-\frac{l_y}{2}}^{\frac{l_y}{2}} \Big\{ K_u\left(u_{0_4}^{+}\right)^2 + K_v\left(v_{0_4}^{+}\right)^2 + K_u\left(u_{0_5}^{+}\right)^2 + K_v\left(v_{0_5}^{+}\right)^2 \\ & + \left(K_{\varphi_x}(\varphi_{x_4}^{+})^2 + K_{\varphi_x}(\varphi_{x_5}^{+})^2\right) \Big\} dy \end{aligned} \tag{4.26}$$

Eventually the penalty term U_p in Eq. (5.17) is the sum of all the penalty terms as:

$$U_p = U_p^{(1,2)} + U_p^{(1,3)} + U_p^{(2,3)} + U_p^{(2,4)} + U_p^{(3,5)} + U_p^b \tag{4.27}$$

Once the expression of the total potential energy is obtained, the minimization is done by applying the Ritz method. The Ritz method seeks the displacement field corresponding to an equilibrium state in the form of series of separable approximate functions with unknown coefficients:

$$\psi = \sum_{m=1}^{M}\sum_{n=1}^{N} \Psi_{mn} X_m Y_n \tag{4.28}$$

where ψ represents the physical degrees of freedom of the structure (u, v, w, φ_x, φ_y) and Ψ_{mn}s represent the corresponding coefficients (U_{ij}, V_{ij}, U_{ij}, $\Phi_{x_{ij}}$, $\Phi_{y_{ij}}$).

After substituting the approximate functions into the total potential energy expression, the functional is obtained in terms of the unknown coefficients of the approximate functions. Thereafter, the equilibrium equations can be found by minimizing the total potential energy functional with respect to these coefficients:

$$\frac{\partial \Pi}{\partial \Psi_{mn}} = 0 \tag{4.29}$$

The approximate functions are complete sets capable of accommodating every possible deformed shape of the structure and are required to have nonzero derivatives to the highest degree of derivatives that appear in the total potential energy expression [100]. Conventionally, the Ritz functions are selected in a way that they satisfy the essential boundary conditions of a specific problem. However, in the present work, the derivation is done using the Legendre polynomials (see Appendix 1) and as explained above, the essential boundary conditions are imposed by modifying the total potential energy expression. The Legendre polynomials have the advantage of orthonormality which guaranties well-conditioned matrices. Adopting the penalty function method makes the developed formulation flexible with respect to the boundary conditions and loading. Furthermore, the derivation of the equilibrium equations involves carrying out numerous integrals which in nonlinear analyses should be repeated multiple times. The employment of orthogonal functions makes the integrations easier and more importantly faster. It is worthy of attention that Legendre polynomials are orthogonal over the interval $[-1\ 1]$ and therefore, to benefit from the aforementioned advantages for an interval of $\left[-{}^{l}/_{2}\ {}^{l}/_{2}\right]$ it is necessary to stretch each Legendre function by a ratio of ${}^{l}/_{2}$ and scale it by a factor of $\frac{1}{\sqrt{l}}$. For an $l_x \times l_y$ plate the functions in x and y directions are defined as:

$$X_i = \frac{L_i\left({}^{2x}/_{l_x}\right)}{\sqrt{l_x}} \tag{4.30}$$

$$Y_j = \frac{L_j\left({}^{2y}/_{l_y}\right)}{\sqrt{l_y}} \tag{4.31}$$

where L_i and L_j are the Legendre polynomials of ith and jth degree respectively

The functions X_i and Y_j inherit the orthogonality characteristic of original Legendre polynomials except that they are orthogonal over the intervals $\left[-{}^{l_x}/_{2}\ {}^{l_x}/_{2}\right]$ and $\left[-{}^{l_y}/_{2}\ {}^{l_y}/_{2}\right]$ respectively.

Given that the continuity in displacements across the interfaces of the different sublaminates is enforced through the penalty function method, each of the sublaminates can be modeled in a separate dedicated coordinate system. Here for all the sublaminates, the origin of the dedicated local coordinate system is located at the center of that particular sublaminate.

4.3.4 Delamination growth assessment

Determination of the possibility of the growth of a delamination under a certain level of loading is done by calculating the SERRs corresponding to the three fracturte modes. As the primary advantage of the employed penalty approach, the distribution of the interlaminar tractions can be found as the product of the relative displacements of the interfaces of zones 2 and 3 and the corresponding stiffnesses. Therefore, the energy release rate corresponding to the three fracture modes can be determined along the edge of the delamination using Irwin's crack closure integrals. The crack closure Integral calculates the energy release rate based on the assumption that the energy dissipated during the growth of a crack is equal to the energy required for closing the same grown crack. The crack closure integrals for a straight crack tip parallel to the y-axis located at $x = x_0$ read as:

$$G_I = \lim_{\delta x \to 0} \frac{1}{2\delta x} \int_{x_0}^{x_0+\delta x} \sigma_z(x-\delta x, y)\ \delta w(x,y) dx \tag{4.32}$$

$$G_{II} = \lim_{\delta x \to 0} \frac{1}{2\delta x} \int_{x_0}^{x_0+\delta x} \tau_{zx}(x-\delta x, y)\ \delta u(x,y) dx \tag{4.33}$$

$$G_{III} = \lim_{\delta x \to 0} \frac{1}{2\delta x} \int_{x_0}^{x_0+\delta x} \tau_{zy}(x-\delta x, y)\ \delta v(x,y) dx \tag{4.34}$$

where σ_z, τ_{zx}, and τ_{zy} are interlaminar stresses in the plane of the delamination and δw, δu, and δv are the relative displacements of the surfaces of the open crack.

Theoretically, in a purely elastic system, the crack tip stresses are singular. However, as in the present method, the bonding of the sublaminates is modeled using finite values for the interlaminar stiffnesses, and therefore, a finite value for each of the crack tip stresses is obtained. Another side effect of using finite values for interlaminar stiffnesses is the occurrence of relative displacements of the sublaminates in the region ahead of the crack. When carrying out crack closure integrals these infinitesimal relative movements are taken into account. Hence, the relative displacements are expressed as:

$$\delta w(x,y) = \left(w_{0_5}(x,y) - w_{0_4}(x,y)\right) - \left(w_{0_3}(x-\delta x, y) - w_{0_2}(x-\delta x, y)\right) \tag{4.35}$$

$$\begin{aligned}\delta u(x,y) = &\left[\left(u_{0_5}(x,y) + \frac{h_2}{2}\varphi_{x_5}(x,y)\right) - \left(u_{0_4}(x,y) - \frac{h_1}{2}\varphi_{x_4}(x,y)\right)\right] \\ &- \left[\left(u_{0_3}(x,y) + \frac{h_2}{2}\varphi_{x_3}(x,y)\right) - \left(u_{0_2}(x,y) - \frac{h_1}{2}\varphi_{x_2}(x,y)\right)\right]\end{aligned} \tag{4.36}$$

$$\delta v(x,y) = \left[\left(v_{0_4}(x,y) + \frac{h_1}{2}\varphi_{y_4}(x,y)\right) - \left(v_{0_3}(x,y) - \frac{h_2}{2}\varphi_{y_3}(x,y)\right)\right] - \left[\left(v_{0_2}(x,y) + \frac{h_1}{2}\varphi_{y_2}(x,y)\right) - \left(v_{0_1}(x,y) - \frac{h_2}{2}\varphi_{y_1}(x,y)\right)\right] \quad (4.37)$$

4.3.5 Contact

Depending on the properties of the sublaminates, the debonded surfaces may tend to interpenetrate. These potential interpenetrations are prevented using a scattered distribution of fictitious springs. To ensure the compression-only behavior of these spring their status (compression/tension) is checked in an iterative process and the individual springs under tension are eliminated from the array of springs. The iterations are repeated until a stable distribution of springs is achieved. The effect of these springs is incorporated in the analysis through the addition of their corresponding potential energies to the expression of the total potential energy of the structure. The energy stored in a rectangular $K \times L$ array of springs can be expressed as:

$$U_c = \frac{1}{2}K_c \sum_{k=1}^{K}\sum_{l=1}^{L} C_{k,l}[w_5(x_k, y_l) - w_4(x_k, y_l)]^2 \quad (4.38)$$

where x_k and y_l are the coordinates of each spring in the delaminated region, $C_{k,l}$ are binary coefficients defining the status (active/inactive) of a spring, and K_c is the stiffness of each spring.

4.4 Results and discussion

A MATLAB program was developed based on the derived formulation and an arc-length method [114] as a solver for nonlinear systems of equations. Compared to a conventional Newton-Raphson method, the arc-length method has the advantage of being able to trace the equilibrium path beyond the onset of instability. To examine the applicability of the methodology and the validity of its results, the program was used to solve certain benchmark problems. For the sake of validating the postbuckling results by comparing them with experimental data [113], the material properties and stacking sequences of the laminate were selected as those used in Ref. [113]. The considered laminates are constructed of 36 plies with an overall thickness of 0.201" and a stacking sequence of $(0/90/0)_{12}$. The orthotropic mechanical properties of the unidirectional composite lamina are listed in Table 4.1.

Table 4.1 Ply orthotropic material properties

E_{11}(GPa)	E_{22}(GPa)	G_{12}(GPa)	ν_{12}
100.7	8.27	3.45	0.25

In the first step to examine the validity of the proposed SERR calculation method, the developed model was used for modeling standard Double Cantilever Beam (DCB) and End-Loaded Split (ELS) tests (as depicted in Figure 4.5) and the results are compared with Finite Element (FE) analysis results obtained using ANSYS® multipurpose commercial software. In FE analyses the 3-dimensional layered element SOLID185 which is a linear element capable of accommodating stress stiffening and large deflection effects was used. The element is constructed with 8 nodes each of which has 3 translational degrees of freedom. Every 3 plies of the laminate were modeled using one layer of brick elements. The laminate was divided into two sublaminates by the delamination plane. The connection between the sublaminates was attained using the Interface element INTER205. The element INTER205 is an 8-node 3D element used with linear solid elements to simulate the adhesion between solid surfaces.

The SERR was calculated using the Virtual Crack Closure Technique (VCCT) applied on a predefined crack path. Obtaining accurate SERR values using VCCT requires a fine mesh especially in the vicinity of the crack tip. The mesh independence was achieved through the incremental enhancement of the mesh quality. To obtain more accurate results on both sides of the crack tip (the closed and open sides) a similar element size was used. The contact between the delaminated surfaces was incorporated in the analysis through the contact facility available in INTER205.

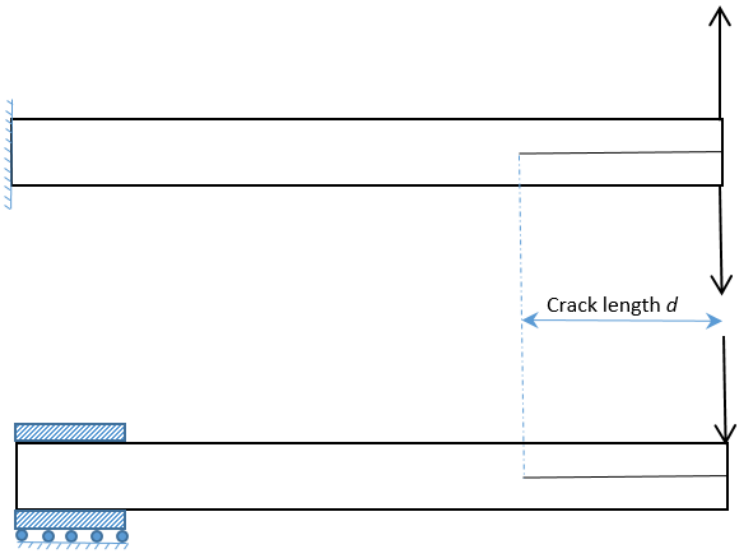

Figure 4.5 Schematic view of the test specimen, loading and boundary condition in DCB (top) and ELS (bottom) tests

Figure 4.6 shows the dimensions used for the DCB and ELS simulations. To demonstrate the applicability of the SERR calculation method for different sizes of crack, three delamination lengths 1", 1.5", and 2" were considered. As per the standard definition of these tests, the delamination was placed in the midplane of the laminate. All the analyses were performed under an arbitrarily selected force of 100N. In all the studied cases, the values of Mode *III* SERR (tearing mode) are negligible and therefore, these results are not presented. However, essentially, the determination of the tearing mode SERR is similar to that for the shearing mode, and in any case, where the values of Mode *III* SERR are of significance the adopted crack closure integrals can be utilized for determining them.

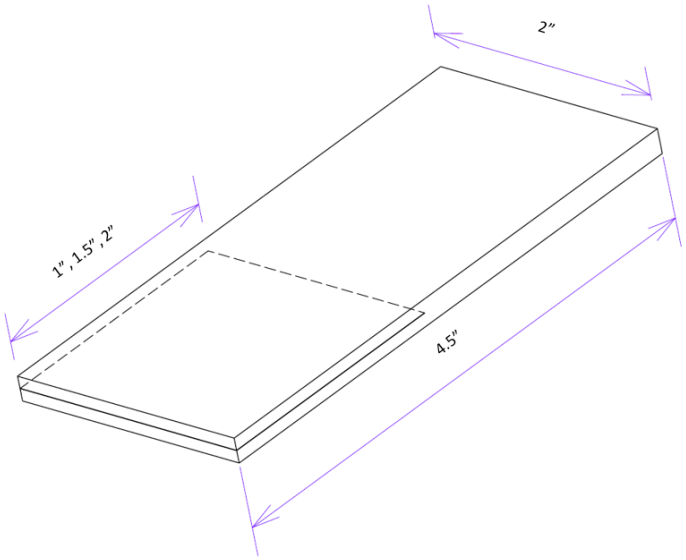

Figure 4.6 Dimensions of the specimen used in DCB and ELS test simulations

Figure 4.7 – 4.9 show the Mode I SERR (G_I) distribution along the edge of the delamination for the three delamination sizes. It can be observed that despite slight oscillations in the results calculated using the present method, the approximated values as well as the shape of their distribution along the crack tip are in good agreement with FE results. Both FE and the present method predict lower SERR values near the longitudinal (parallel to x-axis) edges of the plate. However, the present method predicts a sharper drop in SERR values in these areas. It can be observed that for the smallest delamination the SERR calculated using the present method is smaller than the values calculated using FE analysis. For larger delaminations, however, the estimated values are higher than FE results. It can be deduced that compared to FE analyses the present method predicts a slightly sharper increase in Mode II SERR with the increase in the delamination.

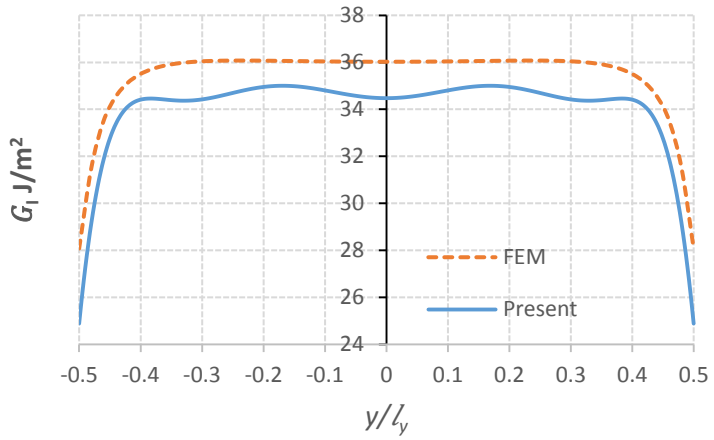

Figure 4.7 Mode I SERR for 1" delamination

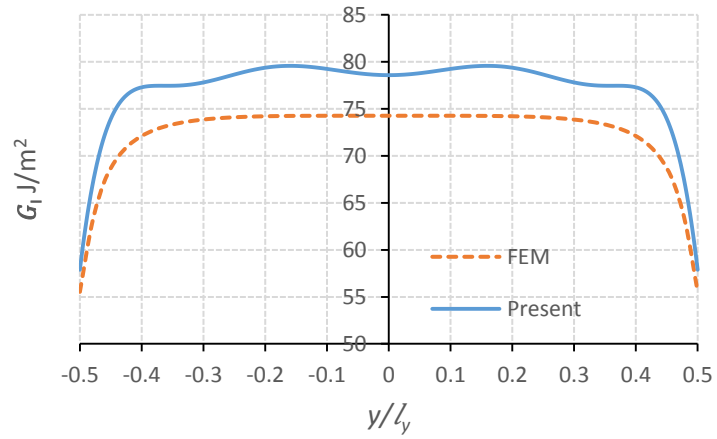

Figure 4.8 Mode I SERR for 1.5" delamination

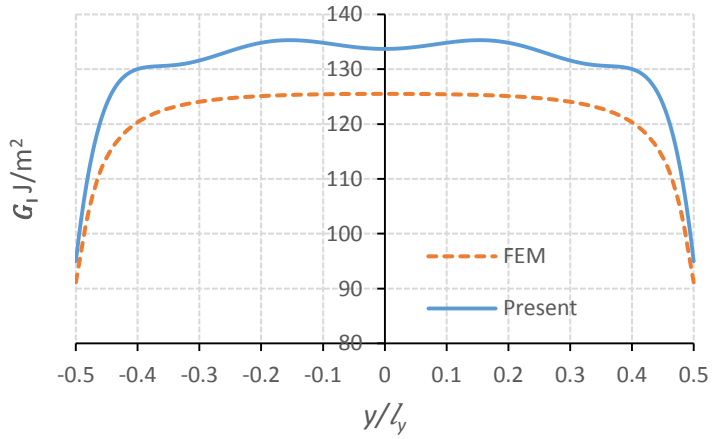

Figure 4.9 Mode I SERR for 2" delamination

Figure 4.10-4.12 depict the predicted Mode *II* SERR (G_I) distribution along the edge of the delamination in an ELS test with the described configuration. These results revealed that for the

ELS test the agreement between FE results and the results obtained using the current method is even closer than that of the DCB test. Unlike in the case of the DCB test, the values calculated for G_{II} are larger in the regions close to the longitudinal edges (parallel to x-axis) and therefore, under pure Mode II loading the propagation of a delamination can be expected to initiate from the sides as opposed to the case of a pure Mode I loading where the propagation is likely to initiate from the middle. For all the studied delamination sizes the values estimated using the present method are very slightly inferior to those obtained using FE analyses. The difference between the FE and present results tend to diminishes for larger delaminations.

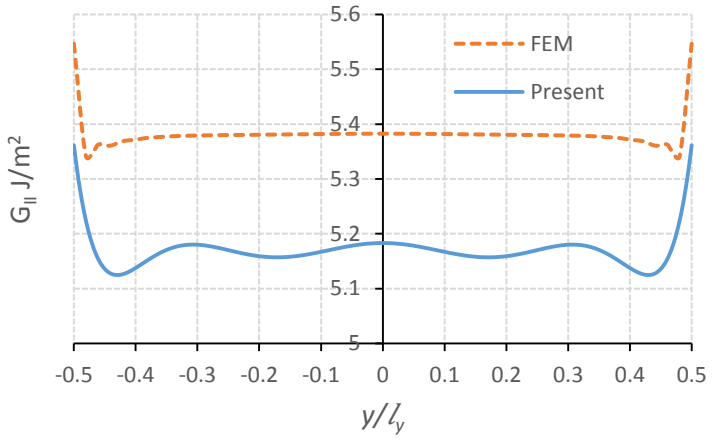

Figure 4.10 Mode II SERR for 1" delamination

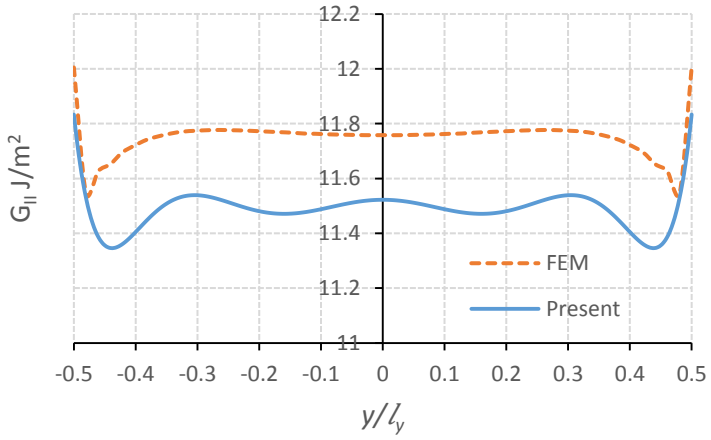

Figure 4.11 Mode II SERR for 1.5" delamination

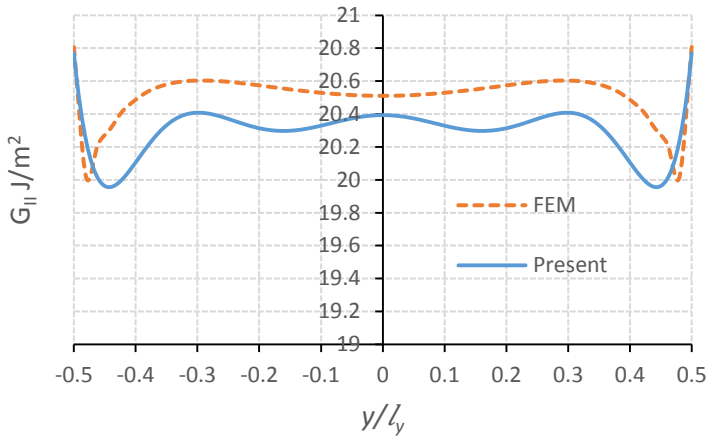

Figure 4.12 Mode II SERR for 2" delamination

In setting up the analyses two factors seem to highly impact the accuracy of the calculated SERRs. These factors are the length of the intermediate region (zones 2&3) and the stiffnesses assigned to the elastic interlaminar adhesions. It was established that the length of the intermediate region should be kept as small as possible however, it should not be smaller than the region ahead of the crack tip where the high gradients of interlaminar tractions are experienced. Regarding the penalty stiffnesses, it was observed that extremely high stiffness would yield highly oscillatory results for the interlaminar tractions and would compromise the accuracy of the results, while low stiffness values may lead to the underestimation of the calculated SERR. Even though finding proper values for these parameters is challenging, It was observed that once the proper values were found for a particular configuration, the same values could be invariably used for different geometrical configurations and loading magnitudes.

After the validity of the proposed method for finding the distribution of the energy release rate was proven, the developed model was used for simulating the buckling and postbuckling behavior of laminated plates with through-the-width delaminations. To probe the validity of the postbuckling results, the obtained results were compared with the experimental data presented in Ref. [113]. The special cross-ply stacking sequence along with the deformed shapes presented in Ref. [113] guarantee that the assumed symmetry boundary conditions are acceptable and would not impose any excessive constraints on the model. Of the samples studied in Ref. [113], two different configurations for which extensive and detailed data was presented in Ref. [113] were selected. The selected samples include a plate containing a midplane delamination of 1.5” of

length and a plate with near-surface delamination of 3” of length. The details of the dimensions of these two specimens are depicted in Figure 4.13.

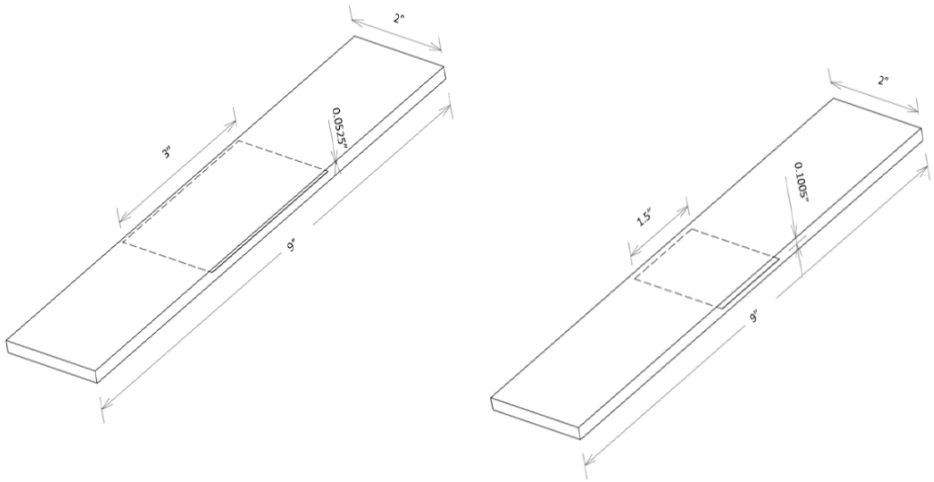

Figure 4.13 The dimensions of the delaminated samples

In the performed analyses, the external loading was applied in the form of an imposed end edge movement (end-shortening). For a perfectly symmetrical laminate subjected to in-plane compressive loading, nonlinear analyses may skip the onset of instability. Therefore, to simulate the postbuckling behavior, preexisting imperfections have to be incorporated. Here, the imperfections are created by applying infinitesimal lateral forces (in the out-of-plane direction).

It was observed that by incorporating low levels of imperfections, the midplane delamination does not open up and the plate experiences a global buckling (Figure 4.14). Figure 4.15 shows the variation of the applied compressive stress with the normalized end-shortening (δ/l_x). The results obtained using the present development show a bilinear behavior. The kink point where the slope of the curve experiences a sudden drop can be regarded as the buckling point. Beyond the buckling point, the correlation is still linear, however, with a remarkably lower slope. In the experimental data, two distinct regions can be distinguished. Up to a certain level of external loading, a fairly linear correlation between the normalized end-shortening and the applied compressive stress is observed. Beyond the aforementioned loading level, a highly nonlinear correlation with a rapid drop (as opposed to the sudden drop in the calculated results) in the slope is noticed. Gu and Chattopkdhyay Ref. [113] regarded the point where the behavior transitions from linear to nonlinear as the buckling point. In both experimental and calculated results, the deviation from the initial linear behavior happens at the onset of lateral deflection. The critical buckling load obtained

using the present method shows close agreement with the experimental data, however, in the predicted postbuckling behavior a more noticeable deviation from experiments is observed. Given the fact that the deviation from the experimental data happens at the same time that the plate starts to deflect laterally (in the out-of-plane direction), the deviation may be attributed to an inconsistency between the bending stiffness of the plate and the bending stiffness calculated using the adopted lamination theory. Furthermore, the accumulation of damage and a gradual change in the shape and size of the delaminated region may contribute to the nonlinear postbuckling behavior in the experiments.

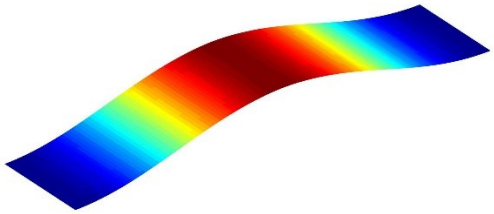

Figure 4.14 Buckled shape of the plate with midplane delamination

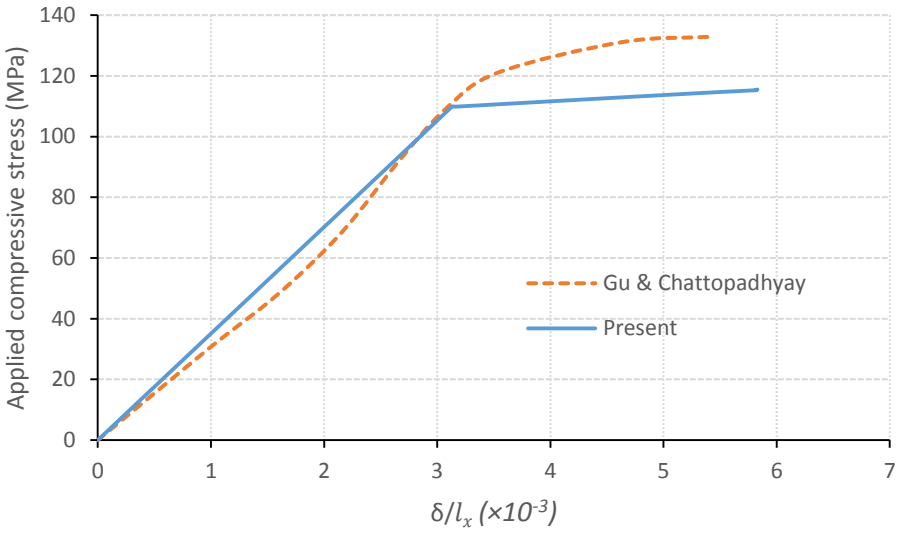

Figure 4.15 Variation of compressive stress with end-shortening for the plate with midplane delamination

As the buckled shape is a global deflection, both sublaminates simultaneously deflect in the same direction. Given the symmetry of the laminate stack up, the direction of the lateral deflection is determined by the initial imperfection. Figure 4.16 shows the applied compressive stress vs the

normalized lateral deflection of the plate at its center point ($^{\delta_t}/_{l_x}$). It can be appreciated that once the buckling load is reached the lateral deflection increases without a significant increase in the compressive stress. The predicted results perfectly agree with experimental data in the critical buckling load at which the out of plane displacement starts. In the postbuckling state, however, the calculated results exhibit a relatively sharper drop in the rate of change of the compressive stress. Despite the difference in the shape of the curves the predicted values seem to be in fair agreement with test results. The negative curvature of the experimental data in the postbuckling region may be interpreted as a gradual loss of stiffness due to damage accumulation and delamination propagation.

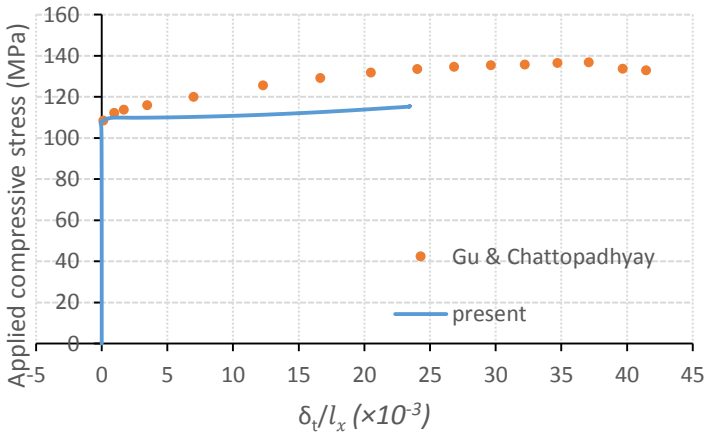

Figure 4.16 Variation of compressive stress vs maximum out-of-plane deflection for the plate with midplane delamination

Figure 4.17 shows the variation of the maximum value of SERR along the edge of the delamination with the normalized end-shortening ($^{\delta}/_{l_x}$) for the plate with the midplane delamination. Given the symmetrical stacking sequence of the laminate, in the prebuckling state, no interlaminar interactions occur in the plane of the delamination (midplane) and thus the SERR is zero. With the emergence of instability and consequently a bending deformation, the value of Mode *II* SERR starts to grow linearly with the applied end-shortening. As the debonded surfaces never lose contact, the delamination does not open and the Mode *I* SERR remains zero. Figure 4.18 depicts the distribution of the Mode *II* SERR along the edge of the delamination at different stages of loading. The top curve exhibits the largest magnitude corresponds to the largest applied end-shortening ($^{\delta}/_{l_x} = 5.78 * 10^{-3}$) and the lower curves correspond to intermediate loading levels in the postbuckling state.

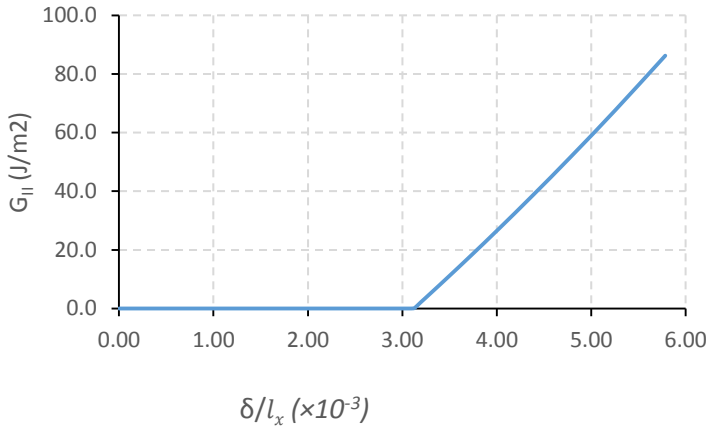

Figure 4.17 Variation of Mode II SERR with end-shortening for the plate with midplane delamination

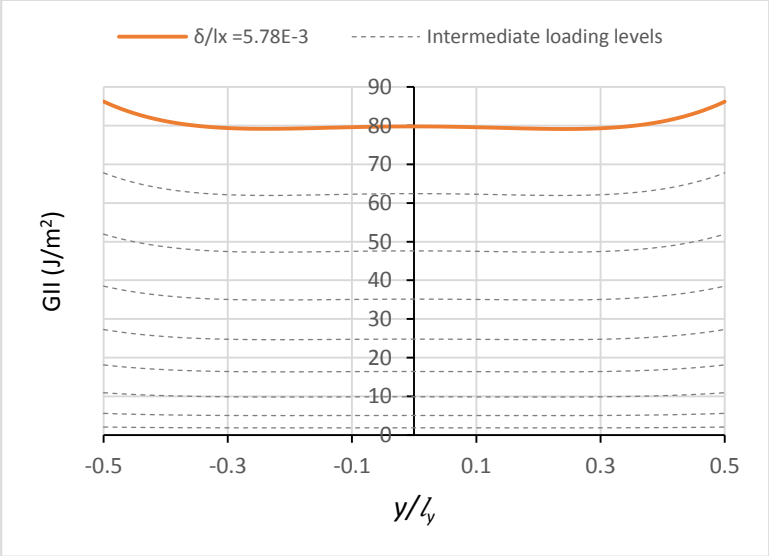

Figure 4.18 Distribution of Mode II SERR in the postbuckling state for the plate with midplane delamination

The instability of the specimen with the near-surface delamination (Figure 4.13 *(a)*) starts with a local buckling in the form of a bulge in the debonded thinner layer (Figure 4.19 left). The local buckling is almost immediately followed by a global deflection in the opposite direction leading to a mixed-mode shape (Figure 4.19 right). Given the larger thickness and consequently larger stiffness of the bottom sublaminate its deflection is dominant and highly impacts the deformation of the thinner sublaminate.

Figure 4.20 shows the variation of the applied compressive stress vs. the normalized end-shortening. Similar to the plate with a midplane delamination, in the prebuckling state the correlation between the compressive stress and end-shortening is linear. However, the results

obtained using the present method show a steeper slope which is an indication of a slight discrepancy between the calculated in-plane stiffness matrix ($[A]$) and that of real composite plate. The slight deviation from a perfectly linear behavior in the experiment is considered to be caused by a sudden growth of the delaminated region [113].

Similar to the experimental data, the present method predicts a nonlinear correlation between the applied compressive stress and end-shortening. It can be observed that the local buckling does not change the behavior of the plate significantly and the linear behavior is mostly disturbed by the emergence of the mixed buckling mode.

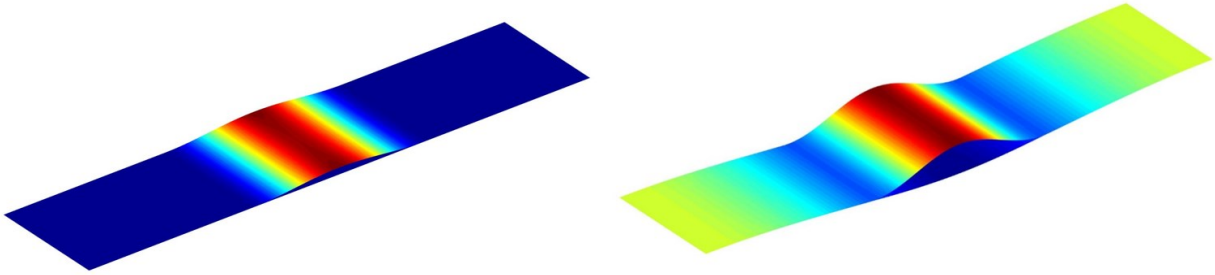

Figure 4.19 local (right) and mixed (left) buckled shapes of the specimen with near-surface delamination

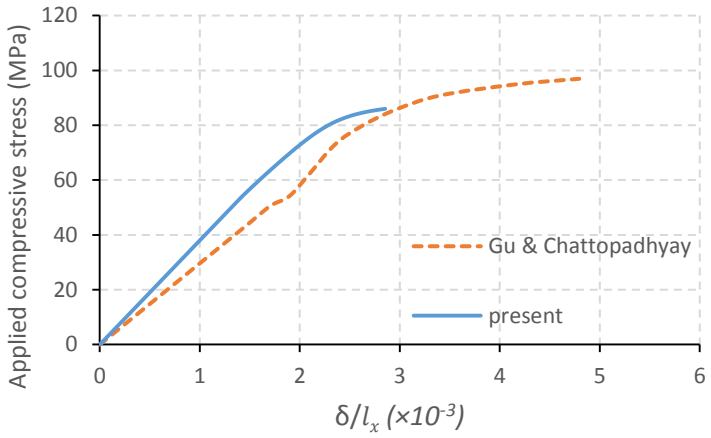

Figure 4.20 Variation of compressive stress with End-shortening for the plate with near-surface delamination

Figure 4.21 depicts the normalized out-of-plane deflection of the center point ($^{\delta_t}/_{l_x}$) of the top and bottom sublaminates (see Figure 4.13) vs the applied compressive stress. The predicted results, as well as the experimental data, show that the thinner (top) sublaminate starts to deflect first and with a further increase in the compressive loading the thicker sublaminate starts to deflect as well. Given the er stiffness of the thicker sublaminate, its deformation drastically affects the shape and the magnitude of the out-of-plane displacement of the thinner sublaminate. The drop in the out-of-

plane displacement beyond the compressive stress of 80 MPa is majorly due to the global deflection of the whole plate rather than the closing of the delamination. The calculated and the experimental results show an excellent agreement in predicting the onset of the local buckling but beyond the onset of the local buckling, the experimental data shows a more rapid loss of stiffness which may be attributed to the gradual growth of the delamination.

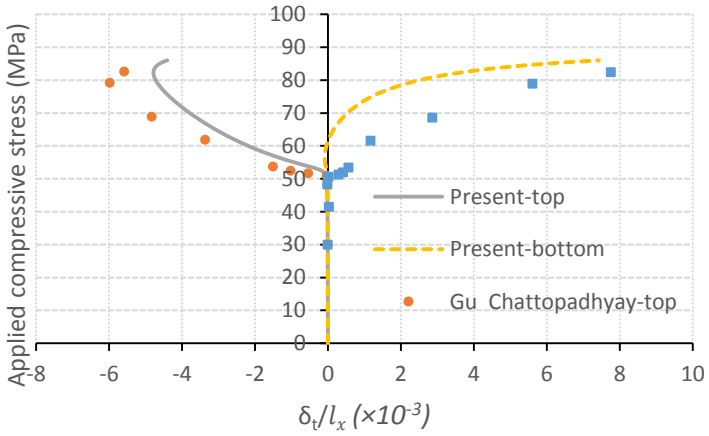

Figure 4.21 Variation of compressive stress vs maximum out-of-plane deflection for the plate with near-surface delamination

Figure 4.22 shows the variation of the maximum values of Mode *I* and Mode *II* SERRs along the edge of the delamination with the normalized end-shortening (δ/l_x). In the prebuckling state both Mode *I* and Mode *II* SERRs have negligible values. However, as buckling leads to the opening of the delamination as well as the bending of the sublaminates, beyond the critical buckling load both SERRs start to rise. Unlike the plate with midplane delamination, the SERRs corresponding to both fracture modes have nonlinear correlations with the applied end-shortening. Figure 4.23 and 4.24 depict the shape of the distribution of the Mode *I* and Mode *II* SERR along the edge of the delamination in different stages of loading. In both figures, the top curve exhibiting the highest magnitudes corresponds to the highest level of applied end-shortening ($\delta/l_x = 2.89 * 10^{-3}$) and the lower curves correspond to intermediate loading levels in the post buckling regime.

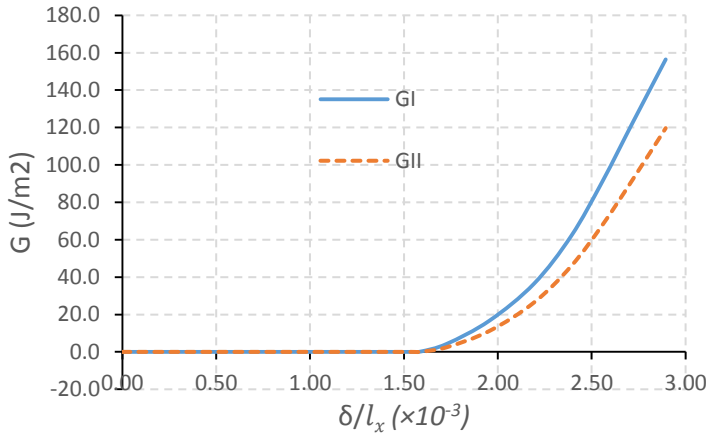

Figure 4.22 Variation of Mode I and Mode II SERR with end-shortening for the plate with midplane delamination

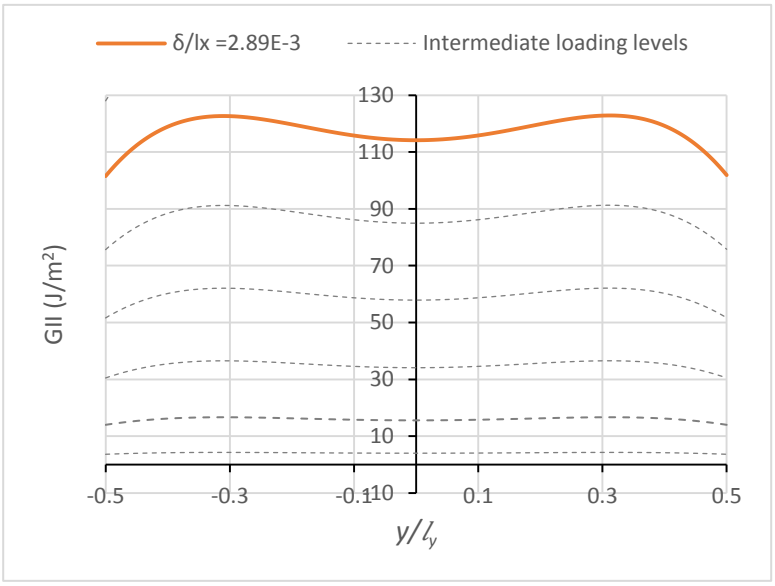

Figure 4.23 Distribution of Mode I SERR in the postbuckling state for the plate with near-surface delamination

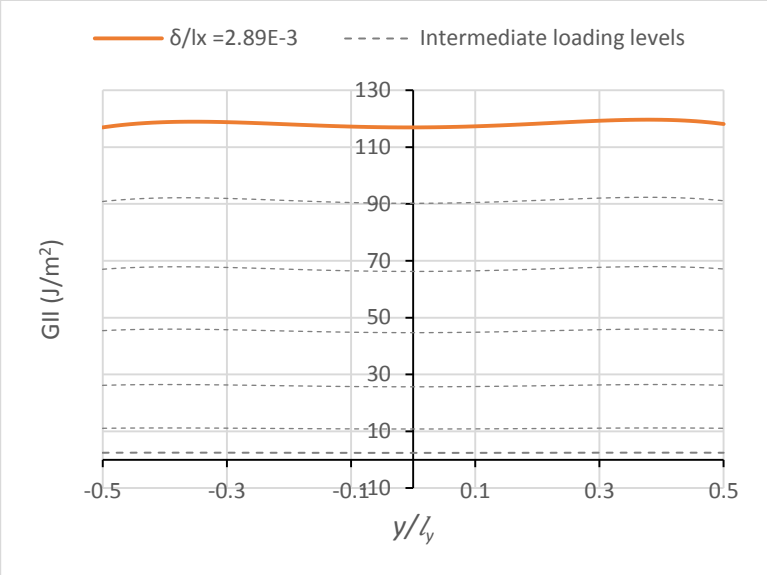

Figure 4.24 Distribution of Mode II SERR in the postbuckling state for the plate with near-surface delamination

Overall, the comparisons made between the calculated results and the experimental data show a fair agreement. In interpreting the comparisons, it should be taken into consideration that while the mathematical model deals with a fixed geometry, in reality, during the tests damage is accumulated and the delamination inevitably grows. This growth changes both the size and the shape of the delaminated region. Therefore, some of the deviations between the results may be attributed to the gradual accumulation of damage in the test samples which is not accounted for in the present simulations.

4.5 Conclusion

A new methodology for modeling the postbuckling behavior of composite plates with through-the-width delamination was developed. The focus of development was the fracture mechanics aspects of the buckling and postbuckling problems. The new technique vastly makes use of the penalty function method for multizone modeling and also for making available the interlaminar data that are required for delamination growth assessment. Through the development and the subsequent validation processes, the following conclusions were drawn.

- In the context of approximate solutions, the use of penalty functions facilitates modeling partitioned structures by circumventing the use of complex approximate functions required to reassure displacement field continuity.

- Through comparison with experimental data it was proved that the new partitioning scheme in conjunction with the penalty function method generates fairly accurate predictions for the behavior of partially delaminated composite plates in the postbuckling state.
- The new partitioning scheme provides a more consistent displacement field ahead of a crack tip in the intact region of a delaminated plate and improves the accuracy of the predicted behavior.
- The proposed technique for determining SERRs using the calculated interlaminar tractions showed promising performance for evaluating the potential growth of the delamination during the postbuckling response of the composite plate (with the pre-existing delamination).
- Despite the satisfactory accuracy of results for SERR, the determination of the influential parameters namely the length of the intermediate region and the stiffness of interlaminar elastic bonds proved to be challenging and requires further study.

Appendix

Legendre polynomials

$$L_0 = 1$$

$$L_1 = x$$

$$L_2 = \frac{1}{3}(3x^2 - 1)$$

$$L_3 = \frac{1}{2}(x^3 - 3x)$$

$$L_4 = \frac{1}{8}(35x^4 - 30x^2 + 3)$$

$$L_5 = \frac{1}{8}(63x^5 - 70x^3 + 15x)$$

$$L_6 = \frac{1}{16}(231x^6 - 315x^4 + 155x^2)$$

$$L_7 = \frac{1}{16}(429x^7 - 639x^5 + 315x^3 - 35x)$$

$$L_8 = \frac{1}{128}(6435x^8 - 12012x^6 + 6930x^4 - 1260x^2 + 35)$$

$$L_9 = \frac{1}{128}(12155x^9 - 25740x^7 + 18018x^5 - 4620x^3 + 315x)$$

$$L_{10} = \frac{1}{256}(46189x^{10} - 109395x^8 + 90090x^6 - 30030x^4 + 3465x^2 - 63)$$

Chapter 5: A unified linear-nonlinear formulation

5.1 Introduction

Generally, the postbuckling behavior of thin-walled structures including composite laminates is determined through nonlinear analyses conducted on a structure having slight imperfections. The main purpose of buckling and postbuckling analyses is predicting the behavior of a structure at and beyond the smallest compressive load that can render a structure unstable. Therefore, to ensure finding the solution corresponding to this smallest loading level, the shape of the imperfections are often inspired by the buckling mode shapes obtained using eigenvalue buckling analyses. In predicting the postbuckling behavior of delaminated composite plates, the imperfections to be incorporated in initial models need to be decided based on the expected buckling mode (local, global or mixed). Given the intricate geometry of delaminated plates, the buckling mode and subsequently the appropriate imperfections to be incorporated in the nonlinear analysis can be determined through the eigenvalue buckling analysis of the intact laminate (without considering the delamination) along with the eigenvalue buckling analysis of the delaminated sublaminate (the thinner sublaminate). As the delaminated region is generally small relative to the overall size of a plate, the overall behavior of the laminated plate can be approximated by analyzing an intact laminate of the same size. At the same time, the behavior of the delaminated layer can be approximated individually as an isolated laminate with restrained edges.

In this chapter through establishing a connection between the eigenvalue buckling and the nonlinear postbuckling solutions, a unified methodology for interrogating the instability behavior of delaminated composite plates is presented. The connection between the linear and nonlinear solutions is demonstrated through the comparison of the results obtained in chapter 3 with the results obtained for similar cases using the formulation presented in chapter 2 for eigenvalue buckling analysis of laminates subjected to in-plane constraints. Furthermore, through the comparison of the results obtained using nonlinear solutions with eigenvalue buckling analyses for intact plates, the efficiency of the nonlinear solution in accommodating the effect of in-plane constraints is examined.

5.2 Problem statement

In this chapter laminates with two different combinations of boundary conditions are considered. In the first series of analyses the material properties, stacking sequences and boundary conditions are the same as those used in chapter 3. However, in analyses involving the delaminated layer individually, a different set of boundary conditions compatible with the edge conditions dictated by the surrounding plate is adopted. Figure 5.1 depicts the explained boundary conditions. In the depicted boundary conditions, the end shortening corresponding to delaminated sublaminate is determined using the prebuckling midplane stains at the edges of the sublaminate. Assuming a relatively uniform strain distribution at the center of the plate the correlation between the global end shortening and normal x-axis strain would read as:

$$\varepsilon_x = \frac{\delta}{l} \tag{5.1}$$

Similarly the local end shortening can be found in terms of the x-axis strain and consequently the global end shortening as:

$$\delta_d = \varepsilon_x d = \frac{\delta d}{l} \tag{5.2}$$

where δ is the overall end shortening applied on the plate and δ_d is the end shortening imposed on the delaminated layer.

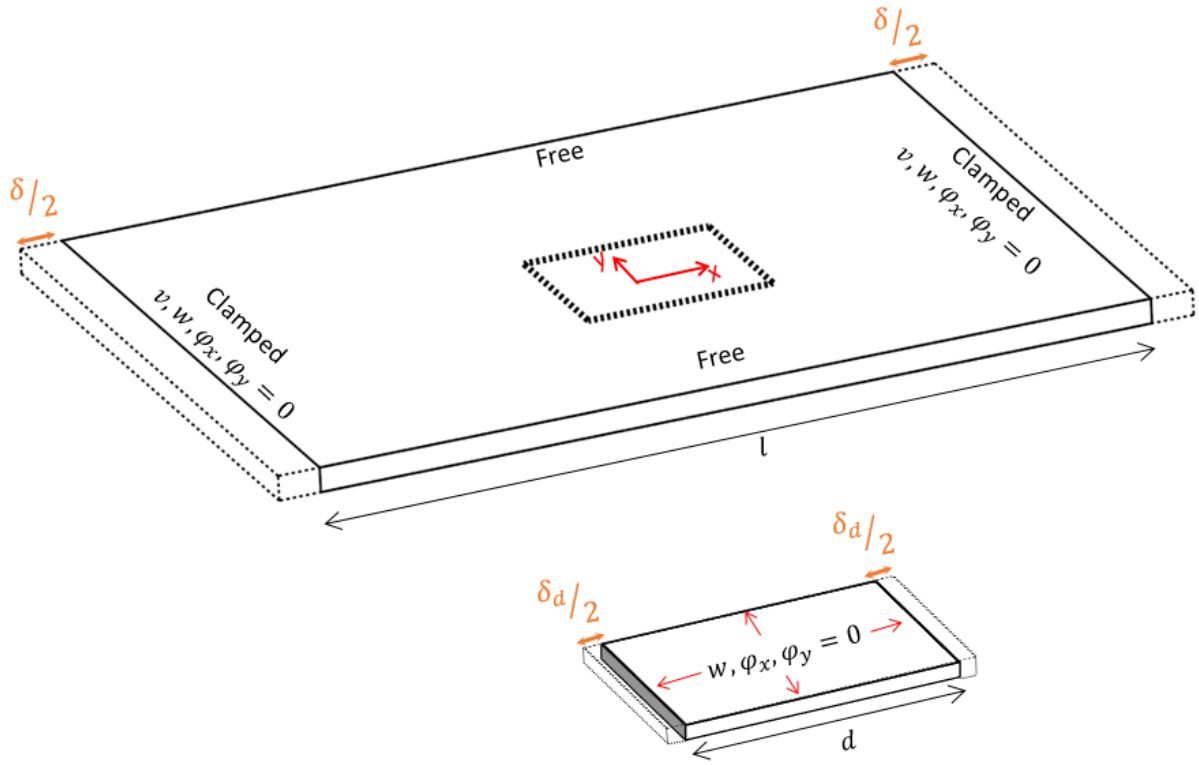

Figure 5.1 Schematic view of the delaminated plate and the debonded sublaminate and the corresponding boundary conditions and loading

The second series of analyses are done on plates with the same boundary conditions as those of chapter 2. Figure 5.2 shows the mentioned boundary conditions.

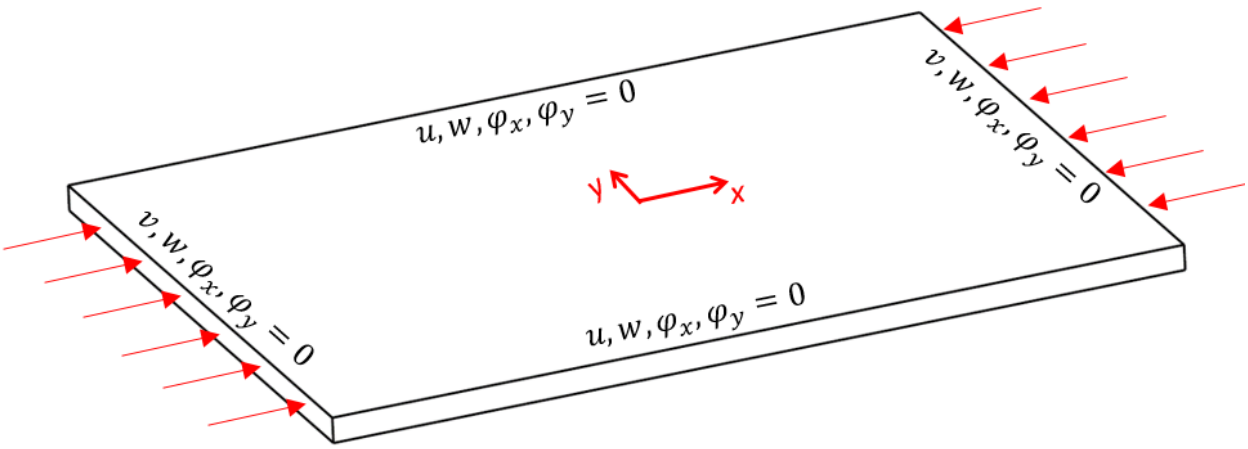

Figure 5.2 Schematic view of laminated plate and boundary conditions

5.3 Results and discussion

In the first step, the results presented in chapter 3 are plotted against the eigenvalue buckling solutions obtained for similar laminates and debonded sublaminates. The analyzed specimens are 150 mm×100 mm plates with different delamination sizes. The plates are considered to be made of a laminate with a stacking sequence of $(0/90/90/0)_3$. The orthotropic material properties and the thickness of the plies are listed in Table 5.1.

Table 5.1 orthotropic material properties and thickness of plies comprising the delaminated plates

E_{11}(GPa)	E_{22}(GPa)	G_{12}(GPa)	ν_{12}	*Ply thickness(mm)*
181	10.3	7.17	0.28	0.2

Figures 5.3-5.5 show the variation of the out-of-plane displacement of the center point of plate (w) with the applied end shortening (δ) for laminates with 30 mm×30 mm, 40 mm×40 mm, and 50 mm×50 mm delaminations respectively. It can be observed that the critical buckling load predicted using the eigenvalue buckling analysis (blue line) for the whole plate is slightly higher than the values predicted by nonlinear solution for an intact plate. This slight difference in the predicted critical buckling loads can be attributed to the higher order terms that are neglected in a linearized buckling analysis. Despite this difference, the eigenvalue buckling results are in fair agreement with the nonlinear solution. In all the studied cases the bottom sublaminate is thicker sublaminate and its deformation follows the overall deformation of the whole plate. Therefore the abrupt rise in the out-of-plane displacement at the center of this sublaminate may be perceived as the emergence of a global deflection. The Comparison of the three figures reveals that the difference between the predicted buckling load for the intact plate and the load under which the delaminated plate experiences a global deflection has a direct correlation with the dimensions of the delaminated region. In Figures 5.3 –5.5 the green horizontal line represents the critical buckling load predicted for the delaminated layer (the top sublaminate) using the eigenvalue buckling analysis. It can be appreciated that regardless of the size of the delamination, the critical buckling loads obtained using the linear analysis for the top sublaminate are larger than those predicted using the nonlinear analyses for the local buckling. The difference between the linear and nonlinear local buckling results seems to be rather insensitive to the size of the delamination. The presented results suggest that the linear buckling solution can reasonably predict the instability threshold for both local and global instabilities.

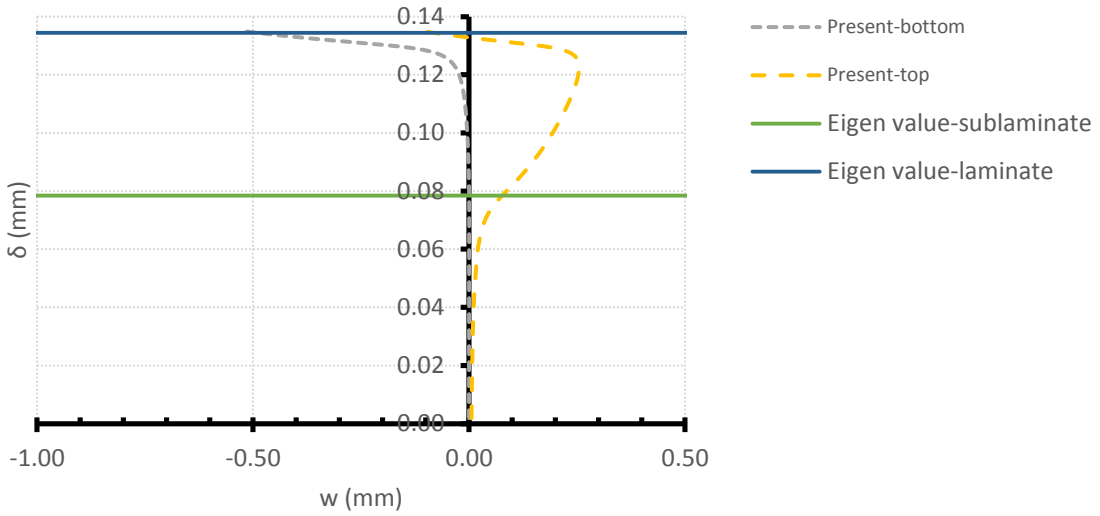

Figure 5.3 Center point out-of-plane displacement vs end-shortening for a plate with a 30 mm×30 mm delamination between the 2nd and the 3rd plies from top

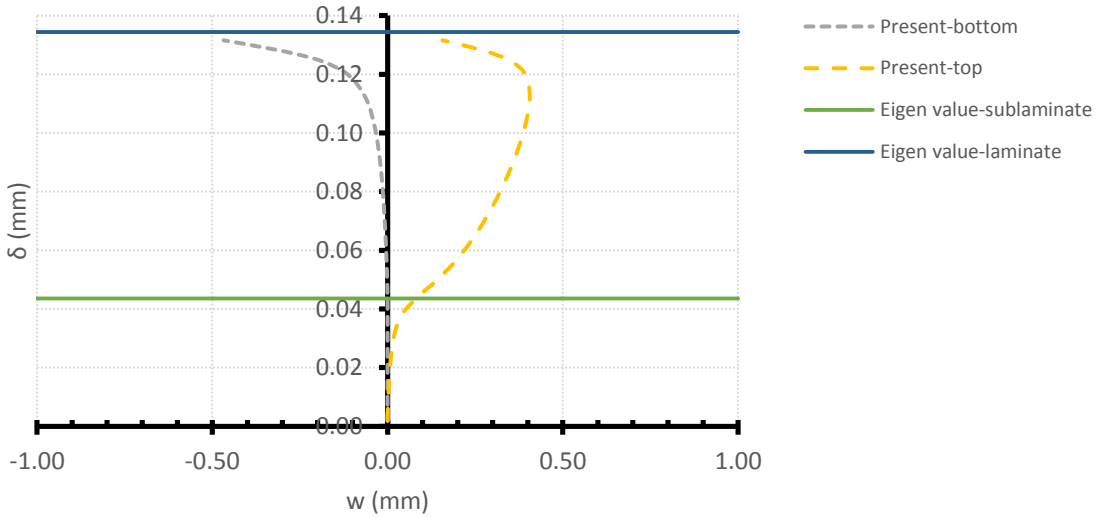

Figure 5.4 Center point out-of-plane displacement vs end-shortening for a plate with a 40 mm×40 mm delamination between the 2nd and the 3rd plies from top

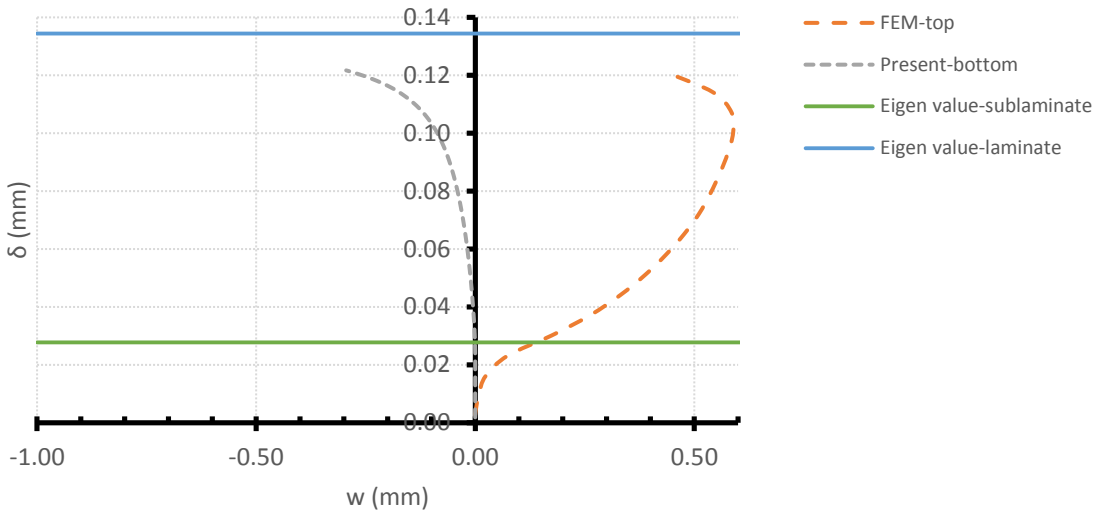

Figure 5.5 Center point out-of-plane displacement vs end-shortening for a plate with a 50 mm×50 mm delamination between the 2nd and the 3rd plies from top

Figures 5.6 and 5.7 present similar results for rectangular shaped delaminations of 30 mm×45 mm, and 30 mm×20 mm sizes respectively. While the results for the plate with the 30 mm×45 delamination show the same behavior as that of the previously discussed plates with square shaped delaminations, the plate with the 30 mm×20 mm delamination exhibits no local instability. The buckling load predicted using the eigenvalue buckling analysis closely matches the buckling load predicted using the nonlinear solution. The eigenvalue buckling analysis predicts a critical buckling load for the delaminated layer which is larger than the critical buckling load of the intact laminate. The higher critical buckling load of the sublaminate can be justified by taking into account that the debonded sublaminate has four clamped edges as opposed to the intact plate two of the edges of which are considered free. Besides the debonded sublaminate has remarkably smaller in-plane dimensions that can potentially lead to higher overall stiffness. Given the fact that the nonlinear analysis predicts a global buckling mode shape only, it can be deduced that in cases where the critical buckling load of the delaminated layer exceeds that of the overall plate a global buckling is to be expected. This argument is reinforced by the results obtained for plates with delaminations located deeper in the thickness of the laminate. Figure 5.8 shows the results for a laminate with a delamination between the 4th and the 5th plies from the top. Given the similarity of the results for the different delamination sizes, for the sake of brevity, only the nonlinear results obtained for the plate with a 30 mm×30 mm delamination are presented. However, eigenvalue buckling results for different sizes of delamination are presented. Obviously, the critical buckling

loads calculated for the three selected sizes of delaminated sublaminate are significantly larger than the critical buckling load predicted for the intact plate. Therefore, in neither of the cases local or mixed-mode buckling can be expected. This finding agrees with the global mode shape obtained for these cases using nonlinear buckling and postbuckling analyses.

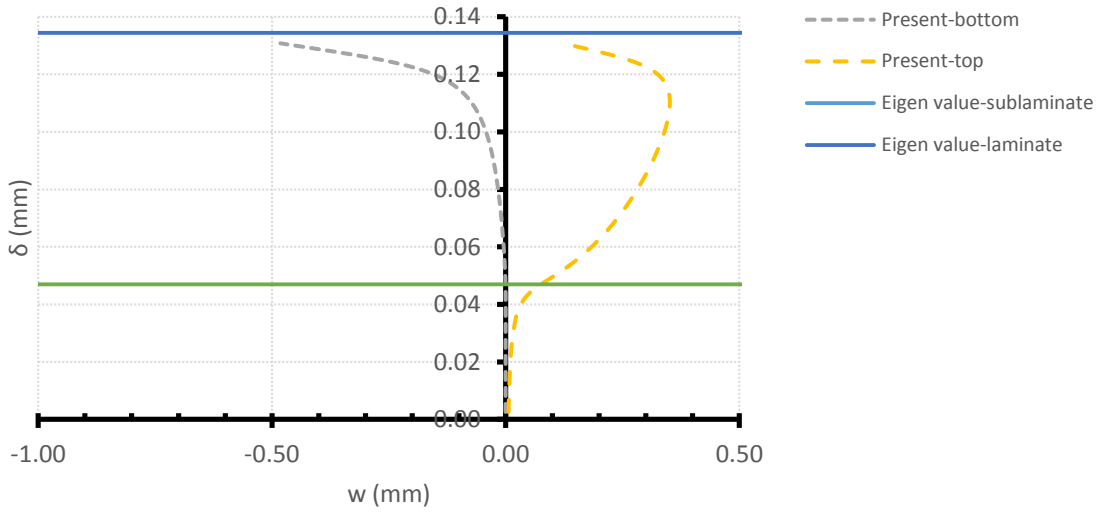

Figure 5.6 Center point out-of-plane displacement vs end-shortening for a plate with a 30 mm×45 mm delamination between the 2nd and the 3rd plies from top

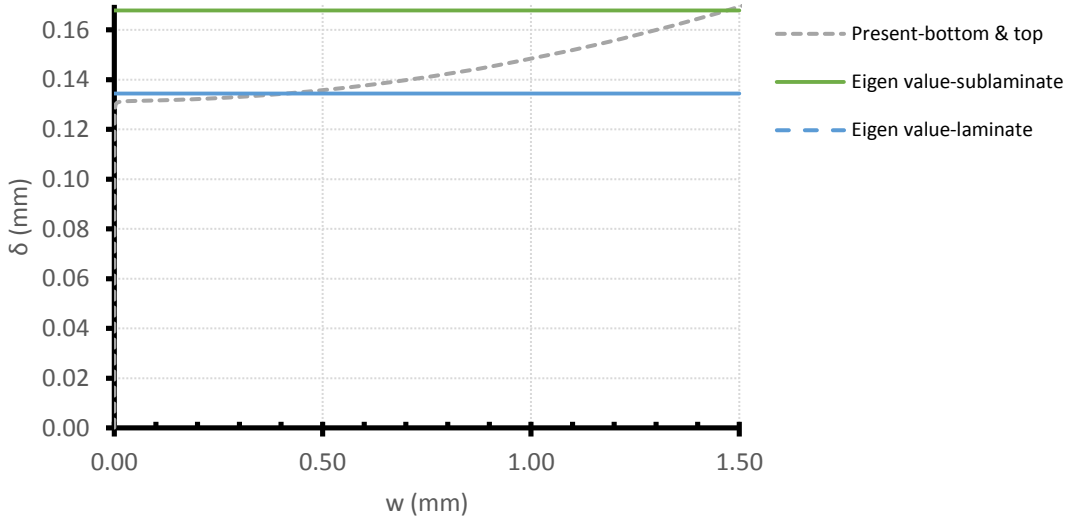

Figure 5.7 Center point out-of-plane displacement vs end-shortening for a plate with a 30 mm×20 mm delamination between the 2nd and the 3rd plies from top

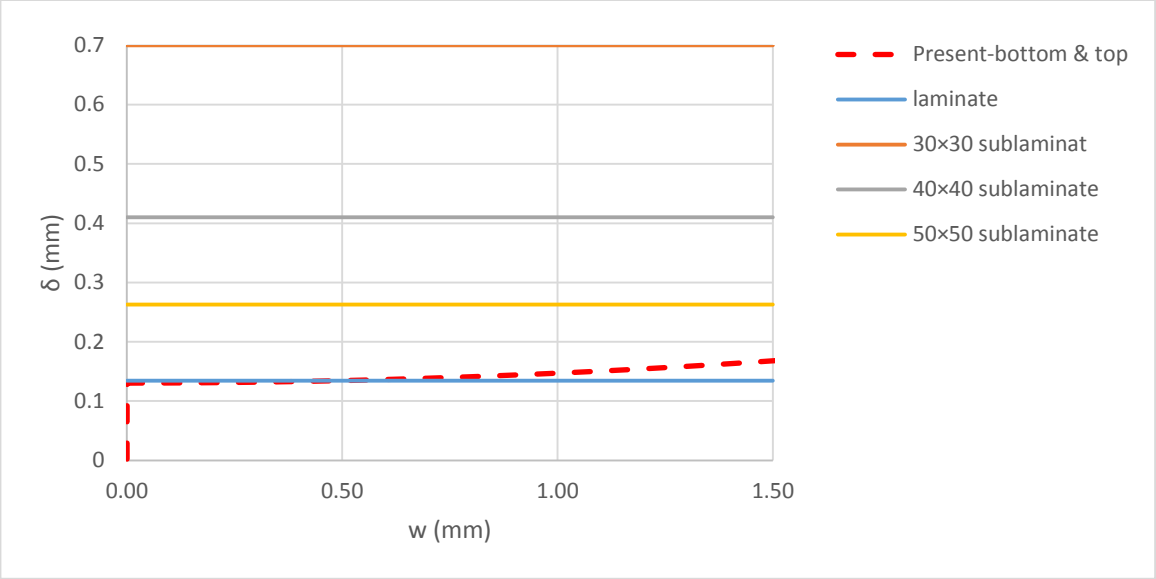

Figure 5.8 Center point out-of-plane displacement vs end-shortening for a plate with a 30 mm×30 mm delamination between the 4th and the 5th plies from top

In the second step to examine the capability of the nonlinear method presented in chapter 3 to properly incorporate the effect of in-plane constraints, a selected set of the results presented in chapter 2 was compared with the results obtained using nonlinear analyses for the same selected cases. The analyses were carried out on laminates with stacking sequences of $[0]_{10}$, $[(0/90)_2/(0)]_s$, $[(\pm30)_2/(30)]_s$, $[(\pm45)_2/(45)]_s$, and $[(\pm70)_2/(70)]_s$. the orthotropic material properties and the thickness of the plies is listed in table 5.2

Table 5.2 orthotropic material properties and thickness of plies comprising the delaminated plates

E_{11}(GPa)	E_{22}(GPa)	G_{12}(GPa)	ν_{12}	*Ply Thickness(mm)*
181	10.3	7.17	0.28	0.2

The analyzed specimens are 10”×10” and 15”×10” plates with no delaminations. The boundary conditions considered are similar to those used in chapter 2 (Figure 5.2). The results presented in Figures 5.9-5.13 show a very good agreement between the critical buckling loads obtained using the nonlinear and eigenvalue buckling analyses, however, it is noticeable that the critical buckling loads predicted using the eigenvalue buckling analysis are always larger than the predictions of the nonlinear analysis. In conducting the nonlinear analyses, the imperfections incorporated in the geometry were inspired by the buckling mode shapes obtained in eigenvalue buckling analyses. It was observed that applying inconsistent imperfections would lead to other buckling shapes with generally larger critical buckling loads. Therefore, to find the imperfect shape which would lead

to the buckling mode corresponding to the smallest critical buckling load, a preliminary eigenvalue buckling analysis seems necessary.

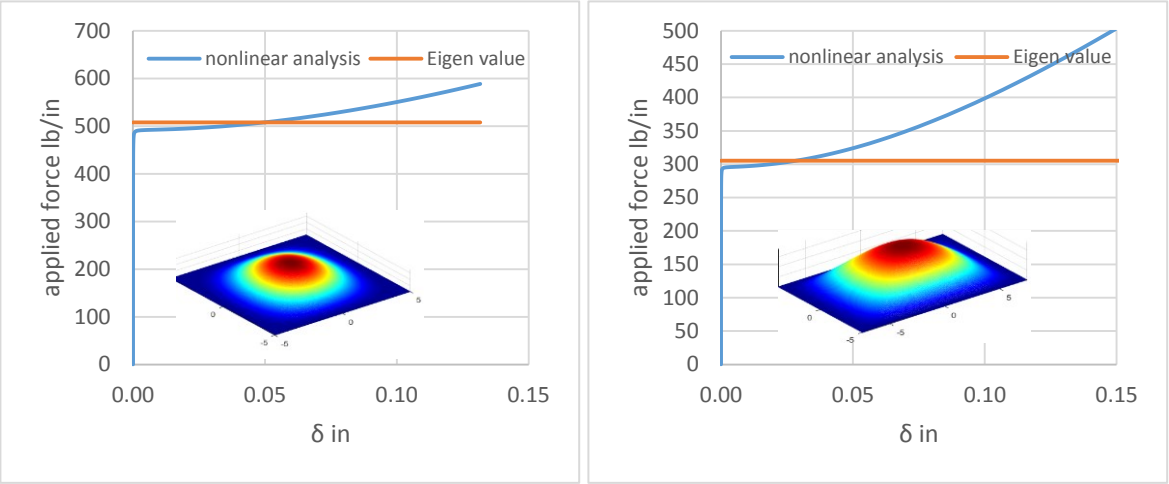

Figure 5.9 Center point out-of-plane displacement vs end-shortening for a 10"×10" plate (left) and a 15"×10" plate with a stacking sequence of $[0]_{10}$

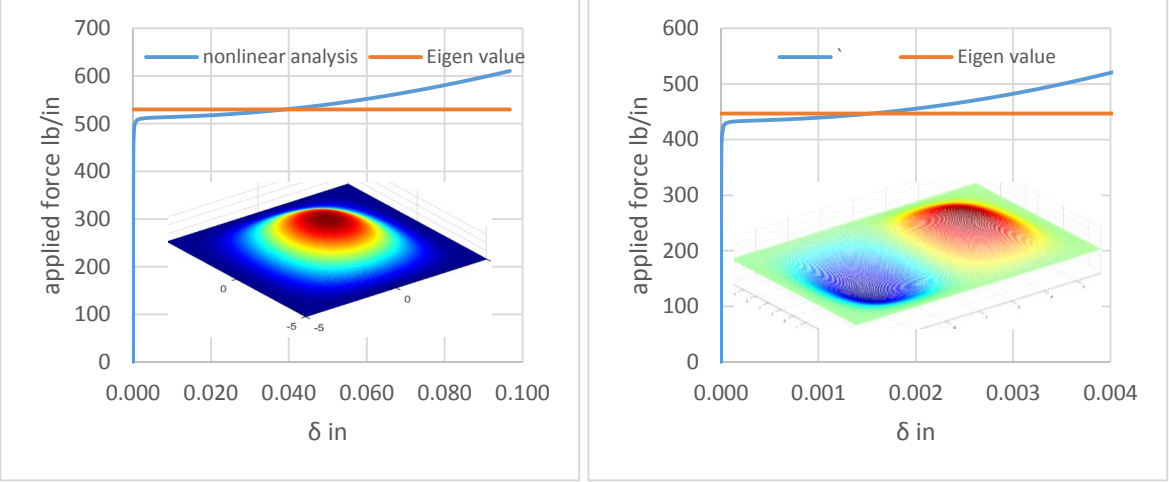

Figure 5.10 Maximum out-of-plane displacement vs end-shortening for a 10"×10" plate (left) and a 15"×10" plate with a stacking sequence of" $[(0/90)_2/(0)]_s$

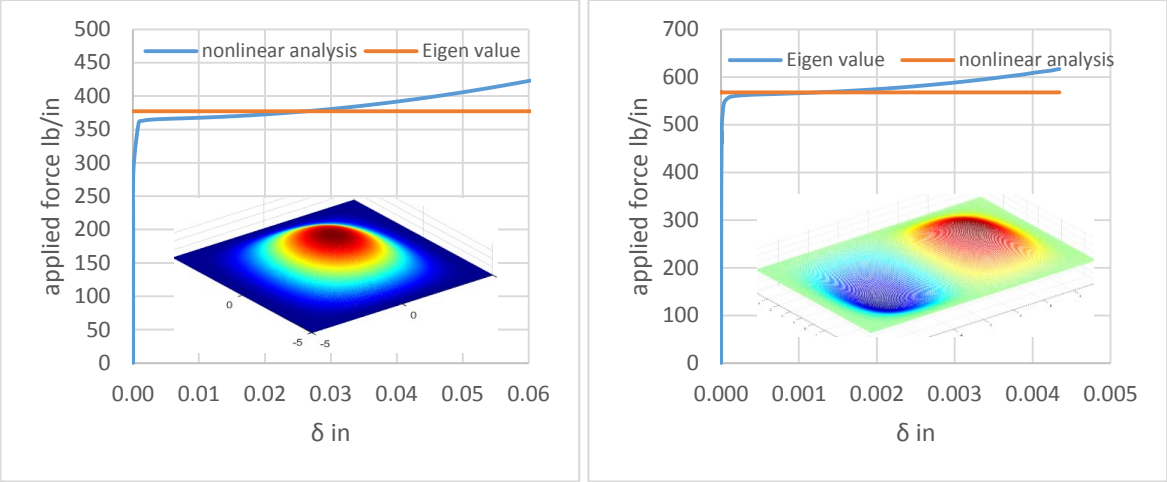

Figure 5.11 Maximum out-of-plane displacement vs end-shortening for a 10"×10" plate (left) and a 15"×10" plate with a stacking sequence of $[(\pm 30)_2/(30)]_s$

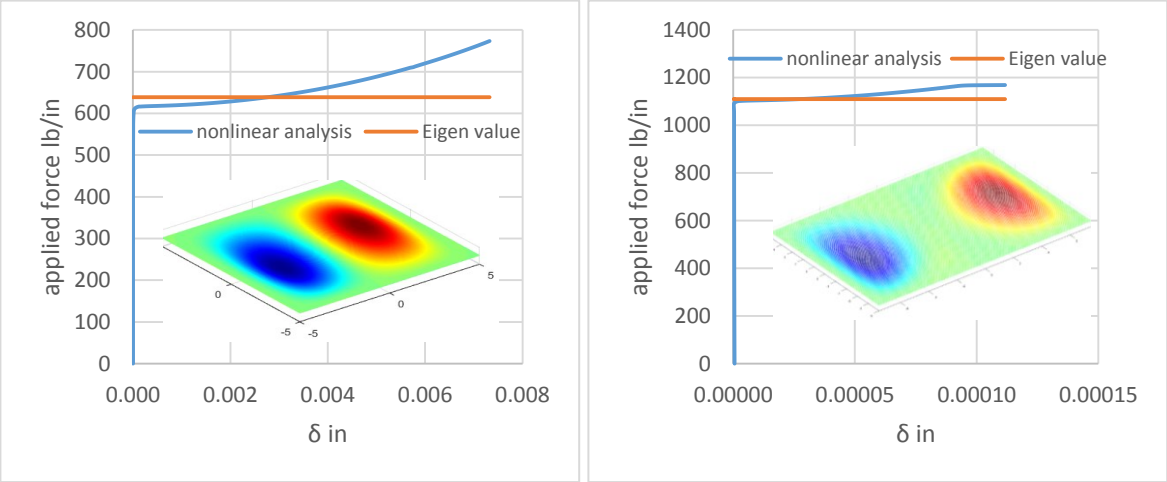

Figure 5.12 Maximum point out-of-plane displacement vs end-shortening for a 10"×10"plate (left) and a 15"×10" plate with a stacking sequence of $[(\pm 45)_2/(45)]_s$

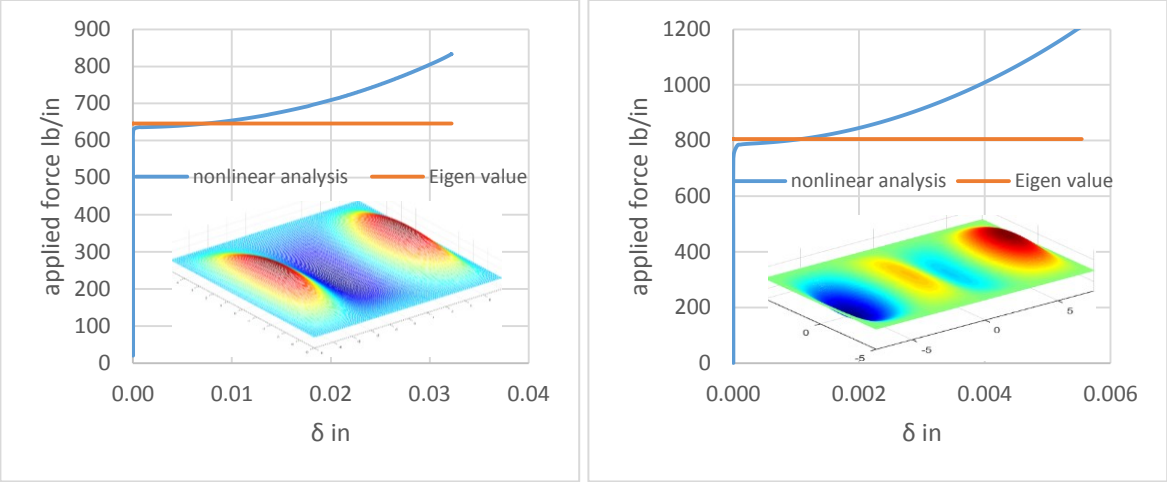

Figure 5.13 Maximum point out-of-plane displacement vs end-shortening for a 10"×10"plate (left) and a 15"×10" plate with a stacking sequence of $[(\pm 70)_2/(70)]_s$

5.4 Conclusions

In this chapter through combining the unique capabilities of eigenvalue buckling analysis and nonlinear postbuckling solution a unified methodology for interrogating the instability behavior of composite laminate with delamination was introduced. In doing so the following conclusions were drawn:

- The postbuckling results obtained using nonlinear analyses critically depend on the shape of the initial geometric imperfection; inconsistent initial imperfections may lead to buckling mode shapes with larger critical buckling loads.
- In order to find the smallest compressive loading level that can render a plate unstable the shape of the imperfections to be incorporated in nonlinear analyses can be determined using the results of eigenvalue buckling analyses.
- The buckling mode of delaminated plates (local, mixed or global) can be determined based on the critical buckling loads of the intact laminate and that of the debonded sublaminate. In cases where the critical buckling load of the sublaminate is significantly smaller than that of the intact plate, a local buckling followed by a mixed buckling shape is to be expected. In cases where the critical buckling load of the debonded sublaminate is larger than that of the intact plate, a global buckling would be the principal buckling mode.

- Agreement of the results obtained using the eigenvalue buckling and nonlinear buckling and postbuckling analyses reveals that despite using a significantly lower number of terms (9 terms × 9 terms) the developed nonlinear solution can very well accommodate the effects of in-plane constraints and the nonuniform prebuckling stress resultant distribution.

Chapter 6: Effect of rotational restraints on the stability of curved composite panels under shear loading

6.1 Foreword

In chapters 2-5 a methodology for predicting the buckling and postbuckling behavior of flat composite laminates with delamination was presented. In real life composite structures, however, panels are not necessarily flat. This is especially significant in the aerospace industry where the majority of the panels comprising the fuselages of aircraft are curved. The abundant use of curved composite panels along with the inevitability of the presence of delaminations in composite materials necessitates extending the applicability of the previously developed methodology to curved delaminated plates. This can be done by repeating the previously undertaken derivations using shell theories capable of accommodating the curvature of curved panels.

Similar to the process leading to the development of the methodology for flat panels, the first step in developing such a methodology for curved panels would be developing a linear buckling solution. In the context of the instability of curved composite panels, this linear buckling solution would serve the same purpose as that of the development presented in chapter 2 for flat plates. The eigenvalue buckling analysis is used for interrogating the instability behavior of intact curved panels as well as that of the sublaminates on the two sides of the delamination plane. Given potentially different boundary conditions of the intact panel compared to the sublaminates, in order for a single buckling solution to be applicable to both, it should be flexible with respect to boundary conditions. This flexibility can be achieved by developing a solution for curved plates subjected to rotational edge restraints.

In this chapter, as the first step in extending the methodology to curved panels, an eigenvalue buckling solution for rotationally restrained curved composite panels based on the FSDT and the Ritz method is presented. The effects of rotational restraints acting upon the edges of the panel are incorporated in the solution using a penalty function method. The penalty function method used for modeling edge restraints provides the facility of simulating the intact curved plates with flexible boundary conditions ranging from simply supported to clamped. The debonded sublaminates, however, are modeled as thin curved films with clamped boundary conditions dictated by the surrounding substrate. In a similar manner, as was explained in chapter 5, through the comparison of the critical buckling loads obtained for the intact curved plate and the sublaminates, the buckling mode (local, mixed, global) of the delaminated panel can be determined. Eventually, the information obtained through the eigenvalue analyses can be used for

determining the proper shape of imperfection to be incorporated in the nonlinear postbuckling analysis.

6.2 Introduction

The high strength to weight ratio of laminated composites makes them perfect candidates for lightweight aerospace structures. However, predicting their mechanical behavior has always been challenging due to their anisotropic material properties. A major criterion in designing composite structures is their buckling strength. Conventionally, buckling analyses are carried out under either simply supported or clamped boundary conditions. However, in real-world applications, namely in aircraft structures, panels are often joined to stiffer structural elements which restrain the rotation of the edges to some extent but not completely. Hence, neither of the aforementioned boundary conditions can perfectly reflect the true condition of the edges. The effect of these structural members on the overall behavior of panels can be accounted for by considering their equivalent rotational and/or torsional stiffness.

The stability of rotationally restrained panels has been the subject of many studies. Depending on the studied aspects, various simulation technics have been adopted by different researchers. The mathematical models mainly differ in the employed plate theories, the considered boundary conditions, and the solution methods.

The Classical Lamination Plate Theory (CLPT) is possibly the simplest and the most widely used theory for modeling the mechanical behavior of laminated composite plates and shells. Despite its wide use, the CLPT is notorious for overestimating the buckling strength of thicker plates and shells [115]. As a remedy, shear deformation theories have been used and proved to more accurately predict the buckling behavior of composite laminates[49,87,116–119].

The solution methods may be classified into the three categories of analytical, approximate, and numerical solutions. Approximate solutions such as the Ritz and Galerkin methods have been most widely used in the literature of restrained composite panels. The Galerkin method as a technique for converting partial differential equations to a weak form has been vastly used in the restrained plate buckling literature. When using the Galerkin method, restraints are imposed either by modifying the solution procedure [120] or by adjusting the displacement functions in a way that they accommodate the stiffness of the restraints automatically [121–123]. The Ritz method has been more widely used especially for simulating the buckling behavior of interconnected composite plates such as in thin-walled beam sections [124–126] or stiffened panels [127]. The Ritz method has also been used in works solely dedicated to the study of the effect of different combinations of boundary stiffness and loadings on the buckling of individual panels [128–131].

A major disadvantage of the Ritz method is its inflexibility with respect to boundary conditions. To remedy this shortcoming, the penalty function method has been used in some research works [117,132]. This approach makes it also possible to take advantage of functions with faster convergence rates while imposing the boundary conditions using penalty functions. In spite of the popularity of the Galerkin and Ritz methods in restrained panel buckling studies, analytical approaches have also been used in several instances [10,133–135].

Apart from analytical approaches, numerical methods such as finite strip [136,137], finite difference [138] and finite element[139] methods have also been used for analyzing the buckling of restrained composite panels. Numerical solutions are highly flexible with respect to geometry, loading and boundary conditions. However, given their high time and computation costs, they are not the best options for preliminary aircraft structure analyses. In general, aerospace structures consist of numerous panels, the performance of which needs to be verified under various conditions. The high number of load case-panels makes analytical and approximate solutions more favorable for preliminary verifications of such structures.

restrained isotropic cylindrical and anisotropic flat plates have been extensively studied, however, to the knowledge of the authors, the only study on the buckling of restrained composite curved panels is dedicated to buckling, postbuckling and crippling responses of these plates, under compressive axial loading [140]. Considering the significant use of cylindrical composite shells in the aerospace industry, studying the buckling behavior of cylindrical restrained panels is of crucial importance. Therefore, in this work, the stability problem of rotationally restrained curved composite panels under shearing forces, and the effect of the influential parameters are investigated.

In the present work, the formulation was developed based on the Sanders-Koiter shell theory and a first-order shear deformation approach. The linear stability equations were obtained on the basis of the minimum total potential energy principle and by employing the Ritz method. The restraints were simulated through a penalty function method. A specific class of laminates was sufficiently studied and characteristic curves were presented using no-dimensional parameters. In order to normalize the effect of torsional members a new non-dimensional parameter is introduced and used in the parametric studies.

6.3 Theoretical approach

In order to model the buckling behavior of curved laminated composite shells, the Ritz method which is based on the principle of minimum total potential energy was used. The formulation was developed based on the Sanders-Koiter shell theory and a first-order shear deformation (FSDT) displacement field. The details of the theory behind the developed formulation are explained in the subsequent sections.

6.3.1 Kinematics of cylindrical shells

In a first-order shear deformation theory, a laminate is treated as an equivalent single layer (ESL) in which, the displacements field is assumed to be of the form[141]:

$$u = u_0(x,y) + z\phi_x \quad (6.1)$$

$$v = v_0(x,y) + z\phi_y \quad (6.2)$$

$$w = w_0(x,y) \quad (6.3)$$

where x and y are the axes of a curvilinear coordinate system, u and v are the in-plane displacements corresponding to x and y directions respectively, w is the out-of-plane displacement, and ϕ_x and ϕ_y are the clockwise rotations of the normal cross-section around y and x-axes respectively. The variables denoted by $_0$ are the displacements associated with the mid-plane of the laminate.

According to the Sanders-Koiter shell theory and by using the displacement field introduced above, the linear mid-plane strains and shell curvatures are expressed in terms of displacements as [141]:

$$[\epsilon] = \begin{Bmatrix} \varepsilon_x^0 \\ \varepsilon_y^0 \\ \gamma_{xy}^0 \\ k_x \\ k_y \\ k_{xy} \end{Bmatrix} = \begin{Bmatrix} \dfrac{\partial u_0}{\partial x} \\ \dfrac{\partial v_0}{\partial y} + \dfrac{w_0}{R} \\ \dfrac{\partial u_0}{\partial y} + \dfrac{\partial v_0}{\partial x} \\ \dfrac{\partial \varphi_x}{\partial x} \\ \dfrac{\partial \varphi_y}{\partial y} \\ \dfrac{\partial \varphi_y}{\partial x} + \dfrac{\partial \varphi_x}{\partial y} - \dfrac{1}{2R}\left(\dfrac{\partial u_0}{\partial y} - \dfrac{\partial v_0}{\partial x}\right) \end{Bmatrix} \tag{6.4}$$

And the out-of-plane shear strains are:

$$[\Gamma] = \begin{Bmatrix} \gamma_{yz} \\ \gamma_{xz} \end{Bmatrix} = \begin{Bmatrix} \varphi_y + \frac{\partial w_0}{\partial y} - \frac{v_0}{R} \\ \varphi_x + \frac{\partial w_0}{\partial x} \end{Bmatrix} \tag{6.5}$$

Considering the nonlinear nature of the buckling phenomenon, nonlinear in-plane strains are also incorporated in the eigenbuckling analysis. These nonlinear strains, which are denoted by the superscript $'$, are expressed as[141]:

$$\epsilon' = \begin{Bmatrix} \varepsilon_x' \\ \varepsilon_y' \\ \gamma_{xy}' \end{Bmatrix} = \begin{Bmatrix} \dfrac{1}{2}\left(\dfrac{\partial v_0}{\partial x}^2 + \dfrac{\partial w_0}{\partial x}^2\right) \\ \dfrac{1}{2}\left[\left(\dfrac{\partial u_0}{\partial y}\right)^2 + \left(\dfrac{\partial w_0}{\partial y} - \dfrac{v_0}{R}\right)^2\right] \\ -\dfrac{\partial u_0}{\partial y}\left(\dfrac{\partial v_0}{\partial y} + \dfrac{w_0}{R}\right) - \dfrac{\partial v_0}{\partial x}\dfrac{\partial u_0}{\partial x} + \dfrac{\partial w_0}{\partial x}\left(\dfrac{\partial w_0}{\partial y} - \dfrac{v_0}{R}\right) \end{Bmatrix} \tag{6.6}$$

6.3.2 Constitutive equations

For a laminate with a thickness of h, when the origin of the coordinate system is located on the mid-plane of the laminate, the elements of the stiffness matrix of the laminate are given by[142]:

$$\left(\mathrm{A_{ij}}, \mathrm{B_{ij}}, \mathrm{D_{ij}}\right) = \int_{-h/2}^{h/2} Q_{i,j}(1, z, z^2)dz \tag{6.7}$$

where Q_{ij}s are the elements of the reduced plane stress stiffness matrix of each ply.

The elements of the stiffness matrix corresponding to the transverse shear deformations are calculated through:

$$H_{\mathrm{ij}} = k\int_{-h/2}^{h/2} C_{i,j}\, dz \quad for \quad i = 4{,}5 \tag{6.8}$$

where C_{ij}s are the elements of the complete stiffness matrix and k is the shear correction factor. Unlike isotropic materials no single value can be prescribed for the shear correction factor of anisotropic laminates. However, both the values prescribed for isotropic plates have been used in the literature [49–52] and were proved to lead to acceptable results. Throughout the present work a correction factor of $\frac{2}{3}$ was used.

The relationship between the vector of force and moment resultants and the vector of midplane strains and curvatures is described by the constitutive equations as follows:

$$\begin{Bmatrix}\{N\}\\ \{M\}\end{Bmatrix} = [S]\{\epsilon\} \tag{6.9}$$

where $[S] = \begin{bmatrix}[A] & [B]\\ [B] & [D]\end{bmatrix}$, $\begin{Bmatrix}\{N\}\\ \{M\}\end{Bmatrix} = \left[N_x\ N_y\ N_{xy}\ M_x\ M_y\ M_{xy}\right]^T$, N_x, N_y, and N_{xy} are membrane force resultants and M_x, M_y and M_{xy} are the moments around y and x-axes and the twisting moment, respectively.

The constitutive equation for transverse shear reads:

$$\begin{Bmatrix}Q_x\\ Q_y\end{Bmatrix} = [H]\{\Gamma\} \tag{6.10}$$

where Q_x and Q_y are resultant shear forces on xz and yz planes, respectively.

6.3.3 Total potential energy

According to the principle of minimum total potential energy, the equilibrium corresponds to a state in which the potential energy functional is stationary. The total potential energy of a restrained panel, in a stability analysis, is expressed as:

$$\Pi = U + U_r + V \tag{6.11}$$

where U is the strain energy, U_r is the potential energy of rotational springs and torsional elements and V is the potential energy of membrane stresses due to an out-of-plane displacement.

The strain energy of the shell is given by:

$$U = \frac{1}{2}\left\{ \int_0^a \int_0^b \{\epsilon\}^T [S] \{\epsilon\} dxdy + \int_0^a \int_0^b \{\Gamma\}^T [H] \{\Gamma\} dxdy \right\} \tag{6.12}$$

where a and b are curved panel axial and circumferential dimensions, respectively. Figure 6.1 depicts the geometry under consideration.

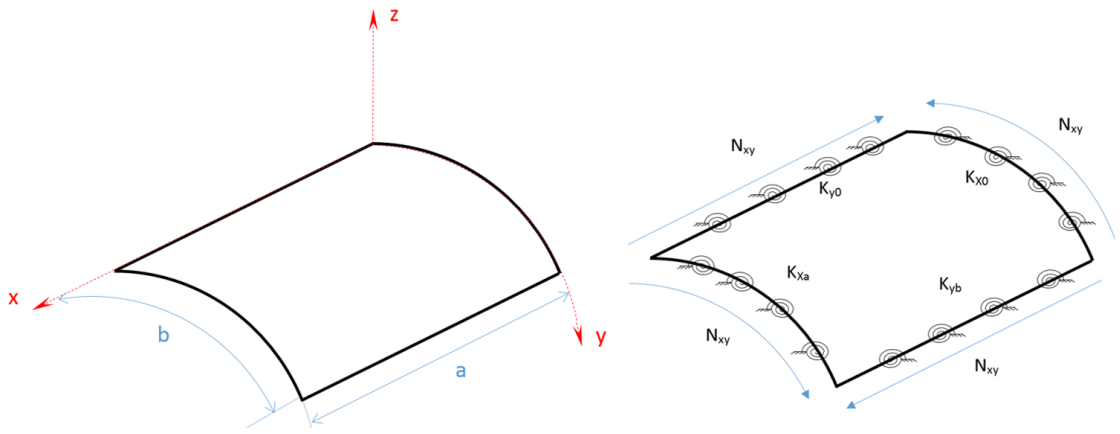

Figure 6.1 Geometry and the coordinate system of the cylindrical shell (left), the arrangement of the rotational springs and applied shear forces (right)

In Eq. (6.12), the first integral is the bending or flexural potential energy and the second integral represents the potential energy of the shearing deformation. The rotational stiffness may be applied as the reaction of rotational springs or as the reaction moment of torsional members such as stiffeners. The potential energy of rotational springs and torsional stiffeners can be written as:

$$\begin{aligned} U_r = \frac{1}{2}\Bigg\{ \int_0^b \Bigg[& K_{x0}(\varphi_x^2|_{x=0}) + K_{xa}(\varphi_x^2|_{x=a}) + GJ_{x0}\left(\frac{\partial \varphi_x}{\partial y}|_{x=0}\right)^2 \\ & + GJ_{xa}\left(\frac{\partial \varphi_x}{\partial y}|_{x=a}\right)^2 \Bigg] dy \\ & + \int_0^a \Bigg[K_{y0}(\varphi_y^2|_{y=0}) + K_{yb}(\varphi_y^2|_{y=b}) + GJ_{y0}\left(\frac{\partial \varphi_y}{\partial x}_{y=0}\right)^2 \\ & + GJ_{yb}\left(\frac{\partial \varphi_y}{\partial x}_{y=b}\right)^2 \Bigg] dx \Bigg\} \end{aligned} \tag{6.13}$$

where K_{x0}, K_{xa},K_{y0}, and K_{yb} are rotational stiffnesses of the rotational springs as shown in Figure 6.1 and GJ_{x0}, GJ_{xa}, GJ_{y0}, and GJ_{yb} are the corresponding torsional stiffnesses.

In real-life structures, these stiffnesses may be determined by assessing and simplifying the members to which a panel is joined. Figure 6.2 illustrates a fuselage skin panel joined to stiffer structural elements such as frames and stringers.

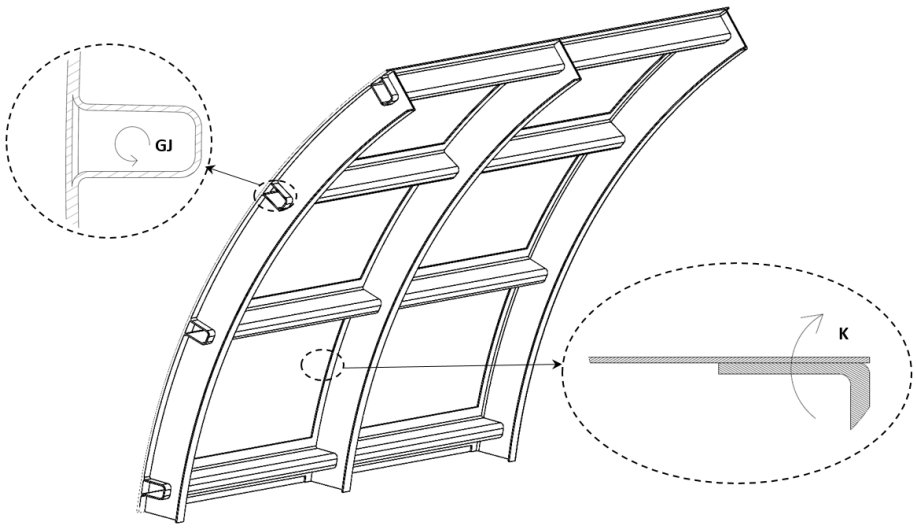

Figure 6.2 Schematic view of a curved panel and its surrounding structure

The energy associated with stress stiffening is[142]:

$$V = \iint_{0\,0}^{a\,b} \{N^0\}^T \{\epsilon'\} dxdy \tag{6.14}$$

where $\{\mathrm{N}^0\} = \left[N_x^0\ N_y^0\ N_{xy}^0\right]^T$ is the pre-buckling stress resultant field and here is assumed to be uniform and equal to the applied load along the edges of a panel In the current study, the curved panel is subjected to pure shear loading, therefore, $\{\mathrm{N}^0\} = \left[0\ 0\ N_{xy}^0\right]^T$.

6.3.4 The Ritz solution

The Ritz method seeks the displacement field corresponding to the buckled shape, in the form of a series of arbitrary displacement functions that satisfy the essential boundary conditions. These functions also need to be linearly independent and to have derivatives up to half the order of the corresponding partial differential equation[100]. The geometric boundary conditions considered in the current work are:

@ (x=0 and x=a): v=0, w=0, ϕ_y =0

@ (y=0 and y=b): u=0, w=0, ϕ_x=0

Thus as the geometric boundary conditions are similar to those of simply supported panels, the trigonometric functions used for simply supported boundary conditions are used for restrained panels as well. The trigonometric functions generally used for a simply supported cylindrical shell with the described boundary condition are[143]:

$$
\begin{aligned}
w &= \sum_{m=1}^{M}\sum_{n=1}^{N} W_{mn} \sin\frac{m\pi x}{a}\sin\frac{n\pi y}{b} \\
u &= \sum_{m=1}^{M}\sum_{n=1}^{N} U_{mn} \cos\frac{m\pi x}{a}\sin\frac{n\pi y}{b} \\
v &= \sum_{m=1}^{M}\sum_{n=1}^{N} V_{mn} \sin\frac{m\pi x}{a}\cos\frac{n\pi y}{b} \\
\varphi_x &= \sum_{m=1}^{M}\sum_{n=1}^{N} \Phi_{mn} \cos\frac{m\pi x}{a}\sin\frac{n\pi y}{b} \\
\varphi_y &= \sum_{m=1}^{M}\sum_{n=1}^{N} \Psi_{mn} \sin\frac{m\pi x}{a}\cos\frac{n\pi y}{b}
\end{aligned}
\tag{6.15}
$$

where M and N are the numbers of terms used in x and y directions respectively and W_{mn}, U_{mn}, V_{mn}, $\boldsymbol{\Phi}_{mn}$, and $\boldsymbol{\Psi}_{mn}$ are the unknown coefficients to be determined through the Ritz method.

Substituting Eqs. (6.12), (6.13), and(6.14) into Eq (6.11) we have the general expression of the total potential energy in terms of displacements and by substituting Eq. (6.15) in that expression we will have the same expression in terms of W_{mn}, U_{mn}, V_{mn}, $\boldsymbol{\Phi}_{mn}$, and $\boldsymbol{\Psi}_{mn}$. The solution is then sought by minimizing the total potential energy with respect to these undetermined coefficients. The resulting system of linear equations reads:

$$
\frac{\partial \Pi}{\partial W_{mn}} = 0,\ \frac{\partial \Pi}{\partial U_{mn}} = 0, \frac{\partial \Pi}{\partial V_{mn}} = 0,\ \frac{\partial \Pi}{\partial \Phi_{mn}} = 0,\ \frac{\partial \Pi}{\partial \Psi_{mn}} = 0, \tag{6.16}
$$

This will lead to a 5M×5N system of equations with a trivial solution. For a non-trivial solution, the determinant of the coefficients of the system of equations is set to zero and the critical buckling load multiplier and the associated mode shape are determined. To do so, for uniformly applied loads, $\{N^0\}$ needs to be written in the form:

$$
\{N^0\} = \lambda\{n^0\} \tag{6.17}
$$

where $\{n^0\} = [n_x\ n_y\ n_{xy}]^T$ is the vector that defines the proportion of each loading direction in the pre-buckled state.

In order to transform the system of linear Eqs.(6.16) into a classical eigenvalue problem, Eq. (6.17) is substituted into Eqs. (6.16) and after rearrangement we have:

$$\begin{aligned}
&\frac{\partial(U+U_r)}{\partial W_{mn}} + \lambda\frac{\partial V}{\partial W_{mn}} = 0\\
&\frac{\partial(U+U_r)}{\partial U_{mn}} + \lambda\frac{\partial V}{\partial U_{mn}} = 0\\
&\frac{\partial(U+U_r)}{\partial V_{mn}} + \lambda\frac{\partial V}{\partial V_{mn}} = 0\\
&\frac{\partial(U+U_r)}{\partial \Phi_{mn}} + \lambda\frac{\partial V}{\partial \Phi_{mn}} = 0\\
&\frac{\partial(U+U_r)}{\partial \Psi_{mn}} + \lambda\frac{\partial V}{\partial \Psi_{mn}} = 0
\end{aligned} \tag{6.18}$$

Putting these equations in the matrix form, we have:

$$[K + \lambda K_s]\begin{Bmatrix}\{W_{mn}\}\\ \{U_{mn}\}\\ \{V_{mn}\}\\ \{\Phi_{mn}\}\\ \{\Psi_{mn}\}\end{Bmatrix} = \{0\}_{5M\times 5N} \tag{6.19}$$

where K is composed of the first terms in Eqs.(6.18) and K_s is the matrix composed of the second terms of the same system of equations.

By multiplying Eq.(6.19) by K^{-1} from left, the solution is found as the inverse of the largest eigenvalue of the matrix $K^{-1}\times K_s$. The eigenvector corresponding to this value demonstrates the buckling mode shape.

6.4 Validation

Using the explained formulation, a MATLAB program was developed and used for parametric studies. All the results presented in this work including the results used for validation and Parametric studies are obtained using 15×15 term solutions. In order to validate the formulation and the program, in the first step, for the special case of isotropic simply supported curved panels the results were compared with the analytically generated curves[144]. The comparison is depicted

in Figure 6.3 and shows an acceptable agreement, however for some values of Z_b the difference rises to a maximum of 8%.

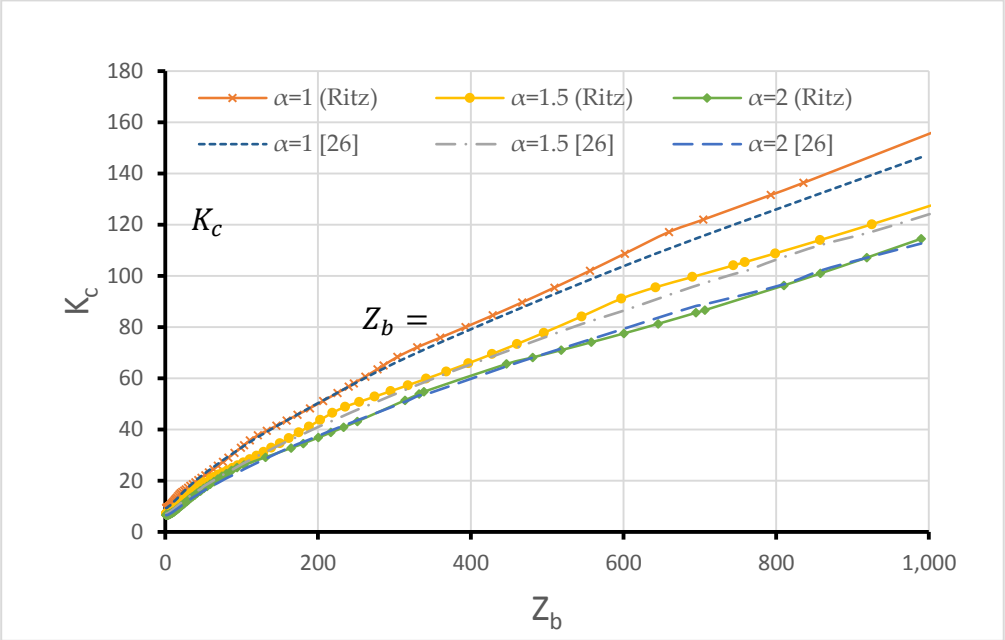

Figure 6.3 Comparison of results for isotropic material with ref [26]

As a second step, the buckling loads calculated using the developed program for a variety of configurations were compared with the same cases solved using ANSYS®. Considering their high levels of anisotropy, $(\pm \Theta / \pm \Theta / \Theta)_s$ laminates were used as complicated enough candidates in the current study. The orthotropic material properties and the ply thickness that was used throughout the current work are listed in Table 6.1 Orthotropic mechanical properties of the composite material.

Table 6.1 Orthotropic mechanical properties of the composite material

E_{11}(GPa)	E_{22}(GPa)	G_{12}(GPa)	ν_{12}	Ply thickness (mm)
127.5	9.4	4	0.33	0.14

The comparisons were done for 200mm×200mm curved panels with a radius of 250mm and different stacking sequences of the aforementioned family. When carrying out the analyses with ANSYS®, SHELL281 which is an eight-node, first-order shear deformation element with a mesh size of 5mm was used. In order to simulate the boundary conditions similar to those imposed by the displacement functions, the shear stress in the curved panels was induced by applying a uniform

azimuthal displacement on one curved edge while keeping the other one azimuthally fixed. To prevent length variation in the other two edges, their axial displacement was constrained.

The results of these comparisons are reported in Tables 6.2 and 6.3 for simply supported and clamped boundary conditions, respectively. The comparisons show an acceptable agreement of the results and the difference never exceeds 5%.

Table 6.2 Comparison of critical shear buckling loads obtained by ANSYS® and the developed program for simply supported boundary condition

Stacking sequence	Ritz (kN/m)	ANSYS® (kN/m)	difference %
$(0)_{10}$	30.14	30.15	-0.01
$(\pm15/\pm15/15)_s$	49.21	51.14	-3.77
$(\pm30/\pm30/30)_s$	82.19	82.83	-0.77
$(\pm45/\pm45/45)_s$	105.72	111.19	-4.91
$(\pm70/\pm70/70)_s$	96.08	95.84	0.25

Table 6.3 Comparison of critical shear buckling loads obtained by ANSYS® and the developed program for clamped boundary condition

Stacking sequence	Ritz (kN/m)	ANSYS® (kN/m)	difference %
$(0)_{10}$	38.81	37.38	3.82
$(\pm15/\pm15/15)_s$	58.71	58.78	-0.13
$(\pm30/\pm30/30)_s$	95.18	97.94	-2.82
$(\pm45/\pm45/45)_s$	119.79	123.20	-2.77
$(\pm70/\pm70/70)_s$	122.71	117.81	4.16

6.5 Results and discussion

In order to report the numerical results in a more insightful manner, the input parameters and the results are presented in the form of non-dimensional units. The non-dimensional parameters that are generally used for characterizing the buckling behavior of composite shells are[145] :

$$\alpha = \frac{a}{b}\left(\frac{D_{22}}{D_{11}}\right)^{1/4} \tag{6.20}$$

$$\beta = \frac{D_{12} + 2D_{66}}{\sqrt{D_{22}\, D_{11}}} \tag{6.21}$$

$$\gamma = \frac{D_{16}}{\left({D_{11}}^3 D_{22}\right)^{1/4}} \tag{6.22}$$

$$\delta = \frac{D_{26}}{\left(D_{11}{D_{22}}^3\right)^{1/4}} \tag{6.23}$$

$$Z = \frac{b^2}{R}\left[\frac{A_{11}A_{22} - {A_{12}}^2}{12\sqrt{A_{11}A_{22}D_{11}D_{22}}}\right]^{1/2} \tag{6.24}$$

$$\bar{\mathrm{N}}_{xy} = \frac{N_{xy}^0 b^2}{\pi^2\left(D_{11}{D_{22}}^3\right)^{1/4}} \tag{6.25}$$

$$\overline{K}_x = \frac{aK_x}{D_{11}} \tag{6.26}$$

$$\overline{K}_y = \frac{aK_y}{D_{22}} \tag{6.27}$$

where α is the non-dimensional aspect ratio, β is the bending orthotropy parameter and γ and δ are the bending anisotropy parameters. Z is the parameter that characterizes the effect of shell curvature and thickness on buckling and is analogous to the Batdorf [145] parameter for curved isotropic shells. $\overline{N}_{xy}$ is the so-called shear buckling coefficient. $\overline{K}_x$ and $\overline{K}_y$ are non-dimensional rotational stiffnesses applied at boundaries parallel to x and y-axes respectively.

In the literature of restrained plates no non-dimensional parameter has been introduced for representing the torsional stiffness of stiffeners. Here, by assessing the balance of moments along the edges of a shell such a parameter was proposed. The balance of moments along the edge $x = 0$ reads:

$$GJ_1 \frac{\partial^2 \varphi}{\partial y^2}|_{x=0} = D_{11}\frac{\partial \varphi_x}{\partial x} + D_{12}\frac{\partial \varphi_y}{\partial y} + D_{13}\left[\frac{\partial \varphi_y}{\partial x} + \frac{\partial \varphi_x}{\partial y} - \frac{1}{2R}\left(\frac{\partial u_0}{\partial y} - \frac{\partial v_0}{\partial x}\right)\right]|_{x=0} \tag{6.28}$$

The essential boundary conditions along the edge *x=0* lead to the vanishing of the second term in Eq.(6.28). After dropping the vanishing term and neglecting the shear deformations and the contribution of in-plane displacements in twist terms, Eq.(6.28) reduces to:

$$GJ_1 \frac{\partial^3 w}{\partial y^2 \partial x}|_{x=0} = D_{11}\frac{\partial^2 w}{\partial x^2}|_{x=0} \tag{6.29}$$

By selecting the dimensions of the domain (curved panel) as the proper scales for x and y we have:

$$GJ_1 \frac{W}{b^2 a} \sim D_{11}\frac{W}{a^2} \tag{6.30}$$

where W is the scale of the out-of-plane displacement.

By analyzing Eq.(6.29) a non-dimensional unit of an order of unity can be introduced to represent the torsional stiffness of a bordering stiffener. The general form of this parameter is presented as:

$$\overline{GJ_x} = \frac{aGJ_x}{b^2 D_{11}} \tag{6.31}$$

Similarly, for the stiffeners joined to the axial edges, the non-dimensional torsional stiffness is defined as:

$$\overline{GJ_y} = \frac{bGJ_y}{a^2 D_{22}} \tag{6.32}$$

Unlike some of the other non-dimensional formulations in the literature, in this work, the formulation was derived in terms of the physical parameters of the problem and then the obtained results were transformed into the non-dimensional forms. Therefore, using the developed program it was not possible to use arbitrary values for orthotropy and anisotropy parameters independently. Hence, the effect of the variation of anisotropy and orthotropy parameters were not comprehensively investigated.

In parametric studies, buckling of laminates with three stacking sequences $(\pm 20/\pm 20/20)_s$, $(\pm 45/\pm 45/45)_s$, and $(\pm 70/\pm 70/70)_s$ were investigated thoroughly. The values of the non-dimensional orthotropy and anisotropy parameters of these laminates are listed in Table 6.2. For the sake of brevity and to avoid reporting similar results, in the following section, the $\bar{N}_{xy} - \alpha$ and $\bar{N}_{xy} - Z$ graphs were plotted for different values of rotational stiffness only.

Table 6.4 Orthotropy and anisotropy parameters of studied laminates

Laminate	β	γ	δ
$(\pm 20/\pm 20/20)_s$	1.37	0.167	0.074
$(\pm 45/\pm 45/45)_s$	2.44	0.22	0.22
$(\pm 70/\pm 70/70)_s$	1.374	0.074	0.167

Figure 6.4-6.6 depict the variation of the shear coefficient $\bar{N}_{xy}$ versus α for the three benchmarked laminates. To generate each curve, the parameters Z, $\bar{K}_x$ and $\bar{K}_y$ were kept constant and α was varied. Z was arbitrarily opted to be equal to 500 and equal values of non-dimensional rotational stiffness values were applied to all the four edges of the panel which is simply designated

by K. As each of these graphs was plotted for a particular laminate, parameters β, γ and δ are necessarily constant.

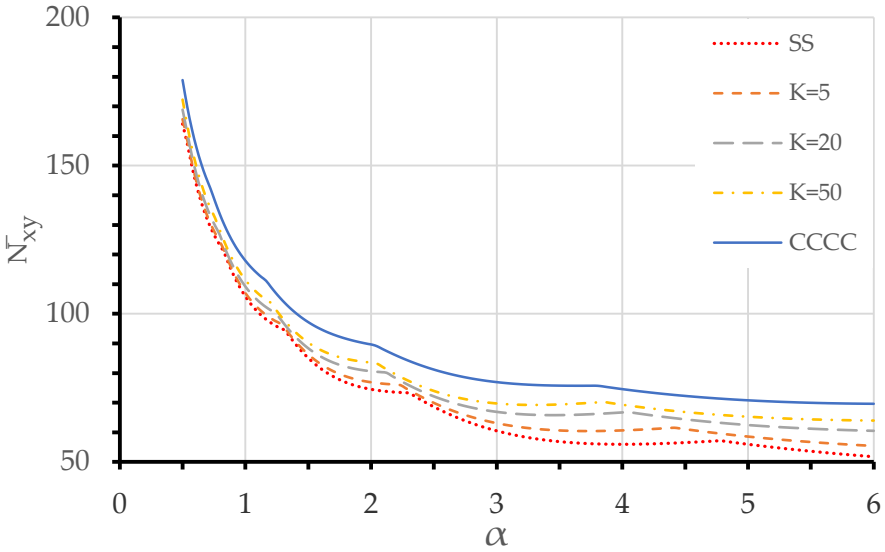

Figure 6.4 Variation of shear buckling coefficient with α for a (±20/±20/20)s laminate

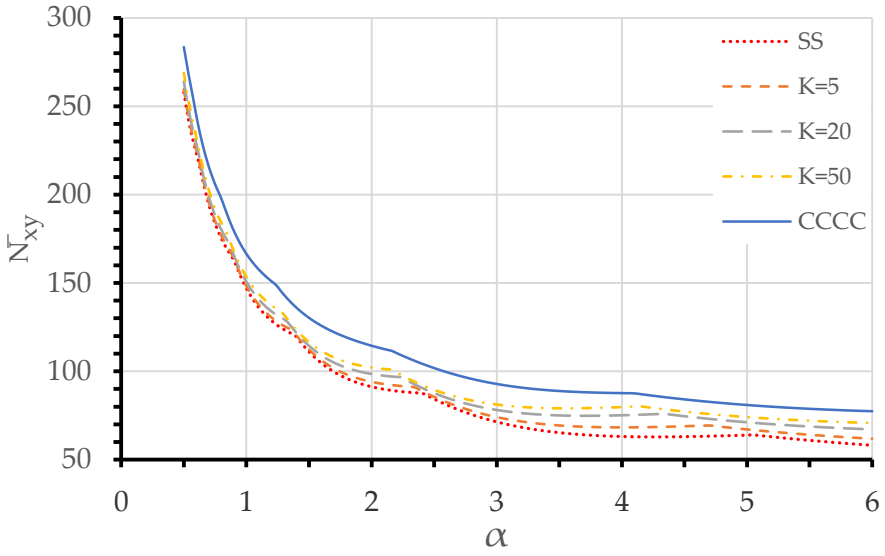

Figure 6.5 Variation of shear buckling coefficient with α for a (±45/±45/45)s laminate

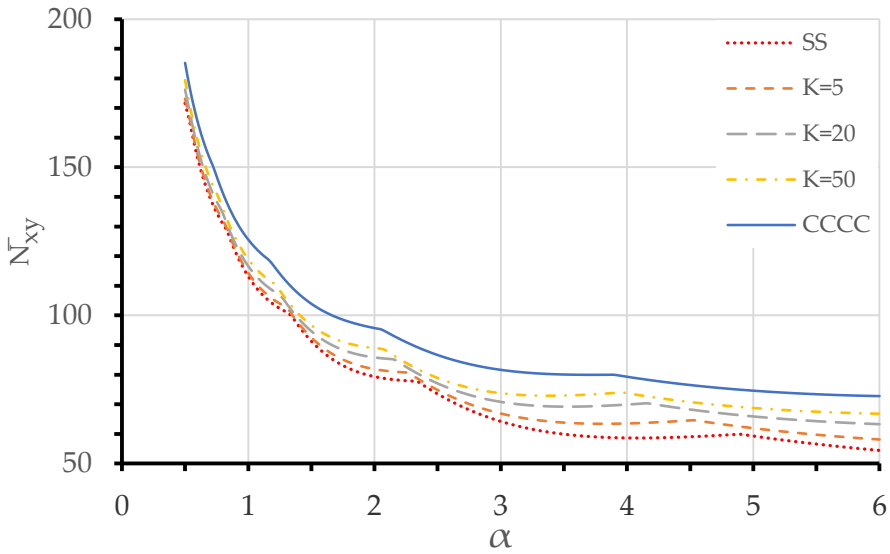

Figure 6.6 Variation of shear buckling coefficient with α for a (±70/±70/70)s laminate

$\bar{N}_{xy} - \alpha$ graphs show that the trend of the variation of the shear buckling coefficient with α is not monotonic. The kink points on the curves represent the aspect ratios at which the mode shapes transition and thus the buckling critical loads fluctuate. It can be observed that applying boundary stiffness not only increases the shear coefficient but also, shifts the aspect ratio at which the mode shapes transition. Figure 6.7 illustrates the mode shapes corresponding to each segment of the curve for the (±45/±45/45)s laminate with simply-supported and clamped boundary conditions. A comparison of simply supported and clamped curves also reveals that the effect of the restraints is more pronounced for shells with larger axial dimensions compared to shells with larger circumferential dimensions.

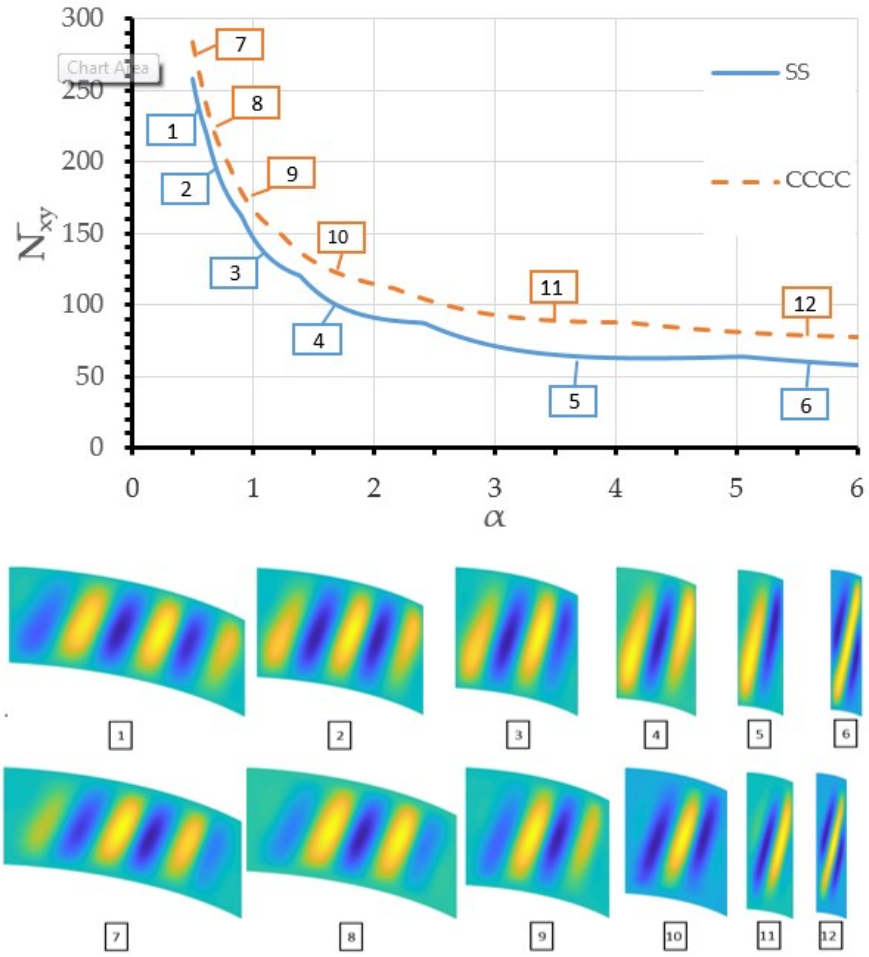

Figure 6.7 Mode shape transition with the variation of α, for a (±45/±45/45)s laminate.

Figures 6.8-6.10 demonstrate the variation of the buckling behavior of curved panels versus Z which for a particular laminate can be implicitly regarded as the effect of curvature on the buckling strength of a cylindrically curved shell. To investigate the effect of this variable solely, the aspect ratio was kept constant to unity. The results are presented for different restraint stiffness values including simply supported and clamped boundary conditions. As these graphs were produced for non-dimensional values they are valid for any configuration regardless of physical properties and dimensions, provided that all other non-dimensional variables be similar.

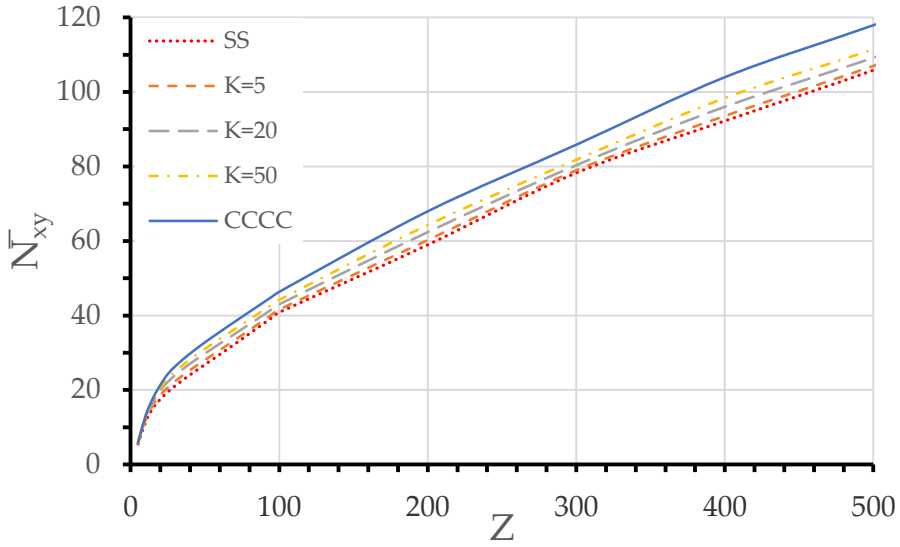

Figure 6.8 Variation of shear buckling coefficient with Z for a (±20/±20/20)s laminate

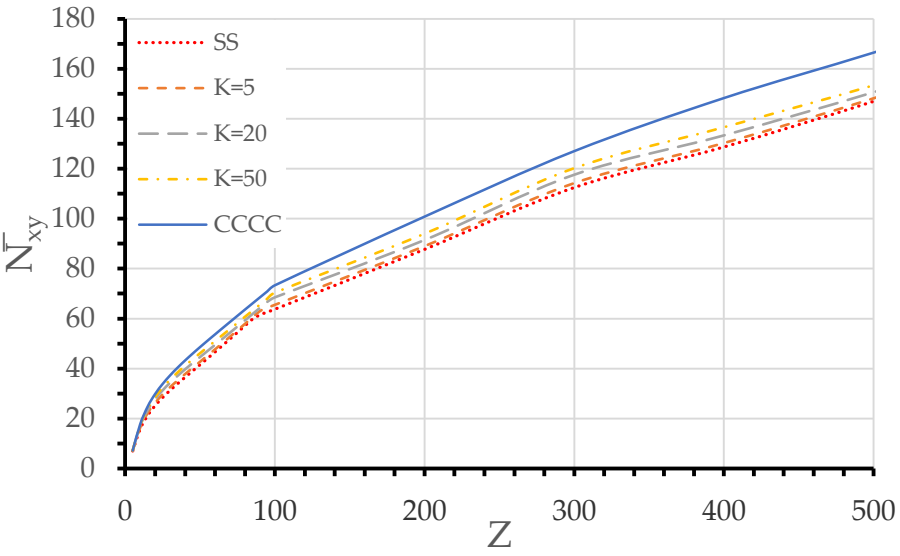

Figure 6.9 Variation of shear buckling coefficient with Z for a (±45/±45/45)s laminate

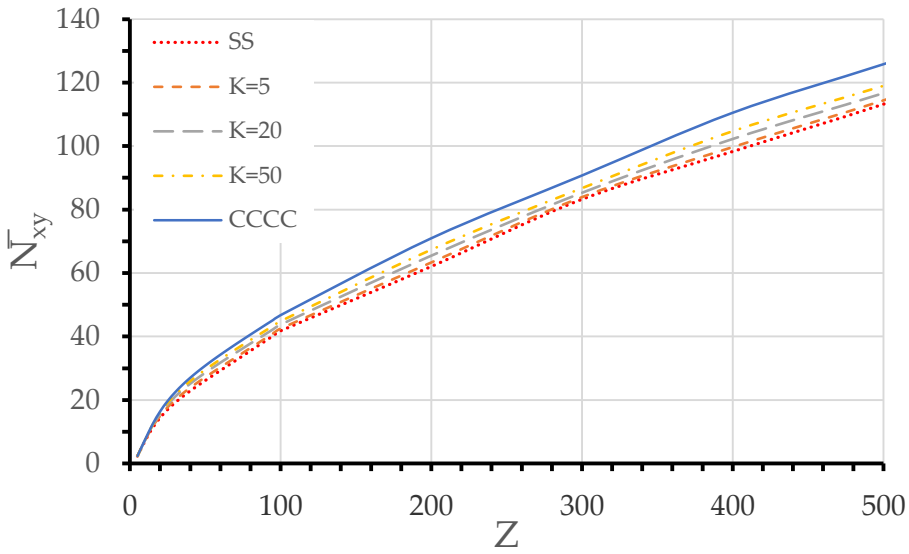

Figure 6.10 Variation of shear buckling coefficient with Z for a (±70/±70/70)s laminate

As in N_{xy}-α curves, kink points are distinguishable on N_{xy}-Z curves as well and the explanation is similar. Figure 6.11 demonstrates the transition of mode shapes with the variation of Z for the (±45/±45/45)s laminate under Simply supported and clamped boundary conditions. This latter phenomenon can be perceived as the effect of curvature on the buckling mode shape. However, attention should be paid to the fact that *Z* is not directly proportional to the shell curvature.

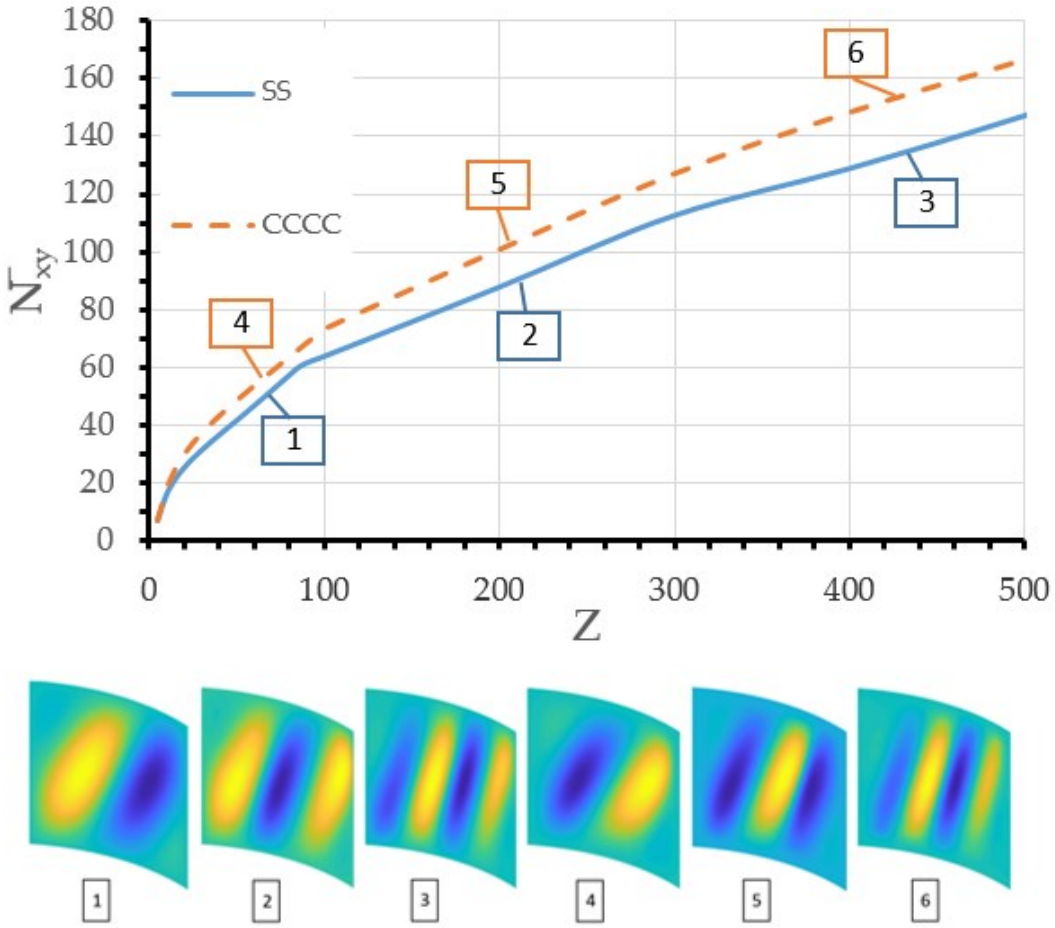

Figure 6.11 Mode shape transition with the variation of Z, for a $(\pm 45/\pm 45/45)_s$ laminate.

As mentioned earlier, the clamped boundary condition can be attained by applying an infinite (a very high numerical value) rotational restraint stiffness. Studying the curves of Figures 6.8-6.10 it was observed that for higher values of Z, the constant K_x and K_y curves get closer to the simply supported case curves rather than the clamped case curves. It can be deduced that for higher values of Z the stiffness required to simulate the clamped boundary condition is relatively higher.

Figures 6.12-6.14 show the variation of the critical buckling load of flat (Z=0) and curved (Z=500) shells versus the non-dimensional restraint stiffness. These results were generated for shells with an α of unity. As expected, the application of both types of rotational restraints leads to a rise in buckling critical force, however, after a certain value of stiffness, the buckling load remains relatively constant. It was observed that compared to curved panels, flat plates experience a sharper rise of buckling strength with the introduction of rotational restraints. Furthermore, it

was noticed that compared to rotational springs, torsional restraints cause a smoother and more gradual increase in the critical buckling force of a shell.

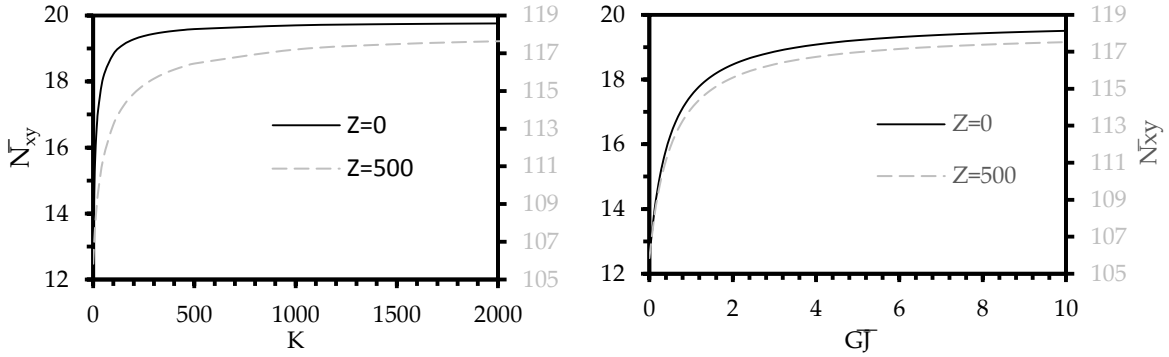

Figure 6.12 Shear buckling coefficient vs. non-dimensional rotational (left) and torsional (right) stiffness for 45a (±20/±20/20)s Laminate

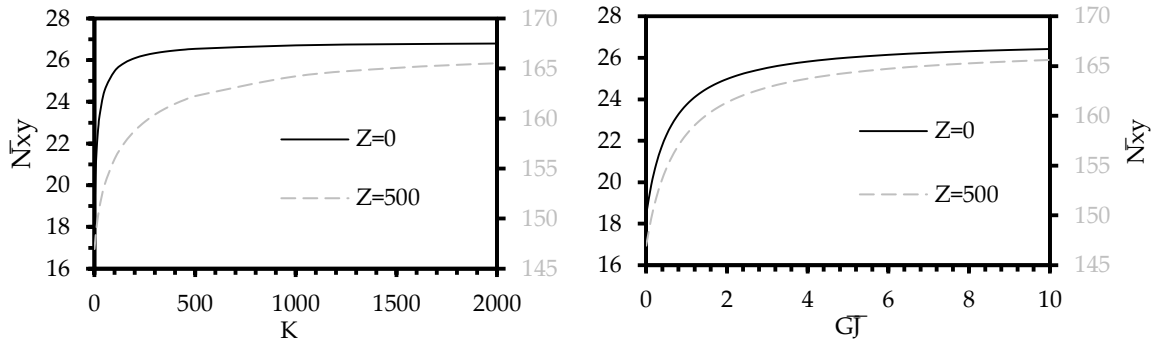

Figure 6.13 Shear buckling coefficient vs. non-dimensional rotational (left) and torsional (right) stiffness for a (±45/±45/45)s laminate

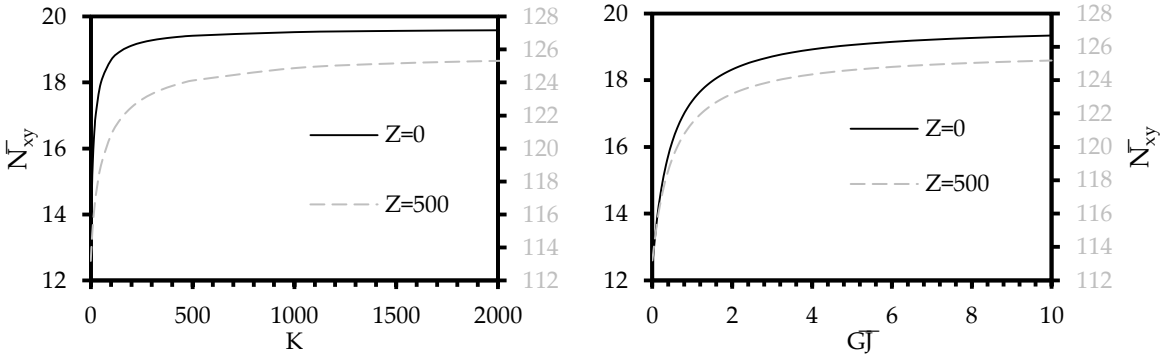

Figure 6.14 Shear buckling coefficient vs. non-dimensional rotational (left) and torsional (right) stiffness for a (±70/±70/70)s laminate

Considering the fact that using a specific material with definite orthotropic properties, it is not possible to vary the orthotropy and anisotropy parameters arbitrarily. To examine the effect of anisotropy parameters on the buckling behavior of restrained panels, a specific characteristic of

the family of ((±45)n,45)s laminates were used. For these laminates, the orthotropy parameter β remains constant with the variation of the number of layers "n" while the anisotropy parameters δ and γ are always equal and diminish by increasing the number of layers "n". Figure 6.15 demonstrates the variation shear buckling coefficient with the parallel variation of anisotropy parameters. Due to the stepwise variation of δ and γ with the number of layers, the reported points are not evenly distributed along the x-axis. Figure 6.15 shows a significant difference between the effect of the variation of δ and γ on the divergence of negative and positive shear buckling coefficients. In other words, for higher values of these parameters, the laminates are more sensitive to the direction of the application of the shear force.

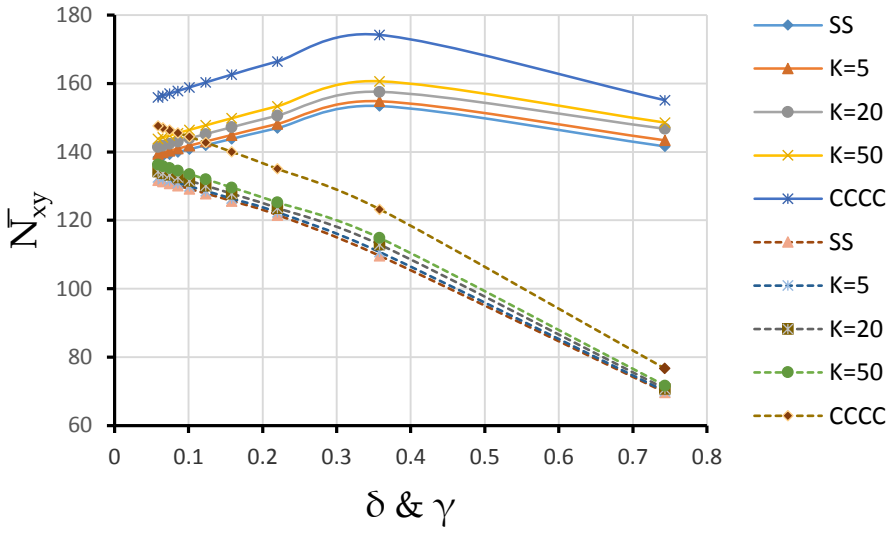

Figure 6.15 Variation of shear buckling coefficient vs. anisotropy parameters δ & γ. Dashed lines correspond to negative shear and continuous lines correspond to positive shear.

6.6 Concluding remarks

The current work is an attempt to simulate and predict the stability behavior of rotationally restrained cylindrical composite shells and also to investigate the effect of the influential parameters on their buckling strength. Through the derivation, validation and parametric studies the following conclusions were drawn.

1. The methodology implemented, including the use of a first-order shear deformation theory and the maximum total potential energy and finally, the Ritz method has proved to be an accurate enough formulation for buckling strength estimation of curved composite panels under pure shear loading.

2. The convergence of the employed trigonometric displacement functions diminishes with increasing the restraint stiffness, however even for clamped case no more than 15 terms are required to attain an acceptable accuracy.
3. In all the studied cases it was observed that a non-dimensional rotational spring stiffness of approximately 6000 or non-dimensional torsional stiffness of 100 is enough for simulating a fully clamped boundary condition and further increasing the stiffness may result in less accurate results due to numerical errors.
4. The generality of the results reported in the non-dimensional forms suggests that the influential physical parameters on buckling of curved panels are the aspect ratio and the ratio b^2/R, thus the curvature of shells cannot be used to characterize their buckling behavior.
5. Despite the fact that the shell thickness affects the *Z* parameter since *Z* is not linearly related to thickness, the ratio t/R may neither be introduced as an influential parameter.
6. The bending anisotropic parameters δ and γ define the difference between positive and negative shear buckling strength of a panel. The conducted parametric studies suggest that the difference between positive and negative critical shear buckling forces grows with an increase in these parameters.
7. In the studied cases, the application of restraints could raise the buckling strength up to 30% and it can be deduced that considering a simply supported boundary condition for restrained panels may lead to a drastic design conservatism.

6.7 Appendix A convergence curves

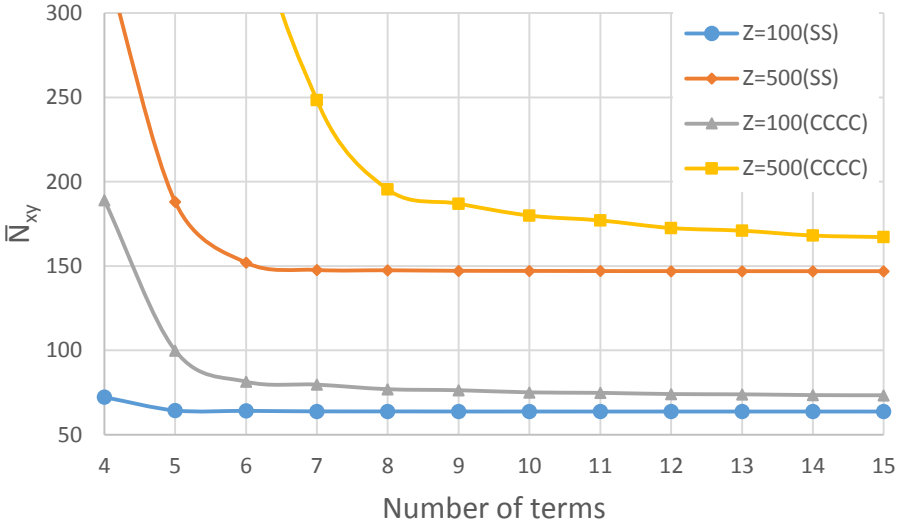

Figure 6.16 Convergence of shear buckling coefficient with number of terms (symmetrical in x &y) for a (±45/±45/45)s laminate with an α of 1

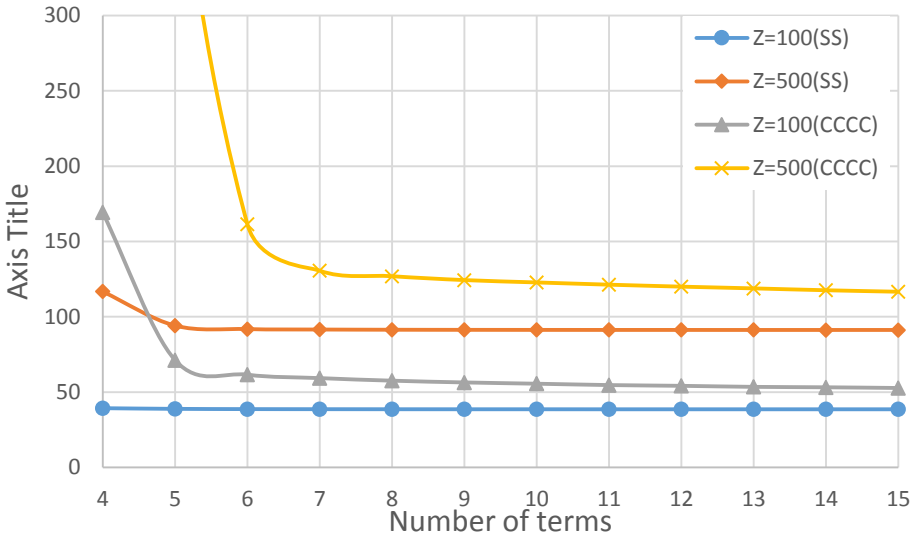

Figure 6.17 Convergence of shear buckling coefficient with number of terms (symmetrical in x &y) for a (±45/±45/45)s laminate with an α of 2

6.8 Appendix B supplementary results

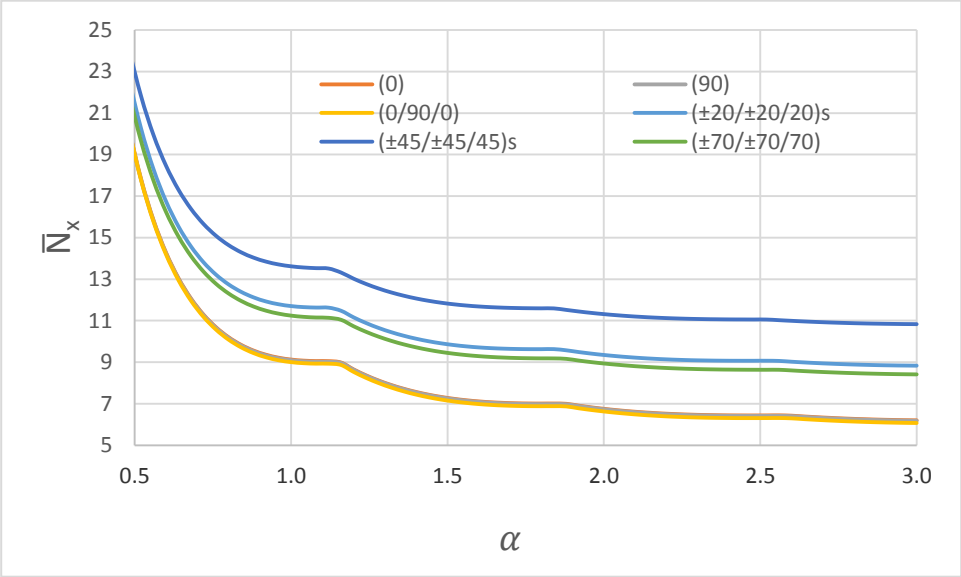

Figure 6.18 Variation of non-dimensional axial buckling load with non-dimensional aspect ratio for selected laminate stack ups with clamped boundary conditions.

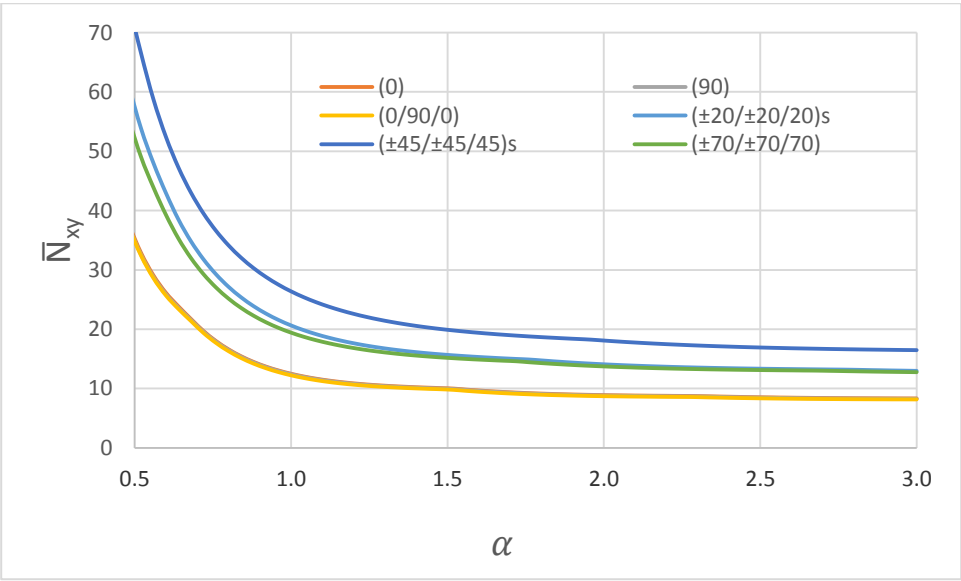

Figure 6.19 Variation of non-dimensional shear buckling load with non-dimensional aspect ratio for selected laminate stack ups with clamped boundary conditions.

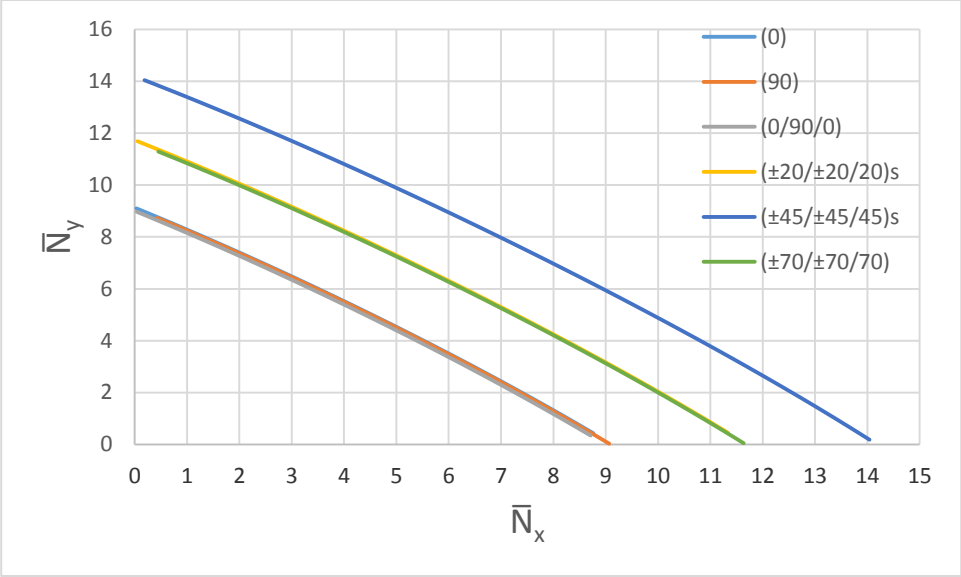

Figure 6.20 Biaxial interaction curves for selected laminate stack ups with clamped boundary conditions.

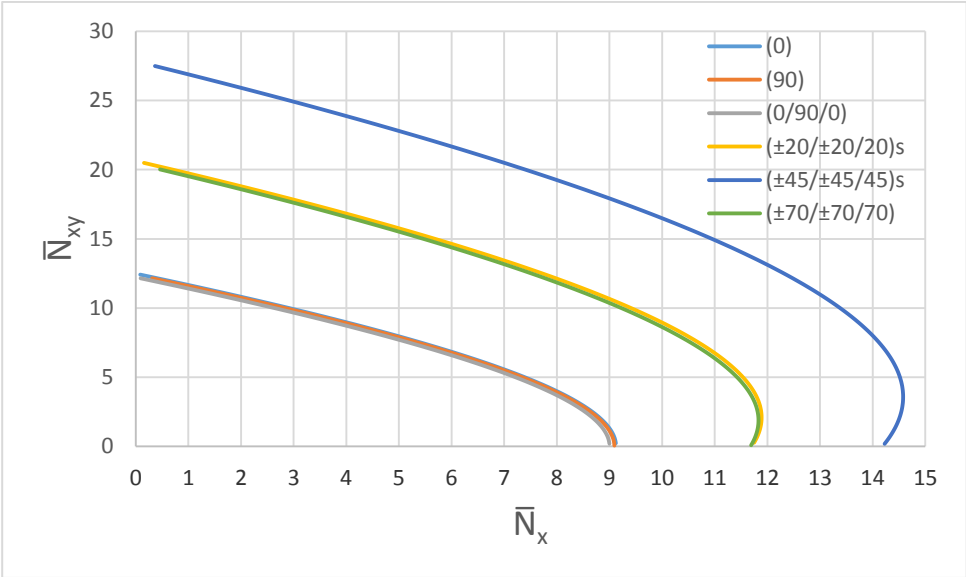

Figure 6.21 Shear-axial buckling interaction curves for selected laminate stack ups with clamped boundary conditions.

Chapter 7: Contributions and conclusions

7.1 Contributions

In this dissertation, a new methodology for investigating the buckling and postbuckling behavior of delaminated composite plates has been presented. The presented techniques include new linear buckling and nonlinear postbuckling solutions offering a wide range of deliverable results. The contributions of these new developments can be summarized as follows:

- A state-of-the-art two-step approximate solution for the buckling problem of laminated composite plates subjected to in-plane constraints was developed. The eigenvalue buckling analysis was based on a calculated prebuckling stress field. The prebuckling stress field was obtained through approximate in-plane stress analysis.
- A novel penalty function based technique for modeling partially delaminated plates was proposed. The new technique divides a laminate into two sublaminates only and compared to older models remarkably reduces time and computation costs in nonlinear analyses. Furthermore, it has the advantage of directly calculating the interlaminar tractions in the plane of an existing delamination.
- A Ritz method based solution using non-continuous approximate functions capable of addressing highly local deformations was proposed. Unlike the conventional Ritz solution, the modified version can easily handle high local gradients of displacements using a reasonably less number of terms. In the particular case of delaminated plates, this technique was used for accommodating the local deformations of the delaminated region. This method was proved to successfully capture the local deformations of the delaminated regions as well as the global deformations experienced in the entirety of the plate.
- A multizone technique for modeling delaminated pates was proposed in which all the continuity and boundary conditions were enforced using penalty functions. The extensive use of penalty functions for imposing essential boundary conditions, makes it possible to use ordinary sets of well-behaved orthogonal approximate functions and develop boundary condition-independent formulations. Another advantage of this approach is the direct access to boundary and interface forces through the penalty functions.
- A technique for calculating the SERR along the borders of a delaminated region was proposed. The new technique has the distinctive advantage of estimating the SERR corresponding to each fracture mode separately. A comparison of the calculated distribution of SERR with the results obtained using FEM and VCCT proved that the

current derivation can accurately predict the magnitude and the shape of the distribution of the SERR along a crack tip.

7.2 Major conclusions

The objective of this thesis work has been to develop a methodology for predicting the buckling and postbuckling behavior of delaminated composite plates capable of addressing the fracture mechanics phenomenon involved in the postbuckling regime. This objective was completely fulfilled by developing a methodology based on the Ritz method for simulating the buckling and postbuckling behavior of delaminated plates. The Ritz solution was formulated in a fashion that it provides the necessary information to be used in fracture mechanics analyses leading to the calculation of SERR distribution along the edges of a delaminated region. The SERR calculation was done using Irwin's Crack closure integrals for the three fracture modes separately. To confirm the performance of the different parts of the developed methodology, the validity of the results yielded by them were verified through comparison with experimental data as well as numerical solutions obtained using FEM.

Through deriving the formulations, developing mathematical models, and solving numerical examples the following conclusions were drawn:

- Under uniaxial compressive loading, the presence of in-plane constraints may cause a significant nonuniformity and biaxilaity in the stress field within a plate. The impact of these constraints on the stress field greatly changes the buckling behavior of the plate. Therefore, excluding the effect of these constraints may lead to erroneous predictions. The proposed two-step solution proved to effectively incorporate the effect of in-plane constraints by basing the eigenvalue buckling analysis on the calculated stress field obtained using an elasticity analysis.
- In employing approximate variational solutions such as the Ritz method, the use of penalty functions for applying essential boundary conditions and restraints waives the need for complicated approximate functions. The use of penalty functions makes approximate solutions flexible with respect to boundary conditions without compromising the accuracy or convergence speed of the solution.
- Approximate solutions and particularly the Ritz method being reliant on continuous approximate functions are not the most suitable options for problems involving highly

localized deformations such as delamination buckling and postbuckling problems. The use of noncontinuous supplementary functions has proved to play the role of a local refinement and can broaden the applicability of such approximate solutions to problems involving a combination of local and global deformations.

- In this thesis, two new partitioning schemes for accommodating the discontinuity posed by delamination were proposed. Both these methods were used in conjunction with a nonlinear variational formulation and were proved to be able to reasonably represent the geometry of a delaminated composite plate. The solutions developed based on these partitioning schemes besides accurately predicting the buckling and postbuckling behavior of delaminated composite plates, have the advantage of yielding the interlaminar tractions in the plane of the delamination.
- The proposed technique for modeling delaminated composite plates using penalty functions sets the ground for marrying approximate solutions with crack closure techniques. This offers the facility of determining the distribution of SERR corresponding to the three fracture modes individually.
- A comparison of postbuckling results with experiments suggests that the deviation of experimental results from the predicted results may be attributed to the calculated stiffness matrices rather than the solution method.
- It was established that through the eigenvalue buckling analysis of the whole plate and the corresponding sublaminates the buckling mode (local, mixed, global) of a delaminated plate can be determined. An a priori knowledge of the buckling mode is essential in determining the shape of the imperfection to be incorporated in the postbuckling analysis of such plates. This necessitates including the linear buckling analysis as an essential element of the overall methodology dedicated to predicting the buckling and postbuckling behavior of delaminated plates.
- It was observed in cases involving a global buckling mode shearing is the dominant fracture mode. In the postbuckling state, the SERR corresponding to the shearing mode varies linearly with the applied end-shortening.
- In plates exhibiting a local buckling mode, the opening mode is the major fracture mode, however, it was observed that a local buckling mode is often followed by a mixed buckling mode where both shearing and opening fracture modes are present. In a mixed

buckling mode, both shearing and opening SERRs have a nonlinear correlation with the applied end-shortening.

- The use of penalty functions for applying rotational restraints on the edges of curved panels provides the facility of predicting the buckling behavior of curved panels with arbitrary rotational boundary conditions ranging from simply supported to clamped without using complicated approximate functions. This facility makes it possible to use a single formulation for analyzing intact curved panels as well as delaminated films.

7.3 Recommendation for future works

The methodology presented in this dissertation fulfills the objectives of this thesis work. However, it can be further expanded to provide more elaborate information on the implications of the existence of interlaminar flaws in composite laminates. Aligned with the achievements of this work the following topics may be suggested as items that could complement the proposed methodology.

- All the formulations of this work are derived based on the FSDT. It has been shown that the FSDT is capable of fairly modeling the behavior of thin to moderately thick laminates in a postbuckling analysis. However, it has been observed that ahead of a crack tip a region can be identified where the FSDT might not be the best representative of the displacement field. In this regard repeating the derivations of this work using the HSDT assumptions may enhance the accuracy of the predicted results especially the SERRs.
- In this work the means for determining the implications of delamination on the performance of flat composite plates are developed, however, in real-life applications, structures are also made of curved composite panels. Therefore, extending the proposed formulation to accommodate curvatures of composite panels can highly contribute to the practicality of the proposed techniques.
- In a significant number of applications, structures are subjected to cyclic loading under which a gradual growth of flaw may be expected. By combining, the proposed solutions with fatigue crack growth equations such as the Paris equation, the use of the present developments can be extended to predict the crack growth rate.

- The current methodology is capable of predicting the onset of the growth of a crack, however, following an infinitesimal propagation of a crack different scenarios may become possible namely the arrest of the crack or its further propagation. By defining the stiffness of the elastic interlaminar bonds as a variable field the movement of a crack front can be traced.
- The penalty function based formulation is compatible with damage mechanics. Therefore, as a next step, the crack closure integrals used in this work for predicting a potential growth of the delaminated region may be replaced by a Cohesive Zone Model (CZM) for modeling the gradual failure process.
- The principles used in chapters 3 and 4 can be extended to problems with two or more delaminations. Doing so would require dividing the laminate by the plane of all the existing delaminations.
- The validity of the predictions made by the developed methodologies may be further examined through the comparison of results with experimental data. Such data can be extaracted from the literature for both through-the-width [7,66,113,146] and embedded [15,62,66] delaminations. In these works, the propagation of the delamination is either studied by analyzing the obtained load-force correlations [113] or using the C-scan technique after the unloading of the tested specimens [15,62]. To obtain a better understanding of the onset of propagation of delamination propagation, future experiments may include monitoring the state of the delamination in realtime using techniques like Ultrasonic, infrared, Radiography, etc [147].

References

[1] S. Sridharan, Delamination Behaviour of Composites, 2008. doi:10.1533/9781845694821.

[2] V. V. Bolotin, Delaminations in composite structures: Its origin, buckling, growth and stability, Compos. Part B Eng. 27 (1996) 129–145. doi:10.1016/1359-8368(95)00035-6.

[3] H. Chai, C.D. Babcock, W.G. Knauss, One dimensional modelling of failure in laminated plates by delamination buckling, Int. J. Solids Struct. 17 (1981) 1069–1083. doi:10.1016/0020-7683(81)90014-7.

[4] H. Chai, C.D. Babcock, W.G. Knauss, One dimensional modelling of failure in laminated plates by delamination buckling, Int. J. Solids Struct. 17 (1981) 1069–1083. doi:10.1016/0020-7683(81)90014-7.

[5] W.L. Yin, The Effects of Laminated Structure on Delamination Buckling and Growth, J. Compos. Mater. 22 (1988) 502–517. doi:10.1177/002199838802200601.

[6] X.R. Zhuo, H.S. Jang, H.G. Beom, Delamination buckling of a thin film bonded to an orthotropic substrate, Int. J. Precis. Eng. Manuf. 16 (2015) 323–333. doi:10.1007/s12541-015-0043-z.

[7] S. Wang, C.M. Harvey, B. Wang, A. Watson, Post-local buckling-driven delamination in bilayer composite beams, Compos. Struct. 133 (2015) 1058–1066. doi:10.1016/j.compstruct.2015.08.012.

[8] G.A. Kardomateas, Initial post-buckling and growth behavior of internal delaminations in composite plates, in: Am. Soc. Mech. Eng., 1993: pp. 1–8.

[9] P.L. Larsson, On multiple delamination buckling and growth in composite plates, Int. J. Solids Struct. 27 (1991) 1623–1637. doi:10.1016/0020-7683(91)90065-N.

[10] G.B. Chai, W.M. Banks, J. Rhodes, The instability behaviour of laminated panels with elastically rotationally restrained edges, Compos. Struct. 19 (1991) 41–66.

[11] K.N. Shivakumar, J.D. Whitcomb, Buckling of a Sublaminate in a Quasi-Isotropic Composite Laminate, J. Compos. Mater. 19 (1985) 2–18. doi:10.1177/002199838501900101.

[12] B.D. Davidson, Delamination Buckling: Theory and Experiment, J. Compos. Mater. 25 (1991) 1351–1378. doi:10.1177/002199839102501007.

[13] W.M. Kyoung, C.G. Kim, Delamination Buckling and Growth of Composite Laminated

Plates with Transverse Shear Deformation, J. Compos. Mater. 29 (1995) 2047–2068. doi:10.1177/002199839502901506.

[14] H. Kim, K.T. Kedward, A method for modeling the local and global buckling of delaminated composite plates, Compos. Struct. 44 (1999) 43–53. doi:10.1016/S0263-8223(98)00117-2.

[15] K.F. Nilsson, L.E. Asp, J.E. Alpman, L. Nystedt, Delamination buckling and growth for delaminations at different depths in a slender composite panel, Int. J. Solids Struct. 38 (2001) 3039–3071. doi:10.1016/S0020-7683(00)00189-X.

[16] G.J. Simitses, S. Sallam, W.L. Yin, Effect of delamination of axially loaded homogeneous laminated plates, AIAA J. 23 (1985) 1437–1444. doi:10.2514/3.9104.

[17] S. Sallam, G.J. Simitses, Delamination buckling and growth of flat, cross-ply laminates, Compos. Struct. 4 (1985) 361–381. doi:10.1016/0263-8223(85)90033-9.

[18] G.A. Kardomateas, D.W. Schmueser, Buckling and postbuckling of delaminated composites under compressive loads including transverse shear effects, AIAA J. 26 (1988) 337–343. doi:10.2514/3.9894.

[19] H.P. Chen, Shear deformation theory for compressive delamination buckling and growth, AIAA J. 29 (1991) 813–819. doi:10.2514/3.10661.

[20] I. Sheinman, Y. Reichman, A study of buckling and vibration of laminated shallow curved panels, Int. J. Solids Struct. 29 (1992) 1329–1338. doi:10.1016/0020-7683(92)90081-4.

[21] C.W. Yap, G.B. Chai, Analytical and numerical studies on the buckling of delaminated composite beams, Compos. Struct. 80 (2007) 307–319. doi:10.1016/j.compstruct.2006.05.010.

[22] M. Kharazi, H.R. Ovesy, Postbuckling behavior of composite plates with through-the-width delaminations, Thin-Walled Struct. 46 (2008) 939–946. doi:10.1016/j.tws.2008.01.005.

[23] M. Kharazi, H.R. Ovesy, M. Taghizadeh, Buckling of the composite laminates containing through-the-width delaminations using different plate theories, Compos. Struct. 92 (2010) 1176–1183. doi:10.1016/j.compstruct.2009.10.019.

[24] H.R. Ovesy, M. Asghari Mooneghi, M. Kharazi, Post-buckling analysis of delaminated composite laminates with multiple through-the-width delaminations using a novel layerwise theory, Thin-Walled Struct. 94 (2015) 98–106. doi:10.1016/j.tws.2015.03.028.

[25] H.R. Ovesy, M. Kharazi, Compressional stability behavior of composite plates with

through-the-width and embedded delaminations by using first order shear deformation theory, in: Comput. Struct., Elsevier Ltd, 2011: pp. 1829–1839. doi:10.1016/j.compstruc.2010.10.016.

[26] J.H. Xue, Q.Z. Luo, F. Han, R.H. Liu, Two-dimensional analyses of delamination buckling of symmetrically cross-ply rectangular laminates, Appl. Math. Mech. (English Ed. 34 (2013) 597–612. doi:10.1007/s10483-013-1694-7.

[27] H.R. Ovesy, M. Taghizadeh, M. Kharazi, Post-buckling analysis of composite plates containing embedded delaminations with arbitrary shape by using higher order shear deformation theory, Compos. Struct. 94 (2012) 1243–1249. doi:10.1016/j.compstruct.2011.11.011.

[28] N. Kharghani, C. Guedes Soares, Behavior of composite laminates with embedded delaminations, Compos. Struct. 150 (2016) 226–239. doi:10.1016/j.compstruct.2016.04.042.

[29] H.J. Kim, C.S. Hong, Buckling and postbuckling behavior of composite laminates with a delamination, Compos. Sci. Technol. 57 (1997) 557–564. doi:10.1016/S0266-3538(97)00011-0.

[30] M.K. Yeh, C.M. Tan, Buckling of Elliptically Delaminated Composite Plates, J. Compos. Mater. 28 (1994) 36–52. doi:10.1177/002199839402800103.

[31] M. Ali Kouchakzadeh, H. Sekine, Compressive buckling analysis of rectangular composite laminates containing multiple delaminations, Compos. Struct. 50 (2000) 249–255. doi:10.1016/S0263-8223(00)00100-8.

[32] A. Tafreshi, T. Oswald, Global buckling behaviour and local damage propagation in composite plates with embedded delaminations, Int. J. Press. Vessel. Pip. 80 (2003) 9–20. doi:10.1016/S0308-0161(02)00152-7.

[33] H. Hosseini-toudeshky, S. Hosseini, B. Mohammadi, Delamination buckling growth in laminated composites using layerwise-interface element, Compos. Struct. 92 (2010) 1846–1856. doi:10.1016/j.compstruct.2010.01.013.

[34] Z. Juhász, A. Szekrényes, Progressive buckling of a simply supported delaminated orthotropic rectangular composite plate, Int. J. Solids Struct. 69–70 (2015) 217–229. doi:10.1016/j.ijsolstr.2015.05.028.

[35] Z. Kutlu, fu K. Chang, Modeling Compression Failure of laminated Composites Containing

Multiple Through-the-Width Delaminations, J. Compos. Mater. 26 (1992) 350–387. doi:10.1177/002199839202600303.

[36] S.F. Nikrad, S. Keypoursangsari, H. Asadi, A.H. Akbarzadeh, Z.T. Chen, Computational study on compressive instability of composite plates with off-center delaminations, Comput. Methods Appl. Mech. Eng. 310 (2016) 429–459. doi:10.1016/j.cma.2016.07.021.

[37] A. Köllner, M. Kashtalyan, I. Guz, C. Völlmecke, On the interaction of delamination buckling and damage growth in cross-ply laminates, Int. J. Solids Struct. 202 (2020) 912–928. doi:10.1016/j.ijsolstr.2020.05.035.

[38] Y. Zhang, S. Wang, Buckling, post-buckling and delamination propagation in debonded composite laminates Part 1 : Theoretical development, Compos. Struct. 88 (2009) 121–130. doi:10.1016/j.compstruct.2008.02.013.

[39] M. Marjanović, D. Vuksanović, Layerwise solution of free vibrations and buckling of laminated composite and sandwich plates with embedded delaminations, Compos. Struct. 108 (2014) 9–20. doi:10.1016/j.compstruct.2013.09.006.

[40] E.J. Barbero, J.N. Reddy, Modeling of delamination in composite laminates using a layer-wise plate theory, Int. J. Solids Struct. 28 (1991) 373–388. doi:10.1016/0020-7683(91)90200-Y.

[41] D.H. Li, Delamination and transverse crack growth prediction for laminated composite plates and shells, Comput. Struct. 177 (2016) 39–55. doi:10.1016/j.compstruc.2016.07.011.

[42] N. Kharghani, C. Guedes Soares, Influence of different parameters on the deflection of composite laminates containing through-the-width delamination using Layerwise HSDT, Compos. Struct. 132 (2015) 341–349. doi:10.1016/j.compstruct.2015.05.040.

[43] I. Sheinman, M. Soffer, Post-buckling analysis of composite delaminated beams, Int. J. Solids Struct. 27 (1991) 639–646. doi:10.1016/0020-7683(91)90218-5.

[44] H. Chai, C.D. Babcock, Two-Dimensional Modelling of Compressive Failure in Delaminated Laminates, J. Compos. Mater. 19 (1985) 67–98. doi:10.1177/002199838501900105.

[45] N. Hu, Buckling analysis of delaminated laminates with consideration of contact in buckling mode, Int. J. Numer. Methods Eng. 44 (1999) 1457–1479. doi:10.1002/(SICI)1097-0207(19990410)44:10<1457::AID-NME545>3.0.CO;2-9.

[46] A. Tafreshi, Delamination buckling and postbuckling in composite cylindrical shells under

external pressure, Thin-Walled Struct. 42 (2004) 1379–1404. doi:10.1016/j.tws.2004.05.008.

[47] A. Tafreshi, Delamination buckling and postbuckling in composite cylindrical shells under combined axial compression and external pressure, Compos. Struct. 72 (2006) 401–418. doi:10.1016/j.compstruct.2005.01.009.

[48] A. Tafreshi, Efficient modelling of delamination buckling in composite cylindrical shells under axial compression, Compos. Struct. 64 (2004) 511–520. doi:10.1016/j.compstruct.2003.09.050.

[49] L.X. Peng, K.M. Liew, S. Kitipornchai, Buckling and free vibration analyses of stiffened plates using the FSDT mesh-free method, J. Sound Vib. 289 (2006) 421–449. doi:10.1016/j.jsv.2005.02.023.

[50] A. Karrech, M. Elchalakani, M. Attar, A.C. Seibi, Buckling and post-buckling analysis of geometrically non-linear composite plates exhibiting large initial imperfections, Compos. Struct. 174 (2017) 134–141. doi:10.1016/j.compstruct.2017.04.029.

[51] M. Aydogdu, T. Aksencer, Buckling of cross-ply composite plates with linearly varying In-plane loads, Compos. Struct. 183 (2017) 221–231. doi:10.1016/j.compstruct.2017.02.085.

[52] M. Song, J. Yang, S. Kitipornchai, Bending and buckling analyses of functionally graded polymer composite plates reinforced with graphene nanoplatelets, Compos. Part B Eng. 134 (2018) 106–113. doi:10.1016/j.compositesb.2017.09.043.

[53] J.M. Whitney, Shear correction factors for orthotropic laminates under static load, J. Appl. Mech. Trans. ASME. 40 (1973) 302–304. doi:10.1115/1.3422950.

[54] P. Gaudenzi, P. Perugini, F. Spadaccia, Post-buckling analysis of a delaminated composite plate under compression, Compos. Struct. 40 (1997) 231–238. doi:10.1016/S0263-8223(98)00013-0.

[55] S.F. Hwang, S.M. Huang, Postbuckling behavior of composite laminates with two delaminations under uniaxial compression, Compos. Struct. 68 (2005) 157–165. doi:10.1016/j.compstruct.2004.03.010.

[56] F. Cappello, D. Tumino, Numerical analysis of composite plates with multiple delaminations subjected to uniaxial buckling load, Compos. Sci. Technol. 66 (2006) 264–272. doi:10.1016/j.compscitech.2005.04.036.

[57] S.L. Donaldson, The effect of interlaminar fracture properties on the delamination buckling

of composite laminates, Compos. Sci. Technol. 28 (1987) 33–44. doi:10.1016/0266-3538(87)90060-1.

[58] R.G. Wang, L. Zhang, J. Zhang, W.B. Liu, X.D. He, Numerical analysis of delamination buckling and growth in slender laminated composite using cohesive element method, Comput. Mater. Sci. 50 (2010) 20–31. doi:10.1016/j.commatsci.2010.07.003.

[59] J.D. Whitcomb, Analysis of instability-related growth of a through-width delamination, NASA Tech. Memo. (1984).

[60] J.D. Whitcomb, Finite Element Analysis of Instability Related Delamination Growth, J. Compos. Mater. 15 (1981) 403–426. doi:10.1177/002199838101500502.

[61] A. Chattopkdhyay, H. Gu, New higher order plate theory in modeling delamination buckling of composite laminates, AIAA J. 32 (1994) 1709–1716. doi:10.2514/3.12163.

[62] K. Wang, L. Zhao, H. Hong, Y. Gong, J. Zhang, N. Hu, An analytical model for evaluating the buckling, delamination propagation, and failure behaviors of delaminated composites under uniaxial compression, Compos. Struct. 223 (2019). doi:10.1016/j.compstruct.2019.110937.

[63] H. Chai, Three-dimensional fracture analysis of thin-film debonding, 1990.

[64] B. Mohammadi, F. Shahabi, S.A.M. Ghannadpour, Post-buckling delamination propagation analysis using interface element with de-cohesive constitutive law, in: Procedia Eng., 2011: pp. 1797–1802. doi:10.1016/j.proeng.2011.04.299.

[65] S. Wang, Y. Zhang, Buckling, post-buckling and delamination propagation in debonded composite laminates Part 2: Numerical applications, Compos. Struct. 88 (2009) 131–146. doi:10.1016/j.compstruct.2008.02.012.

[66] N. Kharghani, C. Guedes Soares, Experimental, numerical and analytical study of buckling of rectangular composite laminates, Eur. J. Mech. A/Solids. 79 (2020) 103869. doi:10.1016/j.euromechsol.2019.103869.

[67] M.A. Crisfield, A fast incremental/iterative solution procedure that handles "snap-through," Comput. Struct. 13 (1981) 55–62. doi:10.1016/0045-7949(81)90108-5.

[68] K. Liang, Q. Sun, Buckling and post-buckling analysis of the delaminated composite plates using the Koiter–Newton method, Compos. Struct. 168 (2017) 266–276. doi:10.1016/j.compstruct.2017.01.038.

[69] S. Nojavan, D. Schesser, Q.D. Yang, An in situ fatigue-CZM for unified crack initiation

and propagation in composites under cyclic loading, 146 (2016) 34–49. doi:10.1016/j.compstruct.2016.02.060.

[70] M. Cetkovic, Thermal buckling of laminated composite plates using layerwise displacement model, Compos. Struct. 142 (2016) 238–253. doi:10.1016/j.compstruct.2016.01.082.

[71] A.W. Leissa, Buckling of composite plates, Compos. Struct. 1 (1983) 51–66. doi:10.1016/0263-8223(83)90016-8.

[72] R.M. Jones, Thermal buckling of uniformly heated unidirectional and symmetric cross-ply laminated fiber-reinforced composite uniaxial in-plane restrained simply supported rectangular plates, Compos. Part A Appl. Sci. Manuf. 36 (2005) 1355–1367. doi:10.1016/j.compositesa.2005.01.028.

[73] M.P. Nemeth, M.P. Nemeth, Buckling Behavior of Long Anisotropic Plates Subjected To Restrained Thermal Expansion and Mechanical Loads Subjected To Restrained Thermal Expansion and Mechanical Loads, 5739 (2016). doi:10.1080/014957300750040122.

[74] M.P. Nemeth, Buckling of long compression-loaded anisotropic plates restrained against inplane lateral and shear deformations, in: 44th AIAA/ASME/ASCE/AHS/ASC Struct. Struct. Dyn. Mater. Conf., 2003: pp. 1–37.

[75] L.-C. Shiau, S.-Y. Kuo, C.-Y. Chen, Thermal buckling behavior of composite laminated plates, Compos. Struct. 92 (2010) 508–514. doi:10.1016/j.compstruct.2009.08.035.

[76] A.N. Sherbourne, M.D. Pandey, Differential quadrature method in the buckling analysis of beams and composite plates, Comput. Struct. 40 (1991) 903–913. doi:http://dx.doi.org/10.1016/0045-7949(91)90320-L.

[77] S.F. Bassily, S.M. Dickinson, Buckling and lateral vibration of rectangular plates subject to inplane loads-a Ritz approach, J. Sound Vib. 24 (1972) 219–239. doi:10.1016/0022-460X(72)90951-0.

[78] S.Y. Kuo, L.C. Shiau, Buckling and vibration of composite laminated plates with variable fiber spacing, Compos. Struct. 90 (2009) 196–200. doi:10.1016/j.compstruct.2009.02.013.

[79] Z. Gürdal, B.F. Tatting, C.K. Wu, Variable stiffness composite panels: Effects of stiffness variation on the in-plane and buckling response, Compos. Part A Appl. Sci. Manuf. 39 (2008) 911–922. doi:10.1016/j.compositesa.2007.11.015.

[80] G. Raju, Z. Wu, B.C. Kim, P.M. Weaver, Prebuckling and buckling analysis of variable angle tow plates with general boundary conditions, Compos. Struct. 94 (2012) 2961–2970.

doi:10.1016/j.compstruct.2012.04.002.

[81] Z. Wu, P.M. Weaver, G. Raju, B. Chul Kim, Buckling analysis and optimisation of variable angle tow composite plates, Thin-Walled Struct. 60 (2012) 163–172. doi:10.1016/J.TWS.2012.07.008.

[82] B.H. Coburn, Z. Wu, P.M. Weaver, Buckling analysis of stiffened variable angle tow panels, Compos. Struct. 111 (2014) 259–270. doi:10.1016/J.COMPSTRUCT.2013.12.029.

[83] M. Song, J. Yang, S. Kitipornchai, W. Zhu, Buckling and postbuckling of biaxially compressed functionally graded multilayer graphene nanoplatelet-reinforced polymer composite plates, Int. J. Mech. Sci. 131–132 (2017) 345–355. doi:10.1016/j.ijmecsci.2017.07.017.

[84] M.Z. Kabir, B. Tavousi Tehrani, Closed-form solution for thermal, mechanical, and thermo-mechanical buckling and post-buckling of SMA composite plates, Compos. Struct. 168 (2017) 535–548. doi:10.1016/j.compstruct.2017.02.046.

[85] R.F. Palardy, A.N. Palazotto, Buckling and vibration of composite plates using the Levy method, Compos. Struct. 14 (1990) 61–86. doi:10.1016/0263-8223(90)90059-N.

[86] A. Nosier, J.N. Reddy, Vibration and stability analysis of cross-ply laminated circular cylindrical shells, J. Sound Vib. 157 (1992) 139–159.

[87] A. Nosier, J.N. Reddy, On vibration and buckling of symmetric laminated plates according to shear deformation theories - Part I, Acta Mech. 94 (1992) 123–144. doi:10.1007/BF01176647.

[88] A. Alesadi, M. Galehdari, S. Shojaee, Free vibration and buckling analysis of cross-ply laminated composite plates using Carrera's unified formulation based on Isogeometric approach, Comput. Struct. 183 (2017) 38–47. doi:10.1016/j.compstruc.2017.01.013.

[89] D.B. Singh, B.N. Singh, New higher order shear deformation theories for free vibration and buckling analysis of laminated and braided composite plates, Int. J. Mech. Sci. 131–132 (2017) 265–277. doi:10.1016/j.ijmecsci.2017.06.053.

[90] A.S. Sayyad, Y.M. Ghugal, On the Buckling of Isotropic , Transversely Isotropic, 2014. doi:10.1142/S0219455414500205.

[91] T. Özben, Analysis of critical buckling load of laminated composites plate with different boundary conditions using FEM and analytical methods, Comput. Mater. Sci. 45 (2009) 1006–1015. doi:10.1016/j.commatsci.2009.01.003.

[92] G.B. Chai, Buckling of generally laminated composite plates with various edge support conditions Gin, 29 (1994) 299–310.

[93] S.T. Smith, M.A. Bradford, D.J. Oehlers, Numerical convergence of simple and orthogonal polynomials for the unilateral plate buckling problem using the Rayleigh-Ritz method, Int. J. Numer. Methods Eng. 44 (1999) 1685–1707. doi:10.1002/(SICI)1097-0207(19990420)44:11<1685::AID-NME562>3.0.CO;2-9.

[94] M. Aydin Komur, M. Sonmez, Elastic buckling of rectangular plates under linearly varying in-plane normal load with a circular cutout, Mech. Res. Commun. 35 (2008) 361–371. doi:10.1016/j.mechrescom.2008.01.005.

[95] K. Liang, M. Ruess, M. Abdalla, The Koiter-Newton approach using von Ka´rma´n kinematics for buckling analyses of imperfection sensitive structures, Comput. Methods Appl. Mech. Eng. 279 (2014) 440–468. doi:10.1016/j.cma.2014.07.008.

[96] P. Dhurvey, Buckling analysis of composite laminated skew plate of variable thickness, Mater. Today Proc. 4 (2017) 9732–9736. doi:10.1016/j.matpr.2017.06.257.

[97] L.W. Chen, L.Y. Chen, Thermal buckling of laminated composite plates, J. Therm. Stress. 10 (1987) 345–356. doi:10.1080/01495738708927017.

[98] S. Tahaei Yaghoubi, S.M. Mousavi, J. Paavola, Buckling of centrosymmetric anisotropic beam structures within strain gradient elasticity, Int. J. Solids Struct. 109 (2017) 84–92. doi:10.1016/j.ijsolstr.2017.01.009.

[99] I.U. Cagdas, S. Adali, Buckling of cross-ply laminates subject to linearly varying compressive loads and in-plane boundary restraints, J. Thermoplast. Compos. Mater. 26 (2013) 193–215. doi:10.1177/0892705711420594.

[100] S. Ilanko, L.E. Monterrubio, The Rayleigh-Ritz Method for Structural Analysis, 2014.

[101] C.M. Wang, Y.C. Wang, J.N. Reddy, Problems and remedy for the Ritz method in determining stress resultants of corner supported rectangular plates, Comput. Struct. 80 (2002) 145–154. doi:10.1016/S0045-7949(01)00168-7.

[102] C.M. Wang, Y.C. Wang, J.N. Reddy, V. Thevendran, Improved Computation of Stress Resultants in the, Managing. 128 (2002) 249–258. doi:10.1061/(ASCE)0733-9445(2002)128:2(249).

[103] L.M. Kachanov, Separation failure of composite materials, Polym. Mech. 12 (1976) 812–815. doi:10.1007/BF00856347.

[104] H. Chai, Buckling and post-buckling behavior of elliptical plates: Part II-Results, J. Appl. Mech. Trans. ASME. 57 (1990) 981–988. doi:10.1115/1.2897671.

[105] H. Chai, Buckling and post-buckling behavior of elliptical plates: Part I-analysis, J. Appl. Mech. Trans. ASME. 57 (1990) 981–988. doi:10.1115/1.2897671.

[106] B. Storåkers, B. Andersson, Nonlinear plate theory applied to delamination in composites, J. Mech. Phys. Solids. 36 (1988) 689–718. doi:10.1016/0022-5096(88)90004-X.

[107] Y. Wan-Lee, Axisymmetric buckling and growth of a circular delamination in a compressed laminate, Int. J. Solids Struct. 21 (1985) 503–514. doi:10.1016/0020-7683(85)90011-3.

[108] N. Kharghani, C. Guedes Soares, Analytical and experimental study of the ultimate strength of delaminated composite laminates under compressive loading, Compos. Struct. (2019) 111355. doi:10.1016/j.compstruct.2019.111355.

[109] S. Wang, Y. Zhang, S. Wang, Buckling , post-buckling and delamination propagation in debonded composite laminates Part 1 : Theoretical development, Compos. Struct. 88 (2009) 131–146. doi:10.1016/j.compstruct.2008.02.012.

[110] C.M. Wang, Y.C. Wang, J.N. Reddy, V. Thevendran, Improved Computation of Stress Resultants in the p-Ritz Method, J. Struct. Eng. 128 (2002) 249–258. doi:10.1061/(ASCE)0733-9445(2002)128:2(249).

[111] D. Bruno, F. Greco, An asymptotic analysis of delamination buckling and growth in layered plates, Int. J. Solids Struct. 37 (2000) 6239–6276. doi:10.1016/S0020-7683(99)00281-4.

[112] J.D. Whitcomb, K.N. Shivakumar, Strain-Energy Release Rate Analysis of a Laminate with a Postbuckled Delamination, NASA Tech. Memo. 89091 (1987).

[113] H. Gu, A. Chattopadhyay, An experimental investigation of delamination buckling and post buckling of composite laminates, Compos. Sci. Technol. 59 (1999) 903–910.

[114] M.A. Crisfield, A fast incremental/iterative solution procedure that handles “snap-through,” Comput. Struct. 13 (1981) 55–62. doi:10.1016/0045-7949(81)90108-5.

[115] J.N. Reddy, a. Khdeir, Buckling and vibration of laminated composite plates using various plate theories, AIAA J. 27 (1989) 1808–1817. doi:10.2514/3.10338.

[116] N. Grover, D.K. Maiti, B.N. Singh, A new inverse hyperbolic shear deformation theory for static and buckling analysis of laminated composite and sandwich plates, Compos. Struct. 95 (2013) 667–675. doi:10.1016/j.compstruct.2012.08.012.

[117] J.L. Mantari, F.G. Canales, Free vibration and buckling of laminated beams via hybrid Ritz

solution for various penalized boundary conditions, Compos. Struct. 152 (2016) 306–315. doi:10.1016/j.compstruct.2016.05.037.

[118] A.K. Upadhyay, · K K Shukla, Post-buckling analysis of skew plates subjected to combined in-plane loadings, Acta Mech. 225 (2014) 2959–2968. doi:10.1007/s00707-014-1205-2.

[119] L. Librescu, A.A. Khdeir, D. Frederick, A shear deformable theory of laminated composite shallow shell-type panels and their response analysis I: Free vibration and buckling, Acta Mech. 76 (1989) 1–33. doi:10.1007/BF01175794.

[120] G.J. Simitses, J. Giri, Buckling of Rotationally Restrained Orthotropic Plates Under Uniaxial Compression, Compos. Mater. 11 (1978) 345–364. doi:10.1177/002199837701100308.

[121] E. Jaberzadeh, M. Azhari, Elastic and inelastic local buckling of stiffened plates subjected to non-uniform compression using the Galerkin method, Appl. Math. Model. 33 (2009) 1874–1885. doi:10.1016/j.apm.2008.03.020.

[122] R. Vescovini, C. Bisagni, Single-mode solution for post-buckling analysis of composite panels with elastic restraints loaded in compression, Compos. Part B Eng. 43 (2012) 1258–1274. doi:10.1016/j.compositesb.2011.08.029.

[123] Q. Chen, P. Qiao, Shear buckling of rotationally-restrained composite laminated plates, Thin-Walled Struct. 94 (2015) 147–154. doi:10.1016/j.tws.2015.04.006.

[124] P. Qiao, G. Zou, Local buckling of elastically restrained fiber-reinforced plastic plates and its application to box sections, J. Eng. Mech. 128 (2002) 1324–1330. doi:10.1061/(ASCE)0733-9399(2002)128:12(1324).

[125] P. Qiao, G. Zou, Local Buckling of Composite Fiber-Reinforced Plastic Wide-Flange Sections, J. Struct. Eng. 129 (2003) 125–129. doi:10.1061/(ASCE)0733-9445(2003)129:1(125).

[126] C. Mittelstedt, Stability behaviour of arbitrarily laminated composite plates with free and elastically restrained unloaded edges, Int. J. Mech. Sci. 49 (2007) 819–833. doi:10.1016/j.ijmecsci.2006.11.011.

[127] D.G. Stamatelos, G.N. Labeas, K.I. Tserpes, Analytical calculation of local buckling and post-buckling behavior of isotropic and orthotropic stiffened panels, Thin-Walled Struct. 49 (2011) 422–430. doi:10.1016/j.tws.2010.11.008.

[128] P. Qiao, L. Shan, Explicit local buckling analysis and design of fiber-reinforced plastic

composite structural shapes, Compos. Struct. 70 (2005) 468–483. doi:10.1016/j.compstruct.2004.09.005.

[129] L. Shan, P. Qiao, Explicit local buckling analysis of rotationally restrained composite plates under uniaxial compression, Eng. Struct. 30 (2008) 126–140. doi:10.1016/j.engstruct.2007.02.023.

[130] P. Qiao, X. Huo, Explicit local buckling analysis of rotationally-restrained orthotropic plates under uniform shear, Compos. Struct. 93 (2011) 2785–2794. doi:10.1016/j.compstruct.2011.05.026.

[131] E. Villarreal, D. Abajo, Buckling and modal analysis of rotationally restrained orthotropic plates, Prog. Aerosp. Sci. 78 (2015) 116–130. doi:10.1016/j.paerosci.2015.06.005.

[132] L.E. Monterrubio, Frequency and buckling parameters of box-type structures using the Rayleigh-Ritz method and penalty parameters, Comput. Struct. 104–105 (2012) 44–49. doi:10.1016/j.compstruc.2012.03.010.

[133] J.W. Pizhong Qiao, Julio F. Davalos, Local buckling of composite FRP shapes by discrete plate analysis, 127 (2001) 245–255.

[134] L.C. Bank, J. Yin, Buckling of orthotropic plates with free and rotationally restrained unloaded edges, Thin-Walled Struct. 24 (1996) 83–96. doi:10.1016/0263-8231(95)00036-4.

[135] S.M.R. Khalili, P. Abbaspour, K. Malekzadeh Fard, Buckling of non-ideal simply supported laminated plate on Pasternak foundation, Appl. Math. Comput. 219 (2013) 6420–6430. doi:10.1016/J.AMC.2012.12.056.

[136] T. Mizusawa, T. Kajita, Vibration and buckling of rectangular plates with nonuniform elastic constraints in rotation, Int. J. Solids Struct. 23 (1987) 45–55. doi:10.1016/0020-7683(87)90031-X.

[137] Q. Chen, P. Qiao, Buckling analysis of laminated plate structures with elastic edges using a novel semi-analytical finite strip method, Compos. Struct. 152 (2016) 85–95. doi:10.1016/j.compstruct.2016.05.008.

[138] J.M. Housner, M. Stein, Numerical analysis and parametric study of the buckling of composite orthotropic compression and shear panels, NASA TN D-7996. (1975).

[139] A. Shirkavand, F. Taheri-Behrooz, M. Omidi, Orientation and size effect of a rectangle cutout on the buckling of composite cylinders, Aerosp. Sci. Technol. 87 (2019) 488–497.

doi:10.1016/J.AST.2019.02.042.

[140] R. ARNOLD, S. YOO, Buckling, postbuckling, and crippling of shallow curved composite plates with edge stiffeners, 26th Struct. Struct. Dyn. Mater. Conf. 23 (1985) 589–598. doi:doi:10.2514/6.1985-769.

[141] N. Jaunky, K. Jr, An assessment of shell theories for buckling of circular cylindrical laminated composite panels loaded in axial compression, Int. J. Solids Struct. 36 (1999) 3799–3820. doi:10.1016/S0020-7683(98)00177-2.

[142] J.M. Whitney, Structural Analysis of Anisotropic Laminated plates, Technomic Publishing Company, Inc., 1987.

[143] R. Ganesan, S. Akhlaque-E-Rasul, Compressive response of tapered composite shells, Compos. Struct. 93 (2011) 2153–2162. doi:10.1016/j.compstruct.2011.02.010.

[144] Elmer Franklin Bruhn, Analysis and Design of Flight Vehicle Structures, Jacobs Publishing, Inc., 1973.

[145] M.P. Nemeth, Nondimensional parameters and equations for nonlinear and bifurcation analyses of thin anisotropic quasi-shallow shells, J. Appl. Mech. 61 (1994) 664–669.

[146] Z. Aslan, M. Şahin, Buckling behavior and compressive failure of composite laminates containing multiple large delaminations, Compos. Struct. 89 (2009) 382–390. doi:10.1016/j.compstruct.2008.08.011.

[147] S. Shoja, V. Berbyuk, A. Boström, Delamination detection in composite laminates using low frequency guided waves: Numerical simulations, Compos. Struct. 203 (2018) 826–834. doi:10.1016/j.compstruct.2018.07.025.